UNIVERSITY OF SOUTHAMPTON

FACULTY OF NATURAL AND ENVIRONMENTAL SCIENCES

School of Ocean and Earth Sciences

Understanding the Extent of Universality in Phytoplankton Spatial Properties

by

Simon Jan van Gennip

Thesis for the degree of Doctor of Philosophy

September 2014

ABSTRACT

UNDERSTANDING THE EXTENT OF UNIVERSALITY IN PHYTOPLANKTON SPATIAL PROPERTIES

Simon Jan van Gennip

Phytoplankton are one of the most visible signs of life in our oceans. They also are a key component of the global carbon cycle and of the marine food web. Their complex patterns at the sea surface are routinely seen in satellite images, though the first observations go back centuries.

The motivation of this thesis is to explore the spatial properties of phytoplankton. Inspired by 'universal' theories for the dynamics of turbulence, several ones have been proposed to explain phytoplankton patchiness as a balance between turbulent stirring by the water and biological processes involving the phytoplankton. The thesis examines the extant theories of plankton patchiness using a novel twin tracer approach, specifically using *in situ* simultaneous Chlorophyll-a and nitrate measurements from a cruise in the North Atlantic. A significant difference is observed between the variability spectra of the two biochemical variables, an outcome potentially explained only by one theory.

More generally, although numerous observations testify to the existence of scaling behaviour of phytoplankton spatial variability, the collation of these studies indicates considerable variability, and hence uncertainty, in the power law behaviour, specifically the value of the spectral 'slope'. The many different techniques used to evaluate the spectrum, the different sources of data, and the geographical and temporal limitations associated with the data all contribute to adding noise and uncertainties in the estimates for the slope and make a comparison between studies difficult. In this thesis, the existence of the universal scaling properties of phytoplankton are tested over a wide range of spatial (sub-regional and regional) and temporal (few days to a year) scales using *in situ*, satellite data and model output. For this purpose a robust method is developed that reliably evaluates the spectrum of phytoplankton. A power-law behaviour in the phytoplankton spectrum is consistently found across the sources of data used and the range of scales studied (from 10 m to 130 km). However, stronger universality for the phytoplankton spectrum, defined as constant or uniform slope, is undermined by the significant variability in spectral slope that is consistently demonstrated across the spatial and temporal scales studied.

Table of Contents

List of tables

List of figures

List of accompanying materials

DECLARATION OF AUTHORSHIP

I, **SIMON JAN VAN GENNIP**

declare that this thesis and the work presented in it are my own and has been generated by me as the result of my own original research.

UNDERSTANDING THE EXTENT OF UNIVERSALITY IN PHYTOPLANKTON SPATIAL PROPERTIES

I confirm that:

1. This work was done wholly or mainly while in candidature for a research degree at this University;
2. Where any part of this thesis has previously been submitted for a degree or any other qualification at this University or any other institution, this has been clearly stated;
3. Where I have consulted the published work of others, this is always clearly attributed;
4. Where I have quoted from the work of others, the source is always given. With the exception of such quotations, this thesis is entirely my own work;
5. I have acknowledged all main sources of help;
6. Where the thesis is based on work done by myself jointly with others, I have made clear exactly what was done by others and what I have contributed myself;
7. [Delete as appropriate] None of this work has been published before submission [or] Parts of this work have been published as: [please list references below]:

Signed: .....

Date:.....

Acknowledgements

I would first and foremost like to thank my supervisors Adrian Martin and Meric Srokosz for their guidance and support over the last four years. I particularly thank them for the inexhaustible patience that they have shown to me, the endless time they have taken to discuss ideas, improve my academic writing, develop my scientific mind and share with me their immense knowledge of oceanography.

I also thank my panel chair, Jon Copley who has assisted in the running of my PhD, the NERC Earth Observation Data Acquisition and Analysis Service (NEODAAS) for supplying the satellite data and Marina Lévy for providing me with the high resolution model data and sharing her modelling expertise.

Thank you to John Allen for his help, particularly in extracting and analysing SeaSoar data and for his guidance, and Mark Hartman for the processing and analysing of the SUV-6 data. I also wish to thank Stuart Painter for always happily helping me and answer my many queries. A particular thanks also go to the Captain, officers, crew, technical staff and fellow scientists aboard RRS Discovery during D369 and to all those who have been involved in the processing of cruise data that may have contributed to this thesis.

Finally, I would particularly like to thank my family who have supported me especially during the writing stage of the thesis, and also Chiara for her enthusiasm, encouragement and formidable editing skills! Thank you to Bastien and Claire for their friendship, to James K. and Dave W. for the numerous runs and cycle rides, and of course a particular thanks to my offices mates in 344-27, Roz, Siân, Sam, Chris and Katsya as well as the numerous other people at NOC.

Abbreviations

AUV	Autonomous Underwater Vehicle
Chl-a	Chlorophyll-a
CTD	Conductivity Temperature and Depth
CV	Coefficient of Variability
DCM	Deep Chlorophyll Maximum
FFT	Fast Fourier Transform
LSP	Lomb Scargle Periodogram
MERIS	Medium REsolution Imaging Spectrometer
MODIS	Moderate Resolution Imaging Spectroradiometer
N	Nitrate
NEMO	Nucleus for European Modelling of the Ocean
OSMOSIS	Ocean Surface Mixing, Ocean Sub-Mesoscale Interaction Study
OWSI	Ocean Weather Station India
P	Phytpplankton
PAP	Porcupine Abyssal Plain
SOOP	Ship Of OPportunity
SUV	UltraViolet Spectrophotometer
Z	Zooplankton
LOBSTER	LODyC Ocean Biogeochemical System for Ecosystem and Resources model

Chapter 1: Introduction

Unlike their biosphere counterparts on land (e.g. grass), phytoplankton, the dominant plant in the ocean, are, like their name suggests, free floating and therefore subject to advection by ocean currents. They are additionally very small (down to 1 µm) but can reach such high abundances in blooms as to discolour water. Phytoplankton display striking spatial variability which is routinely captured by satellite images (Figure 1.1). Its structure, made of complex convoluted filamental patterns covering scales from as small as a millimetre to thousands of kilometres, continually evolves over time. A long history of observations of this phenomenon exists, dating back to the expeditions of de Ulloa and Cook in the 18th century, yet debate continues on what mechanisms control this heterogeneity.

Phytoplankton are a major contributor to the global carbon cycle, through their central position in the biological carbon pump (Sanders *et al.*, 2014), and are responsible for an estimated 50% of global primary production (Field *et al.*, 1998, Behrenfeld *et al.*, 2006). At scales of 1-10 km and 10-100 km (the submeso and mesoscale respectively), energetic features such as eddies and fronts are strong drivers of export and primary production as they regulate lateral and vertical transport of nutrients and biomass (Martin and Richards, 2001, Oschlies, 2002, McGillicuddy *et al.*, 2003, Chelton *et al.*, 2011). Those same physical features, through stirring and mixing combined with biological processes (e.g. such as nutrient uptake by phytoplankton for growth and grazing by zooplankton), generate inhomogeneous distributions in the concentration of phytoplankton and other biogeochemical tracers. This heterogeneity can affect estimates of production and export (Levy and Martin, 2013) for which precise estimates are needed e.g. for climate studies of the carbon cycle. Therefore, being able to understand the considerable spatial heterogeneity associated with phytoplankton distributions is essential for further developing our understanding of ocean biogeochemical dynamics and interactions. This has been a motivation for this research study.

As the spatial structure of phytoplankton spans a large range of length-scales, many different processes are involved with their influence varying over this range. The mesoscale range, bounded by the length-scale of the largest eddy (up to few 100 km and decreasing with increasing latitude) and the length-scale above which ocean circulation ceases to be fully three dimensional (~1 km), has attracted much interest, notably because in this range the physics and

the biology act on similar time-scales of order of a few days. This study is primarily focussed on this range.

The following sections provide a context and motivation for the thesis, first by discussing previous observations of phytoplankton patchiness, specifically through the use of spectra, and second by describing the current theories for what controls such patchiness.

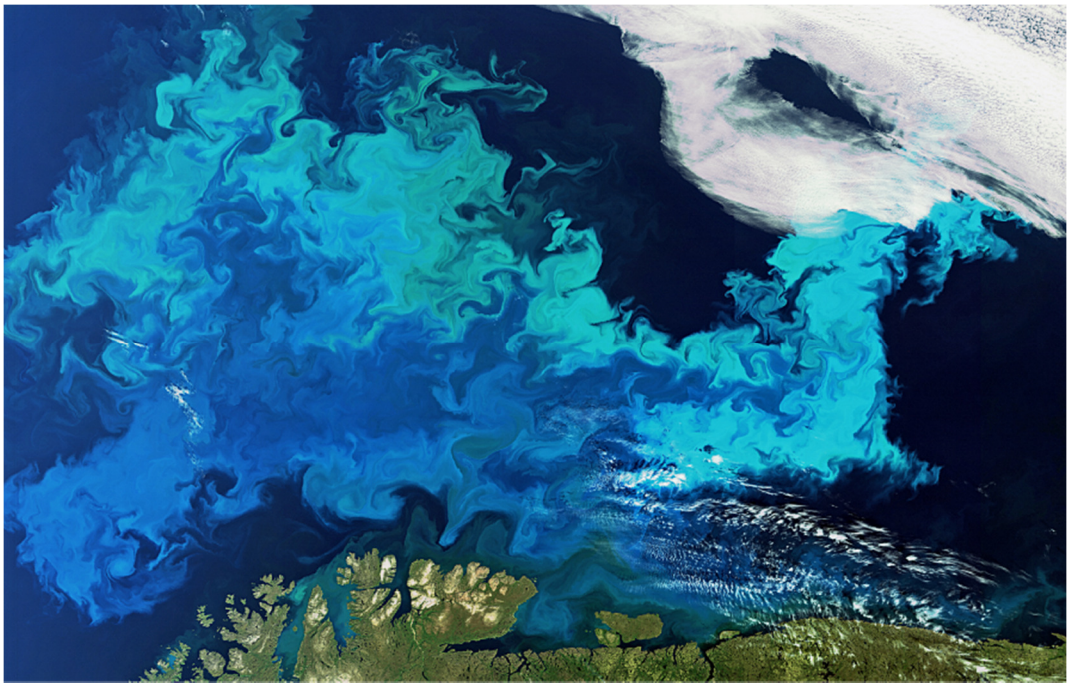

Figure 1.1: *Phytoplankton bloom across the Barents Sea captured by Envisat's MEdium Resolution Imaging Spectrometer (MERIS) on the 24th August 2011. Note the structure present across scales, with the filamental nature of the patchiness illustrative of the role played by ocean turbulence in the pattern formation. The different colours of the ocean reveal the density of phytoplankton population within water parcels with light blue patches being highly concentrated. The picture is approximately 500 km by 350 km.*

1.1. Scaling and universality

The advent of the fluorimeter (Lorenzen, 1966) and the first satellite capable of measuring ocean colour (1978) provided stepping stones for phytoplankton patchiness research. The fluorimeter, through long transect continuous chlorophyll-a (Chl-a) measurements, revealed that phytoplankton structure did not consist of a series of independent patches but that patches were interconnected. Later on, ocean colour provided for the first time two dimensional synoptic maps of Chl-a, revealing the intricate spatial structure of convoluted and filamental patterns evocative of the action of the stirring and mixing of the flow (see Figure 1.1).

Using spectral analysis, which decomposes the variability observed in the data series into the contribution from individual length-scales, it was found that phytoplankton variability was present across a range of length-scales and displayed scaling properties between them. Indeed, numerous observational studies describe the phytoplankton spectrum as following a power law (Gower *et al.*, 1980, Smith *et al.*, 1988, Yoder *et al.*, 1993, Washburn *et al.*, 1998, Martin and Srokosz, 2002). In other words, when plotted in log-log space, the spectrum is characterised by a straight line. The gradient of this line or slope describes how variability is partitioned between wavenumbers (inverse of the length-scale). This is expressed in mathematical terms as follows: $P(k) \propto k^{\alpha}$ where k is the wavenumber, $P(k)$ the power function of k, and α the slope of the line in log-log space. For phytoplankton patchiness the slope (or equivalently 'exponent') is invariably negative. The steeper the line the more variability is observed at large relative to small scales. The observations indicating such scaling behaviour cover many intervals of length-scales: as short as 10 m– 1 km (Platt, 1972, Fasham and Pugh, 1976, Seuront *et al.*, 1999) to the submesoscale (1-10 km) (Smith *et al.*, 1988) and the mesoscale (Lekan and Wilson, 1978, Strutton *et al.*, 1997) and many other overlapping intervals.

Inspired by 'universal' theories for the dynamics of turbulence, where a similar decreasing trend of variability with decreasing length-scale is seen e.g. velocity fluctuations (Kolmogorov, 1991), the idea of a universal spectrum for phytoplankton has been proposed. Several theories attempt to explain phytoplankton patchiness as a balance between turbulent stirring by the water and biological processes involving the phytoplankton.

Between the large length-scale (of order of 1000 km)at which kinetic energy is being introduced and the short one (of order of cm) at which it is dissipated, kinetic energy decays following a power law under the influence of the stirring and mixing of the oceanic flow (Kraichnan, 1967). A similar transfer of variability across a range of length-scales has been proposed for

phytoplankton, on the assumption that forcing of phytoplankton variability occurs at a scale larger than the range being considered. For example, for scaling behaviour at the mesoscale, forcing would consist of winter convection which forces nutrient gradients at basin scale.

The structure imposed by the flow on passive non-reactive tracers depends on the turbulence model advocated. Decay in a two dimensional regime (most applicable to scales greater than 1 km) follows α=-1 whilst a faster decay (more applicable to smaller scales) with α=-5/3 occurs in a three dimensional turbulence model (Powell and Okubo, 1994).

Based on the argument that the physical time-scale associated with turbulent motion decreases with length-scale, typically meaning that large eddies have longer time-scales than smaller eddies, and that the time-scale of the biology remains relatively constant with scale, two regimes have been distinguished (Denman and Platt, 1976, Denman *et al.*, 1977). At small scales, where the eddy time-scale is shortest, the physics dominate and therefore should dictate the spatial distribution of phytoplankton which should therefore share the same spectral properties with physical scalars such as temperature. In contrast, as scales become larger, a critical length-scale exists past which the physical processes are slower than biological ones allowing the biological processes to influence the spatial structure of phytoplankton. How biology is predicted to change the structure imposed by the flow at this larger scales is not consistent between theories, with biological models shown to either redden or whiten the phytoplankton spectrum (Powell and Okubo, 1994).The transition scale or 'knee' at which processes decouple, has been predicted to be within the range 0.2 – 20 km (Denman and Platt, 1976).

The notion of a competition of time-scales has fuelled several other theories which are discussed in the next section.

Throughout this thesis, the definition for universality is that the spectrum has the same shape everywhere at all times. The spectrum may have different slopes for different length ranges but these ranges and slopes remain constant across region and time. This thesis explores the hypothesis that universal scaling properties exist for phytoplankton patchiness. This research project will focus on open ocean cases only and therefore disregard coastal shelf zones which have their own biological and physical complexities. Both satellite colour data and high resolution global plankton models are better suited to the open ocean.

1.1.1. Observations in spectral slope

Combined together, observations seem to suggest that a universal explanation for phytoplankton spatial variability does not exist. Large variability in slope is observed at both the mesoscale — with values ranging from -1.05 (Martin and Srokosz, 2002) to -3.04 (Smith *et al.*, 1988) — and submesoscale — with values between -0.48 (Yoder *et al.*, 1993) and -3.28 (Washburn *et al.*, 1998). A more detailed review is available in Mackas *et al.* (1985) and Martin (2003) .

It is not clear whether the differences observed are geographical or temporal because studies did not take place in the same location or at the same time. No investigation of phytoplankton patchiness exists that have taken place for one location at regular intervals over the course of the year for example. Temporal variation have been observed over an 8-week period (Horwood, 1978) but covered only small scales (<3 km). Differences in slopes between regions have been measured (Barale and Trees, 1987) but were obtained with data from different times of year.

Beside variability in slope values for phytoplankton, no consistency is found between spectra of phytoplankton and physical tracers. For example, agreement with theoretical predictions would show phytoplankton slope flattening relative to temperature at large scale (Denman and Platt, 1976). Cases for which this is observed (Lovejoy *et al.*, 2001) are balanced by those that display the opposite (Lekan and Wilson, 1978) or those that show no change at all (Mahadevan and Campbell, 2002).

A general consensus regarding the structure of the patchiness of plankton is therefore difficult to obtain. This is partly due to the scarcity of observations in space and time. It is clear that a larger number of observations are needed. However, it is uncertain whether the differences are due to methodological issues or because of true variability, either spatial or temporal. How much this variability is due to the choice of method therefore needs to be determined. It therefore seems premature to conclude non-universality in phytoplankton scaling properties on the basis of such a small number of spectral studies.

1.1.2. Differences in methodology

Many different methods exist to estimate the spectrum of a variable. Amongst the phytoplankton studies, one dimensional spectra (Platt and Denman, 1975), two dimensional spectra (Gower *et al.*, 1980), autocorrelation spectra (Mackas and Boyd, 1979), semi variograms (Yoder *et al.*, 1993) and structure functions (Seuront *et al.*, 1999) have been used. A main

difference is whether regularly or irregularly spaced data is used, an issue addressed in Chapter 7.

Additionally, the data can be modified in order to reduce the noise in the spectral estimation. A finite data series is equivalent to a longer one looked at through a window for which values outside view are equal to 0. Hence, sharp changes exist at the edges of that window. This can introduce bias in the spectral estimations. Therefore by smoothing the start and end of the data series to create a more gradual change, such bias can be reduced. Different windows have been used to reduce the bias. In phytoplankton studies, data have been windowed using a Hann window (Weber *et al.*, 1986, Washburn *et al.*, 1998), pre-whitening window (Mackas and Boyd, 1979) and a cosine window (Smith *et al.*, 1988, Martin and Srokosz, 2002). While the choice of a window can somewhat be arbitrary, it is clear that the method can affect the outcome, as shown in Chapter 2. Whereas a question worth asking about studies in the literature is whether a different spectral slope would have been obtained had another method been used, and consequently whether when comparing slopes between studies we are simply comparing the effects of different methodologies.

Furthermore, some slope estimates are obtained with limited spatial coverage, sometimes using a single transect just tens of kilometres long. Given the noisy nature of spectral analysis (Jenkins and Watts, 1968), do such estimates give a robust estimate of the slope? Averaging estimates of spectral power by using a number of transects or by splitting long transects into subsets is generally recommended for obtaining more robust values (Emery and Thomson, 2001) but this has not always been done. Given so it is unclear how many transects are needed to obtain a robust estimate of signals with a power-law relationship with length-scale. Different spatial coverage also means that the slopes have been estimated over different, if overlapping, ranges of length-scales with no consistency in ranges covered across studies.

Different sources of data are also being used for estimating the spectra of phytoplankton, mainly Chl-a estimates obtained either from ship surveys from fluorimeter fitted on the underway sampling system or on a towed undulating vehicle (Hodges and Rudnick, 2006), but also from remotely sensed data from satellites (Mahadevan and Campbell, 2002) or airplanes (Yoder *et al.*, 1993). Bacterioplankton variability has also been investigated using flow cytometry (Martin *et al.*, 2008). This is of relevance because *in situ* and remotely sensed estimates do not necessarily capture the same variability (Yoder *et al.*, 1993). Estimates from satellite sensors are averages over a pixel (typically 1 km x1 km) but *in situ* estimates are at a point, effectively at scales of one metre. It is not currently known what the differences are between spectra obtained

with point estimates – like *in situ* data – and average estimates – like satellite data. Therefore, a further point is raised regarding a fair assessment of phytoplankton universal scaling properties to date; whether spectra obtained from different types of data can be compared.

Only by developing a common approach for consistently evaluating the spectrum of phytoplankton, the question of whether phytoplankton spectrum displays universal properties can be addressed robustly.

1.2. Theories for patchiness

In this section the extant theories of phytoplankton are reviewed but first a broad overview of the mechanisms involved in generating and modulating patchiness are given.

1.2.1. Broad overview

Phytoplankton need light and nutrients to build organic matter using photosynthesis. Light requirements therefore limit their existence to the sun-lit 100 m or so surface layer of the oceans. In many regions the surface layer sees nutrient quickly being consumed following its upwelling from depth. Various physical processes resupply the surface layer with nutrients (Klein and Lapeyre, 2009), acting on different time and spatial scales. Winter convection through the wind cooling driven deepening of the mixed layer replenishes the surface layer with nutrient rich waters at basin scale. The magnitude of this annual process increases with latitude, with permanently stratified subtropical waters benefiting little from this process. However, it has been argued that as much as 50 % of their annual nutrient budget for these regions is obtained from physical processes at the mesoscale (McGillicuddy *et al.*, 2003). For example, strong nutrient upwelling has been observed within eddies through the shoaling of isopycnals (McGillicuddy *et al.*, 1998). At even smaller scale (1-10 km), eddy interactions form dynamically active filaments and fronts capable of generating strong vertical velocities (Pollard and Regier, 1992, Pidcock *et al.*, 2010) and driving primary production through nutrient upwelling (Strass, 1992, Allen *et al.*, 2005). The availability of nutrient act as a 'bottom up' control on phytoplankton structure and biomass.

A 'top down' control also exists through grazing by zooplankton populations. Their spatial structure is also patchy and to a certain level reflects the spatial structure of their food source.

Their greater ability to swim and aggregate gives them a better control on their own structure. Most studies show zooplankton spectra to be flatter than phytoplankton (Mackas and Boyd, 1979, Horwood, 1981, Weber *et al.*, 1986, Tsuda *et al.*, 1993) but as mobility and behaviour vary with size, different sized species have different spatial structure (Martin and Srokosz, 2002) with some displaying a steeper spectral slope than phytoplankton structure. Biogeochemical models do not capture this complexity and often only have one zooplankton component. Modelling studies show that parameters such as grazing rates and zooplankton mortality greatly impact the phytoplankton structure (Abraham, 1998). The effect of top down control on phytoplankton structure is however difficult to understand due to the non-linear reaction between the two interacting populations but also the scale at which the grazing pressure is exerted (Steele and Henderson, 1992). The top down control is not the focus of this research study and will therefore not be investigated. Rather, accent is placed on the bottom up control and how the different pathways for nutrient injection may affect the phytoplankton spatial structure.

Horizontal advection, the dominant physical process at the mesoscale, redistributes the introduced variance across length-scales through stirring and mixing. In the case of larger scale forcing of nutrient such as winter convection, the oceanic mesoscale advection cascades large scale variability to small scale (e.g., Abraham, 1998, Hernández-García *et al.*, 2002). However, such cascades can also be generated by small scale nutrient injections associated with mesoscale and submesoscale features (Lévy, 2003). Such episodic nutrient upwelling generates strong structure in the phytoplankton field. At such scales, this may lead to flatter slopes. It is clear that whatever the routes used by nutrients to reach the euphotic layer and the scales at which it does so, their impact on how phytoplankton are distributed is critical.

Beside physical drivers of patchiness, the structure of phytoplankton is also influenced by the biological processes that alter its concentration. For phytoplankton these consist of uptake of nutrients, growth, death and grazing by zooplankton. All biogeochemical reactive tracers are advected by a common flow, yet as discussed below, there is no consensus on whether these tracers can display different spatial scaling (Mahadevan and Campbell, 2002). The incomplete understanding of these biological interactions within a turbulent flow and the difficulty of sampling the mesoscale means much previous work has been theoretical or numerical. Nevertheless several theories exist that predict how biological reactions affect the spatial properties of phytoplankton and the components of its ecosystem.

1.2.2. Theories

There are four theories that seek to explain how phytoplankton spatial variability is structured across a range of length-scales.

The first theory (Denman and Platt, 1976, Denman *et al.*, 1977) is based on the argument that the time-scale associated with turbulent motion may decrease with length-scale but the biological response time is invariant with scale. At small scales, where physical processes act fastest, the spectral slope of phytoplankton should be identical to that of physical variables such as temperature. In contrast, at longer length-scales, the biological processes are quickest, and so patterns of spatial variability in phytoplankton can diverge from those of physical tracers. More specifically it has been predicted that there is a knee in the spectrum, not mirrored in physical variables, associated with a flattening of the phytoplankton slope at larger scales. The knee is argued to occur where biological and physical time-scales match. The second theory (Hernández-García *et al.*, 2002) takes the notion of a single biological time-scale further, arguing that it will be common to all interacting components of the planktonic ecosystem. In this scenario the ecosystem components, whether nutrients, phytoplankton or zooplankton, are predicted to have identical spectral slopes. This theory additionally assumes that a single time-scale can describe the effect of the turbulent stirring. The third theory (Bracco *et al.*, 2009) argues that the biological time-scale associated with each constituent of the ecosystem is determined by how quickly it responds to perturbation in its environment. Consequently, zooplankton are argued to react more slowly than phytoplankton and accordingly predicted to have different spectral slopes to nutrients and phytoplankton which respond on shorter time-scales. The fourth theory (Lévy and Klein, 2004) challenges the idea of a 'cascade' of variability from large scales to small scales, a central tenet in the theories for physical turbulence, which have been used as a basis to explain power law behaviour in spectra. Although variability is still transferred to smaller scales by stirring, the upwelling of nutrients at a range of intermediate scales, particularly within the mesoscale and submesoscale, injects extra variability. The response to such localized enhancement of phytoplankton growth is ephemeral and often significantly perturbs the ecosystem relative to background conditions. A consequence is that spectral slopes for different components of the ecosystem no longer need match (Lévy and Klein, 2004, Lévy *et al.*, 2005).

1.2.3. Testing theories

Although as discussed earlier, numerous observations already exist for phytoplankton patchiness, they have proved very variable and insufficient to distinguish between theories. The reasons for this have already been discussed (Sections 1.1.1. and 1.1.2.). One way to avoid these issues is to examine differences between a variety of tracers simultaneously. For example, if a theory predicts different spectral slopes for different biochemical tracers, the theories can be tested by simultaneously examining another component of the ecosystem that strongly interacts with and moves like phytoplankton.

Cases exist for which phytoplankton and zooplankton structure have been compared (Mackas and Boyd, 1979, Tsuda *et al.*, 1993, Martin and Srokosz, 2002). Unlike phytoplankton, zooplankton possess motility which result in behavioural mechanisms such as swarming, mating or predator avoidance that influence the way zooplankton are distributed in space (Folt and Burns, 1999). This does not make zooplankton an ideal ecosystem component alongside phytoplankton to test the above theories because zooplankton do not behave like phytoplankton and therefore it is not clear that they should have the same spatial properties. Observations are once again inconclusive. Zooplankton may have more small-scale structure than phytoplankton and therefore display a flatter spectral slope (Horwood, 1981, Weber *et al.*, 1986, Tsuda *et al.*, 1993). However, cases also exist showing a zooplankton spectral slope similar in strength (Piontkovski *et al.*, 1997) or steeper (Martin and Srokosz, 2002) than that of phytoplankton, suggesting the relationship between them is not simple. Additionally, different sized zooplankton are shown to have different spectra slopes (Martin and Srokosz, 2002). With the range of zooplankton size spanning four orders of magnitudes – from µm to tens of mm – and having varying mobility capabilities, it is not clear whether a unifying spectrum for all zooplankton species can be expected.

Nutrients however are not motile and are advected like phytoplankton making them a more reliable component with which to test the theories. This requires simultaneous high resolution nitrate and Chl-a measurements. Such dataset are now available and will be used to test these theories in this thesis (Chapter 3).

1.3. Research objectives

This thesis aims to further understanding of the patchiness of phytoplankton in the open ocean using a multidisciplinary approach, combining *in situ* and satellite observations, as well as numerical predictions from a model. More specifically, the thesis tackles the following specific objectives:

- To develop a robust methodology to reliably measure the spectrum of phytoplankton (**Chapter 2**).
- To test extant theories of phytoplankton patchiness (**Chapter 3**).
- To evaluate whether phytoplankton power spectra in different regions of the open ocean share the same properties (**Chapter 4**).
- To investigate whether phytoplankton spectral slopes vary significantly over time-scales of days (**Chapter 5**).
- To evaluate whether temporal variations over a period of months exceed variations in slope between regions (**Chapter 5**).
- To measure if the difference in nitrate and phytoplankton spectral slope is consistent in time (**Chapter 5**).
- To explore if there is a seasonal pattern in phytoplankton spectral slopes (**Chapter 5**).
- To investigate if satellite data can capture seasonal cycle in spectral slope (**Chapter 6**).
- Determine whether satellite and *in situ* data are consistent for the study of phytoplankton patchiness (**Chapter 6**).
- To determine whether phytoplankton spectral slope is insensitive to how an area is mapped (**Chapter 6**)

In **Chapter 2** a method that reliably estimates the power spectra of phytoplankton and that can be applied consistently throughout the thesis will be presented. For this, the sensitivity of the different spectral methods against a range of power-law signals simulating phytoplankton variability and the effect of windowing on improving the estimates is investigated. Inherent problems such as uneven spacing, associated with dealing with real data (whether from *in situ* or remote-sensing) are also covered.

Chapter 3 tests extant phytoplankton patchiness theories using a novel twin tracer approach, specifically using *in situ* simultaneous Chl-a and nitrate measurements from a cruise in the North Atlantic.

Chapter 4 investigates the universality of phytoplankton spatial properties by evaluating spectral slope of phytoplankton from different regions obtained using an identical methodology and *in situ* Chl-a measurements

In **Chapter 5**, the potential existence of temporal variability in phytoplankton spatial properties is evaluated using numerical output from a model. This chapter also tackles issues raised concerning spatial and temporal limitations of *in situ* data by investigating phytoplankton spectral properties over larger spatial and temporal scales.

The question of whether *in situ* and satellite give consistent results for phytoplankton patchiness is addressed in **Chapter 6** using simultaneous *in situ* and satellite measurements. The sensitivity of the slope estimate to sampling method and the size of the area mapped is also examined. Satellite data are also used to test temporal patterns observed in model spectral predictions.

In the final chapter (**Chapter 7**), results are synthesized and a broader view is taken to discuss the key findings of the thesis and to relate them to the thesis' original overarching question of whether universal properties in phytoplankton patchiness exist and whether they can be measured accurately.

Chapter 2: Can the spectrum of phytoplankton be reliably estimated?

2.1. Motivations

Why spectra?

Because bio-physical interactions are intimately connected across spatial scales (Prairie *et al.*, 2012) with biological and physical processes acting upon multiple scales, spectral analysis is a particularly well suited tool with which to evaluate the spatial structure of phytoplankton. By estimating the spectrum, which quantifies the distribution of the variability across scale, the contribution of a range of scales towards setting that variability can be studied.

In addition, the spectrum is a valuable tool as a measure for patchiness given that phytoplankton spatial structure has been shown to have a power law spectrum over a range of scales, and therefore can be described with only one number - the slope of log spectrum against log wavenumber.

Why analyse spectra?

The lack of uniformity in methodology of previous observational studies (see introduction chapter) for estimating the power spectrum of phytoplankton has the consequence that a rigorous comparison of phytoplankton spatial structure across regions, time, but also types of data (e.g. *in situ*, satellite or models) has not previously been possible.

The development of a methodology that robustly quantifies the slope of the phytoplankton power spectrum and is capable of processing the different types of data is therefore a prerequisite for this research project. Given issues of noise associated with spectral analysis, the different options available to reduce its impact and the varying nature of the different type of data studied, a thorough investigation of the capacity and limits associated with each method is evaluated here. In addition, given the range of potential slopes that the phytoplankton power law signal can display, it is important to verify whether methods successfully estimate the spectra for all such possible slope values.

The aim, therefore, of this chapter is simply to determine how the phytoplankton spectrum can best be reliably measured, whatever the type of data, the strength of the power law, or the quantity of data available.

2.2. Type of data and consequence for spectral method

For this research project three types of data are studied. Firstly, data obtained from *in situ* surveys are investigated (Chapter3 and 4), followed by model output (Chapter 5) and satellite data (Chapter 6). Before developing a common analysis procedure a quick description of the different data is necessary.

In situ data used in this study consists of surveys for which high resolution measurements are obtained along parallel transects oriented in the North-South or East - West direction (see, for example, Figure 2.1). Depending on the survey, between 4 and 9 transects are available. Measurements were collected with a vehicle towed by the ship and undulating through the water column between the surface and around 400 m depth (Figure 2.2).More details can be found in Chapter 3 and 4 as well as the reports for cruises D321 (Allen, 2008), D369 (Zubkov, 2012) and D381 (Allen and Naveira-Garabato, 2012). Measurements are evenly spaced with an interval of 5 m in the horizontal. The horizontal period of each undulation is approximately 4 km. If data at a specific depth are investigated, this can cause the data to be unevenly spaced because the actual horizontal period is affected by ship motion and weather conditions.

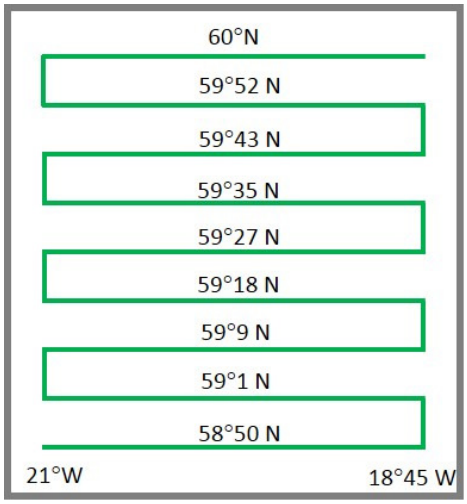

Figure 2.1*: Typical trajectory of a ship sampling in a radiator style an area of size 130 km by 130 km. This setup was taken from a survey during the D321 cruise in the North Atlantic in 2007 (see Chapter 3). It is used to simulate a phytoplankton signal upon which spectral methods are tested.*

Model output analysed in this thesis (see Chapter 5) are available on a regular grid with 1/9° resolution generating data points approximately 11.8 km apart in the x and y direction (Figure 2.3a).

The satellite data used for this study consist of 1 km resolution 'snapshot' images of ocean colour from the Moderate Resolution Imaging Spectroradiometer (MODIS) satellite (Figure 2.3b). The data can be obstructed by the presence of clouds (see Chapter 6) leaving gaps. Composite images, products obtained from averaging data over several days, are less affected by clouds. However, by averaging, some of the phytoplankton structure is smoothed out. These products are therefore not considered.

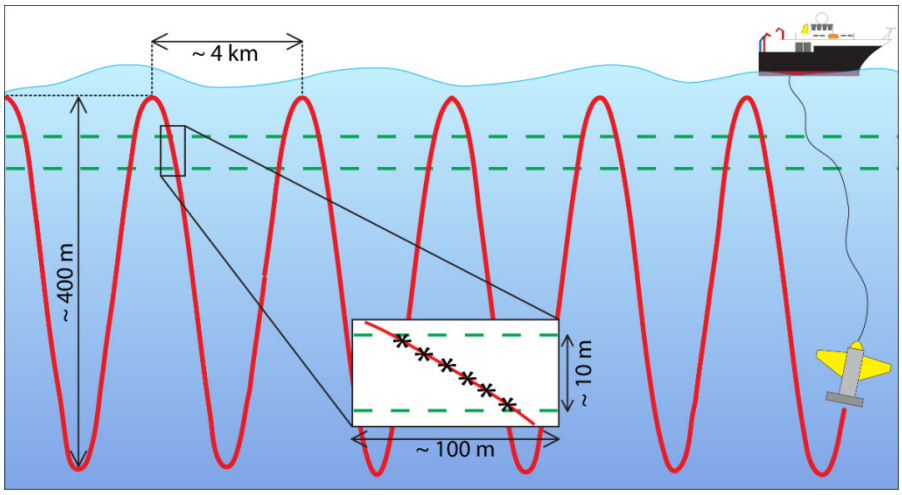

Figure 2.2: *Cartoon of the collection of data using an undulating SeaSoar vehicle towed by the ship. The vehicle traverses the water column to ~400 m depth. One full cycle has a period of ~ 4 km and generates two vertical profiles. Data are collected every ~5 m horizontally. Selecting data for a fixed depth range, here 10 m, generates clusters of around 20 points which are used for calculating the spectrum at 10-100 m length-scales. Averages of each of the clusters over the entire transect (130 km), provide spatial information for length-scales 8 – 130 km.*

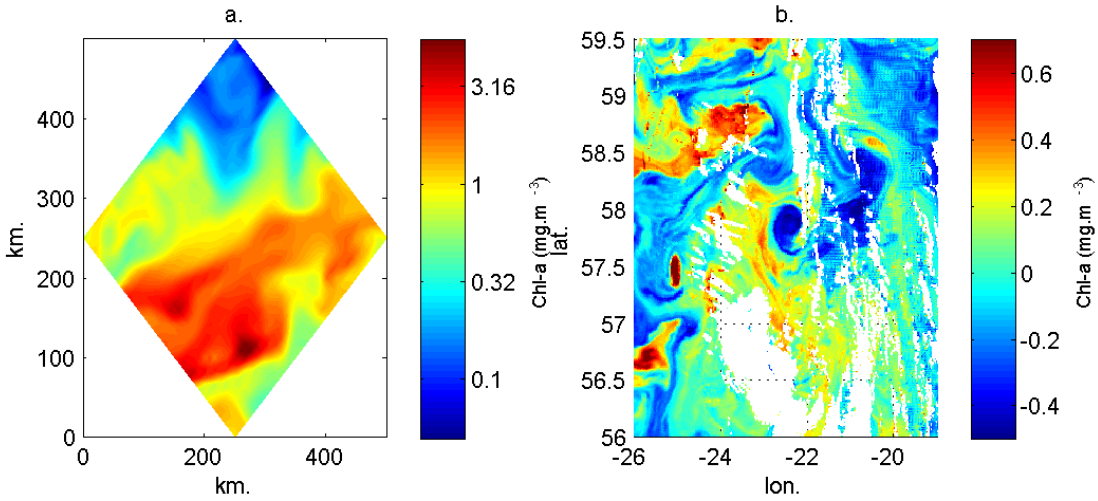

Figure 2.3: *Example of data for model predictions (a.) and satellite measurements of Chl-a (b.). Pixels for both data are evenly spaced with size 11.8 km and 1 km respectively. Note the presence of gaps due to clouds in the satellite data visible as white areas.*

Although the types of data have varying uniformity, spatial coverage and resolution, a requirement is that results across data types can be compared. This means that care is needed when evaluating the spectrum.

The most restricting of the datasets is that collected *in situ*. The parallel transects only sample finely in one direction (Figure 2.1). Because of this, and because the majority of previous studies (Chapter 1) analyse one-dimensional spectra, this is the approach used here.

Only the *in situ* data provides information at the smaller ranges of scales studied (10-100 m). However, *in situ*, satellite and model all provide data at the larger scales (8-130 km). Given that at larger scales *in situ* data points are approximately 4 km apart and measured over transect of around 130 km long, information on variability is only complete for length-scales within the range 8-130 km. The minimum length-scale of 8 km is obtained because a minimum of two sampling intervals are needed to capture a cycle and estimate the level of variability for that length-scale. However, model output are ~12 km apart which means their spectrum can only be investigated for a minimum length-scale of 24 km and not 8 km as for satellite and *in situ*. This difference was tolerated so that the already narrow range of length-scales used for *in situ* spectra was not further reduced.

2.3. Simulating a phytoplankton signal with a power law spectrum

Prior to evaluating the different spectral methods, it is important to construct a phytoplankton signal for which the spectral slope can be set so that it is known. The signal can then be used to evaluate each spectral method and its ability to recover the pre-defined slope value.

Previous observational studies found phytoplankton variability to be a power law signal with slope -3.3 ≤α≤ -0.5 (see Chapter 1 Section 1.1.). For this investigation, the different spectral methods are therefore tested against signals of power-law slopes covering the entire range of these observed values.

Knowing the slope of the spectrum and the range of length-scales covered, the simulated phytoplankton signal can be constructed with Fourier series. Fourier series reproduce a periodic signal $f(x)$ by superimposing a number of sinusoidal functions, such that:

$$f(x) = \sum_{j=1}^{n} A_j cos(\omega_j x + \varphi_j),$$

where the amplitude A_j and wavenumber ω_j of each wave *j* are determined by the chosen slope of the power spectrum and the range of length-scales respectively. The phase φ_j for each wavenumber ω_j however is not set by choosing the slope and is therefore chosen randomly from a uniform distribution on [0, 2 π].

Note that the spectrum from observational data only describes the energy distribution of the signal in wavenumber space for a limited range of length-scales, bounded by the lowest wavenumber detectable $\omega = {}^{1}/_{T} = {}^{1}/_{130}$ km^{-1} set by the length of the transect (*T*), and the highest wavenumber $\omega = {}^{1}/_{2\Delta} = {}^{1}/_{8}$ km^{-1} set by the sampling interval (Δ). In reality, the signal's energy spans beyond this range. Energy from outside the range studied was accounted for in the signal construction by using a wider range of wavenumbers bounded by $\omega = {}^{1}/_{260}$ (km^{-1}) and $\omega = {}^{1}/_{0.005}$ (km^{-1}). The reason for the high frequency to be so high relative to the range of length-scale evaluated in the spectrum is because the signal includes the frequencies of the *in situ* data used later. Equally, given that traditional spectral techniques estimate the power at wavenumber multiples of the lowest wavenumber sampled, $\omega = {}^{1}/_{T}$, the resolution of the spectrum i.e. the interval between wavenumbers, is therefore equal to ${}^{1}/_{T}$. For the signal construction, a finer resolution of ${}^{1}/_{10T}$ was chosen so to generate a closer approximation of a continuous signal.

2.4. Estimating spectra of phytoplankton for evenly spaced data

The data used in this research study which satisfy the condition of being evenly spaced are model output, cloud-free satellite data and *in situ* data at the smaller range of scales (10-100 m).

2.4.1. Fast Fourier Transform

One of the most common method for estimating the power spectrum of a periodic signal is the Fast Fourier Transform (FFT) but it requires evenly spaced data. It is a computationally efficient means of computing the discrete Fourier transform. The discrete Fourier Transform provides a mean to represent the signal in the wavenumber domain by describing the signal's amplitude and phase as a function of wavenumber.

When a signal *s* is sampled discretely with N data points which are separated by a regular interval Δ, the discrete Fourier components S_k can be calculated at length-scales multiple of that interval, with the following equivalent wavenumbers:

$$\omega_k = \frac{k}{N\Delta}. \qquad \text{where } k = 0, \dots, N-1,$$

with $\omega_c = \frac{1}{2\Delta}$, the Nyquist critical wavenumber, corresponding the highest resolved wavenumber.

The Fourier transform of the signal generates the following components:

$$S_k \equiv \sum_{n=0}^{N-1} s_n e^{2\pi i k n/N}$$

The Fourier components S_k are complex numbers containing the information on the amplitude and the phase of the signal at each wavenumber.

The spectrum of the signal is then obtained by taking the amplitude squared P (or also power) at each wavenumber such that:

$$P(0) = P(\omega_0) = \frac{1}{N^2}|S_0|^2$$

$$P(\omega_k) = \frac{1}{N^2}[|S_k|^2 + |S_{N-k}|^2]$$

Wavenumbers indexed from N/2+1 to N-1 correspond to the negative frequencies. The symmetric properties between negative and positive wavenumbers mean that their amplitudes squared are equal, $|S_k|^2 = |S_{N-k}|^2$. In the spectrum calculation, the wavenumbers between 1 and N/2 only are considered, so the power is multiplied by 2 to account for all the variability in the system.

Whether in space or in wavenumber domain, the overall energy within the signal is conserved and therefore, following Parseval's Theorem (Jenkins and Watts, 1968), the following equation should hold:

$$\sum_{n=1}^{N} |s_n|^2 = \frac{1}{N}\sum_{k=1}^{N} |S_k|^2$$

2.4.2. Reducing noise in spectra when using evenly spaced data

To reduce the level of noise in the spectra, a number of techniques exists. They either improve the reliability of the spectral estimates for each wavenumber band (block averaging) or reduce the leakage of energy that occurs from one wavenumber band to neighbouring ones (windowing, pre-whitening). They are each discussed in turn.

Block averaging the data

One method for reducing the level of noise in the final spectrum is through splitting the data series into many segments of equal length. For each of those segments, calculating the spectrum provides a spectral estimate for each wavenumber band. A more reliable spectrum can then be obtained by averaging these estimates for each band. The study of shorter records, however, affects the range of length-scales covered by the spectrum. Indeed, the largest wavenumber resolved is (*1/T*) for a given transect length *T*. By partitioning a transect into K segments, the lowest wavenumber resolved becomes *K/T*.

A greater number of segments can be obtained by allowing for an overlap between segments. The effects are dual. Firstly, a larger number of estimates for each wavenumber band is generated, improving the final spectrum estimate. Secondly, by overlapping segments, data points are used in more than one segment and their position within the segments changes. This causes data points to be given equal weight when evaluating the spectrum because the position of a point, whether central or at the margin of a transect/segment, influences the spectral estimate. This is particularly true when data are windowed (Emery and Thomson, 2001) (see windowing section below).

In this research study, only the smaller length-scale range (10-100 m) is evenly spaced for *in situ* data. As this range is already quite narrow, *in situ* transects are kept intact to maintain as large as possible a spectral range. Block averaging can still be applied to *in situ* data (Chapter 3 and Chapter 4), however, because transects are available for every upward and downward profile of the towed instrument (Figure 2.2). Hence, the spectrum can be estimated by averaging over the available transects.

Overlapping of segments can be applied to satellite data and model predictions. The only condition is that long enough transects are selected such that segments of 130 km long which

are equal to the large length-scale range (8-130 km) *in situ* transects (see Section 2.5.), can be extracted.

Windowing the data

The problem with obtaining data along a transect is that the data extend either side of the section sampled and so it is as if one is looking through a window that is rectangular. The consequence is that abrupt changes occur at the edges of the window of data and can cause the spectral power to be biased. More specifically, the Fourier transform of a finite transect consists of a main lobe and many side lobes of smaller amplitude. The size of these side lobes can be a source of estimation errors and can cause power to leak into neighbouring wavenumber bands.

One strategy to address this is to reduce the sudden change at the edges by having a more tapered shape, gradually changing the observed values from zero at the edge to their full true value at the centre of the 'window'. A benefit of this approach is that the resultant Fourier transform has smaller side lobes. This technique of 'windowing' the data is done by convolution of a specific window with the data transect. It effectively multiplies each data point in the series by the value of the window at that particular position. It therefore significantly modifies each data point according to its position in the data series. One such windows is the Hann window which has been used in many phytoplankton spectral studies (Weber *et al.*, 1986, Washburn *et al.*, 1998). It is obtained by multiplying a rectangular window $w_R(n)$ by one period of a cosine to obtain a bell-shaped window such that:

$$w_H(n) = w_R(n)\cos^2\left(\frac{\Omega_M}{2}\right),$$

and $\Omega_M = {}^{2\pi}/_{M}$ where M is the window length in samples.

Pre-whitening

Spectral leakage can also be reduced by 'whitening' the data prior to the spectral estimation. Whitening involves operating on the data so that the spectral slope becomes flatter or 'whiter'. If, like in the case of phytoplankton, the spectrum is originally 'red' i.e. dominated by low frequency components, such a step reduces leakage of these components and therefore allows a better estimation of weaker spectral components of higher wavenumber (Emery and Thomson, 2001). As will be seen below, slopes less than -2 are particularly susceptible to steeper

estimation due to leakage. Whitening is particularly recommended for signals with slopes steeper than -2 (Coles *et al.*, 2011).

Because the observed slope for phytoplankton spectra is typically between -3 and -0.5 first order differencing of the data is often applied which effectively adds 2 to the slope. First order differencing is a discrete form of differentiation. The Fourier transform of a differentiated function is $i\omega S(\omega)$where ω is the wavenumber and $S(\omega)$ is the Fourier transform of the original function. Hence, the spectrum of a first order differenced transect is $\omega^2|S(\omega)|^2$. The squared wavenumber component of the spectrum is seen to add 2 to the spectral slope. If the spectrum for the original data is required it can be recovered by dividing the first order differenced spectral estimates by their wavenumber squared.

2.4.3. Calculating uncertainties in the slope

The slope of the spectrum is calculated by linear regression of the log of the power estimate against the log of the wavenumber. Using a bootstrap technique the uncertainty in the spectral slope estimate can also be estimated. Suppose there are 5 transects. By pooling spectral estimates from all transects there are 5 estimates for each wavenumber band. If we pick estimates from bands at random we can estimate the spectrum slope using this sub-set of the spectral data as above. For this study, this is done by using all the estimates obtained from all segments or transects. A multitude of subsets, here 10,000, are then generated by randomly selecting 90% of the power spectral estimates, allowing repetition. For each subset, the average power is calculated at each wavenumber and the slope then calculated. The mean and standard deviation of the distribution of the 10,000 slopes from the bootstrapping gives the mean spectral slope and its uncertainty respectively. A sensitivity test showed that using a larger number of subsets did not affect the estimates.

2.4.4. Results

The artificial data used to illustrate the ability of the different methods to recover the spectral slope mimics the shorter length-scale range of *in situ* data (see Figure 2.2), later discussed in Chapter 3 and Chapter 4. Here the data consist of 10 repeat transects of 20 measurements each, with data 5 metres apart, obtained over 100 m horizontal sections every ~4 km from a transect 130 km long. The estimation of the spectrum therefore spans the range 10 m - 100 m. Results

for a satellite (Chapter 6) or model (Chapter 5) setting are qualitatively the same except for the range of length-scales covered.

Spectral estimates are obtained using FFT. Three cases are investigated. Spectral estimates are calculated using the raw, windowed (Hann) and pre-whitened data. By raw data is meant data which has not been processed. Block averaging is applied to all three cases by averaging the estimates obtained from the multiple transects. Scenarios with 10, 20 and 40 transects are investigated. The slope value is obtained by linear regression of the logged estimates and logged wavenumbers. An example of artificial data, spectral estimation and linear regression is displayed in Figure 2.4.

For each signal of pre-defined slope, 50 artificial data sets are generated to evaluate the uncertainty of the estimated slopes. A distribution of slope estimates is obtained from the 50 data sets from which the mean and standard deviation are used and plotted in Figure 2.5. An average uncertainty for all signals with slopes -3.5<α<-0.5 is given in Table 2.1.

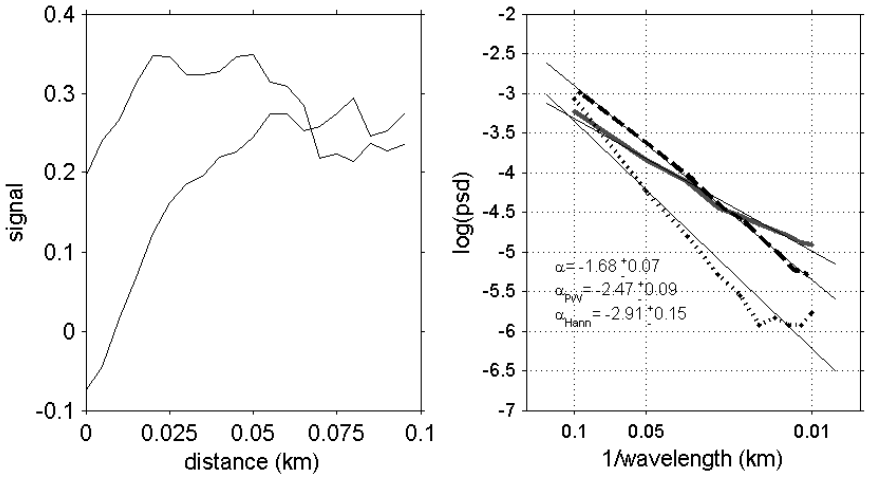

Figure 2.4*: Example of two simulated transects of power law signals S(x)=k$^{\alpha}$ with α=-2.5 and random phase (a.) used to test the Fast Fourier Transform (FFT) spectral analysis method. Estimated spectra (b.) are obtained using 10, 20 or 40 transects of 100 m with data points 5 m apart. FFT on its own (solid line), using a Hann window (dotted line) and with prewhitening (dashed line) are evaluated. The mean spectra are are obtained by averaging the spectral estimates at each wavelength. The slope is obtained by linear regression of the log mean spectral estimates over log of wavelength.*

Both FFT methods using raw data (Figure 2.5a) and windowed data (Figure 2.5b) provide inconsistent estimates of the true signal slope. FFT with raw data cannot be trusted for estimating signals with slope steeper than -2. Specifically, the method would not be capable of distinguishing between signals of different power law if both are steeper than -2. This would be

possible for signals with flatter slopes, note however that the method consistently evaluates the slope to be flatter by approximately 0.25 (Figure 2.5a).

FFT using windowed data (Figure 2.5b) differs from FFT using raw data in that it can distinguish between signals of different power-law regardless of their strength. The estimation of the slopes however is not correct for the steeper slopes evaluated. This error increases for signals with increasingly steeper slopes.

In contrast, the FFT method using whitened data (Figure 2.5c) provides a robust estimate of the slope across the full range of exponents. When using datasets made of 10 transects, the difference with the original slope remains below 0.07 except for the case where a signal with slope -0.5 is estimated for which a difference of 0.21 is observed. Cases using 20 and 40 transects were also examined. The average error decreases to 0.05 and 0.03 respectively. On the other hand estimations for slope -0.5 are not improved.

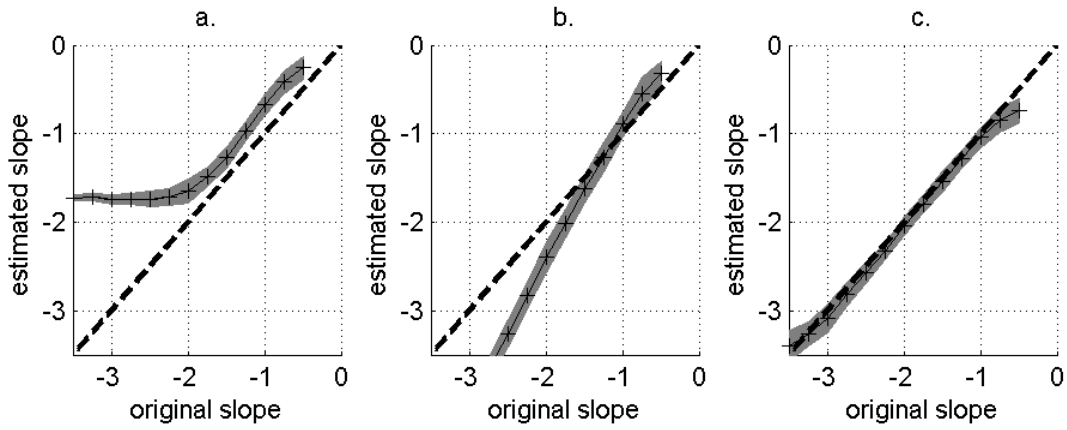

Figure 2.5*: Estimates of spectral slope for evenly spaced data using FFT on its own (a.), with Hann window (b.) and with pre-whitening (c.). The uncertainty in slope estimates (shaded grey) corresponds to one standard deviation either side of the mean estimate.*

Uncertainties in slope estimation were evaluated in two ways. Firstly, the standard deviation of the slope was estimated for each artificial dataset using bootstrapping. The standard deviation associated with the slope estimate decreased from 0.16 to 0.11 to 0.07 when using 10, 20 and 40 transects (Table 2.1). Secondly, the experiment is repeated 50 times and a distribution of the 50 bootstrapped mean slopes is obtained. From this distribution, the mean slope and standard deviation are taken to evaluate the consistency in the method. The standard deviation for the cases of 10, 20 and 40 transects varied from 0.13, to 0.10 to 0.07 respectively.

2.5. Estimating spectra of phytoplankton for unevenly spaced data

With unevenly spaced data, FFT cannot be used. Using interpolation to render irregularly spaced data evenly spaced is not recommended as, beside the subjectivity that lies in the choice of interpolation method (e.g. linear, cubic, spline), the interpolation distorts the data and introduces noise particularly at high wavenumber (Mudelsee, 2010). However, spectral estimation methods exists that can deal directly with unevenly spaced data.

2.5.1. Lomb Scargle Periodogram

One method suitable for calculating spectra for uneven data is called the Lomb Scargle Periodogram (LSP) (Lomb, 1976, Scargle, 1982, Press *et al.*, 2007). The technique consists of estimating a spectrum using a least square fit of sine and cosine waves.

The LSP is defined by:

$$P_N(\omega) \equiv \frac{\left[\sum_j (s_j - \bar{s}) \cos \omega (x_j - \tau)\right]^2}{\sum_j \cos^2 \omega (x_j - \tau)} + \frac{\left[\sum_j (s_j - \bar{s}) \sin \omega (x_j - \tau)\right]^2}{\sum_j \sin^2 \omega (x_j - \tau)};$$

where s_j are the measurements obtained at position x_j in the data series, and $\bar{s}$ is the mean value.

$$\bar{s} \equiv \frac{1}{N} \sum_1^N s_j \ ,$$

and

$$\omega = 2\pi f,$$

τ is a time shift that makes $P_N(\omega)$ independent of shifting the x_j's by any constant. It is defined by the relation:

$$\tan(2\omega\tau) = \sum_j \sin 2\omega t_j \Big/ \sum_j \cos 2\omega t_j.$$

The ability to fit chosen wavelengths by least squares means that the method can be applied to unevenly spaced data to estimate the periodogram P_N for pre-defined wavenumbers ω. The pre-defined wavenumbers were chosen so that spectral variability was evaluated at length-scales

evenly spread in log space. This is useful when evaluating the slope of the spectrum. If the spectrum follows a power law, such a uniform distribution of estimates across log (length-scale) allows an unbiased estimate of slope when applying a linear regression to power versus wavenumber. Otherwise, estimates evenly spaced across length-scales in real space would lead to a disproportionally large number of estimates at the shorter end of the scale range.

Table 2.1: *Uncertainties associated with the use of different spectral method (FFT and LSP) for evenly and non-evenly spaced data. Uncertainties correspond to the mean value from uncertainties obtained for the slope estimation of signal with slopes -3.5<α<-0.5. For each artificial dataset, the standard deviation of the slope is calculated using bootstrapping. The uncertainty of the mean slope is obtained by calculating the slope for 50 artificial datasets and taking the standard deviation of the distribution. Methods are tested with raw, windowed and pre-whitened data. The effect of the number of transects on the uncertainty of the slopes is also tested. The uncertainty of the Pre-whitening is not applicable (N/A) to unevenly spaced data.*

		Raw data		**Windowed data (Hann)**		**Pre-whitened data**	
	Nb tr.	Mean Std slope	Uncertainty mean slope	Mean Std slope	Uncertainty mean slope	Mean Std slope	Uncertainty mean slope
FFT (even data)	10	0.14	0.10	0.14	0.16	0.16	0.13
	20	0.09	0.07	0.09	0.11	0.11	0.10
	40	0.06	0.05	0.06	0.07	0.07	0.07
LSP (uneven data)	4	0.25	0.24	0.23	0.25	N/A	N/A
	8	0.14	0.23	0.13	0.24	N/A	N/A
	20	0.08	0.16	0.08	0.16	N/A	N/A

2.5.2. Results

The data potentially having uneven spacing are from *in situ* and satellite, in the event of uneven undulations of the sampling instrument or cloud coverage within the studied area, respectively.

To illustrate the ability of the method, an artificial phytoplankton data set is once again generated. Again, the case study simulates an *in situ* scenario with the data collected by an undulating vehicle (see Figure2.2). The data are approximately 4 km apart along a 130 km transect. The data points are unequally spaced, mimicking the uneven undulations of the vehicle. To simulate unevenly spaced data (analogous to that investigated in Chapter 3), a 5 m resolution data set is created with data points having a mean separation of 4 km but with a

uniformly distributed random perturbation added, varying between -0.5 and 0.5 km and. Scenarios with 4, 8 and 20 transects are carried out.

Two cases using LSP are studied. The first estimates the spectrum using the raw data series and the second one uses data that has been windowed (Hann). Data cannot be whitened if they are irregularly spaced. Spectral variability is estimated for wavenumbers 1/130 km^{-1}, 1/100 km^{-1}, 1/80 km^{-1}, 1/65 km^{-1}, 1/50 km^{-1}, 1/30 km^{-1}, 1/20 km^{-1}, 1/15 km^{-1}, 1/10 km^{-1}, 1/8 km^{-1} so that estimates are evenly spaced in log space. The power spectral slope estimates are obtained using the bootstrapping approach detailed previously. An example of artificial data, spectral estimation and linear regression is displayed in Figure 2.6.

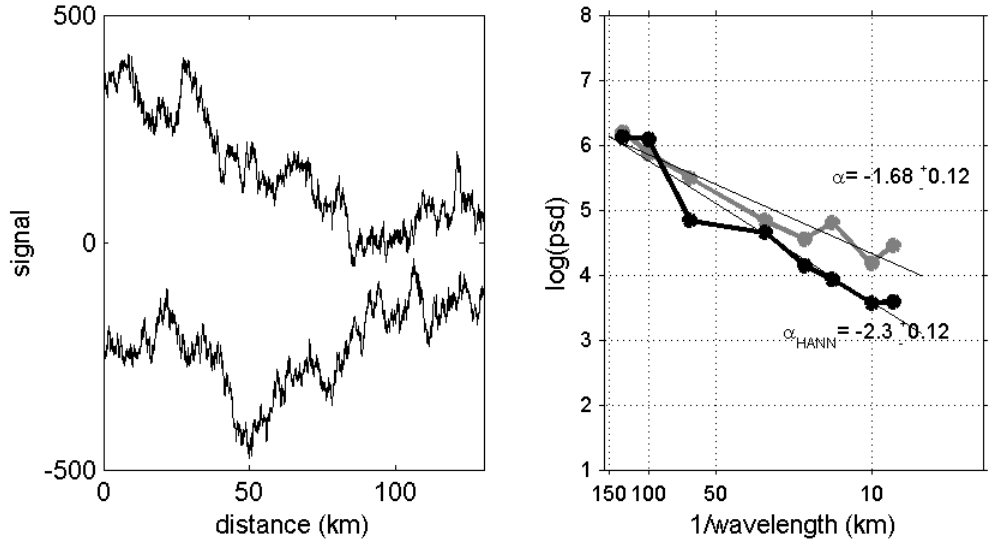

Figure 2.6*: Example of two simulated transect of power law signal $S(x)=k^{\alpha}$ with $\alpha=-1.8$ and random phase (a.) used to test the Lomb Scargle Periodogram (LSP) spectral analysis method. Estimated spectra (b.) are obtained using 8 transects with data points approximately 4 km apart. LSP on its own (grey) and with a Hann window (black) are evaluated. The mean spectra are obtained by averaging the spectral estimates at each wavelength. The slope is obtained by linear regression of the log mean spectral estimates over log of wavelength.*

Neither LSP methods, using raw or windowed data, are consistent in how accurately they estimate the slope. The first technique (Figure 2.7a) performs well for signals with slope flatter than -2 with a reasonably consistent flatter slope estimated. The closest evaluation occurs for slopes from -2 to -1.5, with an under evaluation of mean 0.11. For signals with flatter slope, this difference increases gradually to 0.35 for a signal with near white spectrum of slope -0.5. For signals with steeper slopes than -2, the difference between original and estimated slope becomes larger than 0.25 past -2.1. Beyond signal slopes of -2.5, the estimated slope remains around the value -2.

Windowing the data (Figure 2.7b) does not improve the estimation. The curve of estimated slopes also starts flattening below value -2. Whilst the technique with no windowing consistently estimates flatter slopes, that using windowing estimates steeper slopes for original slope values between $-2.5<\alpha\leq-1.25$ and flatter ones for $-1.25<\alpha\leq0$. For signals with slope past -2, the method's estimation stagnates around the value -2.5.

Focusing only on signals with slopes flatter than -2, a comparison of the absolute difference between estimated and original slope shows that with windowing an average difference of 0.24 is observed. This is higher than the 0.22 observed when data is not windowed.

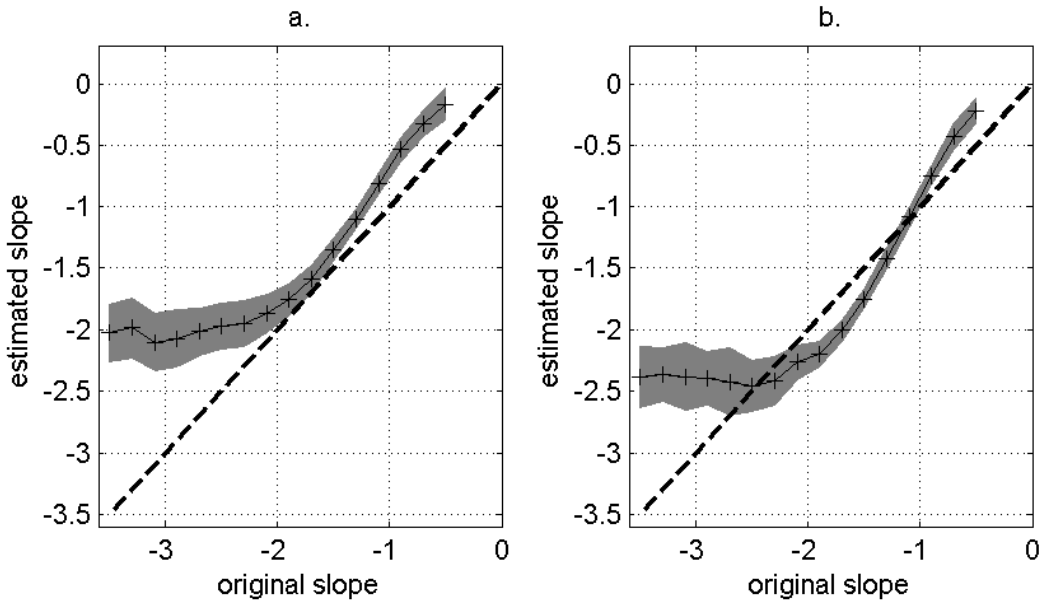

Figure 2.7: *Estimation of power spectral slope for unevenly spaced data. Estimates are calculated using Lomb Scargle Periodogram on its own (a.) and having applied a Hann window (b.). For each signal of slope α, 50 artificial data sets are generated to evaluate the uncertainty in the mean slope estimate. For each artificial data set, 20 transects are used to estimate the spectral slope. The uncertainty is represented in shading using one standard deviation either side of the mean estimate obtained from the distribution of the 50 mean slope estimates.*

The standard deviation associated with the slope estimation for each run was also calculated. It was found to be similar across the range of slope values. Using 4 transects, the averaged standard deviation was 0.25, decreasing to 0.14 and 0.08 when using 8 and 20 transects respectively. Uncertainties were similar using windowed data.

The fluctuation of the slopes for the 50 artificial data sets varied with the steepness of the signal's slope. Larger uncertainties were found for steeper signals (see shaded interval in Figure 2.7). The uncertainty is also larger when a smaller number of transects are used. For slopes flatter than -2, one standard deviation is 0.23 to 0.21 and 0.11 for the cases with 4, 8 and 20 transects respectively.

2.6. Discussion

A number of points with regards to future investigations, including the ones carried out in later chapters, can be made on the basis of the above analysis.

When data is unevenly spaced, spectral slope evaluation using LSP performs reasonably well for signals with power law behaviour weaker than -2. Overall, windowing does not improve the estimation of the slope, therefore there is no basis for the extra processing of the data. However, for signals with slopes steeper than -2 neither method is sensitive or accurate enough to distinguish between them robustly. The method with no windowing is therefore preferred for the analysis.

Similar conclusions can be made for FFT analysis of evenly spaced raw and windowed data which are not suited for the analysis of a signal with such a wide range of possible slope values. The first method cannot distinguish between signals with slopes steeper than -2, whilst the second consistently over estimates the slope. However by whitening the data prior to the spectral estimation, reliable values across the range of slopes investigated are obtained. The overall performance of the FFT method with whitening makes it a method of choice for evaluating the spectrum of phytoplankton for evenly spaced data.

More specifically it is now possible to discuss the relative applicability of the above methods to the investigations in this thesis.

Comparing the power law of two signals

In the situation that the spectra of two variables are studied (e.g. nitrate and phytoplankton as in Chapter 3), it is important that their relative slope difference can be measured accurately.

For unevenly spaced data, if both signals have slopes flatter than -2, their difference can reliably be estimated with the LSP method, with a greater number of transects reducing the uncertainty. If just one variable has a slope steeper than -2, the difference in slopes will be found but may be underestimated due to the saturation of the method beyond slopes of -2. For the case where both variables have slopes steeper than -2, the method will not be able to measure the difference accurately.

For evenly spaced data, the technique using FFT with whitened data will accurately capture the difference independent of the signal's slope steepness.

Comparing slopes across different ranges of length-scales

An additional problem that underestimation of steep slopes may cause is when a spectral slope for one variable is estimated for two separate length-scale ranges (e.g. 10 m – 100 m and 8 km -130 km as in Chapter 3 and 4) using different methods. What may appear as a shift in power law behaviour between ranges of length-scales may simply be a consequence of the change in method. For example, if the true slope is -3 for *in situ* data (Chapter 3 and 4) then FFT with pre-whitening will get it right at small scales but estimate it to be about -2 for large scales.

Comparing spectra of one variable over time and geographically

Another problem occurs when the spectrum of one variable e.g. phytoplankton, is evaluated for different regions (Chapter 4) or time of year (Chapter 6). The risk with unevenly spaced data is that the differences in the estimated spectra with space or time may not reflect the true variability because signals with steep slopes are poorly evaluated. The suitability of the method will depend on the question being asked. For instance, the method is capable of revealing the existence of variability in slope but may not be able to quantify precisely the amplitude of that difference.

Quantity of data

Significant uncertainties can be associated with the slope estimates, as illustrated by the shaded confidence interval in Figures 2.4 and 2.5. These uncertainties increase when smaller number of transects are available. In the case of satellite data for which larger areas than *in situ* can be studied, this can be addressed by setting a threshold for the minimum of transects required to obtain a good approximation of the slope. In the case of *in situ* data, often the lack or limited amount of data available for analysis is an inevitable feature of making measurements at sea.

2.7. Summary

I have investigated the behaviour of the different methods for calculating spectra under conditions similar to those to be studied in the following chapters. It has been demonstrated that it is possible to measure phytoplankton spectra for both cases of evenly and unevenly spaced data, if the limitations of the methods are understood.

Chapter 3: Comparing phytoplankton and nitrate spectra

3.1. Introduction

The complex patterns observed in marine phytoplankton distributions arise from the interplay of biological and physical processes, but the nature of the balance remains uncertain centuries after the first observations. Previous observations have shown a consistent trend of decreasing variability with decreasing length-scale (see Chapter 1). Influenced by similar scaling found for the properties of the water the phytoplankton inhabit, 'universal' theories have been proposed that simultaneously explain the variability seen from meters to hundreds of kilometres.

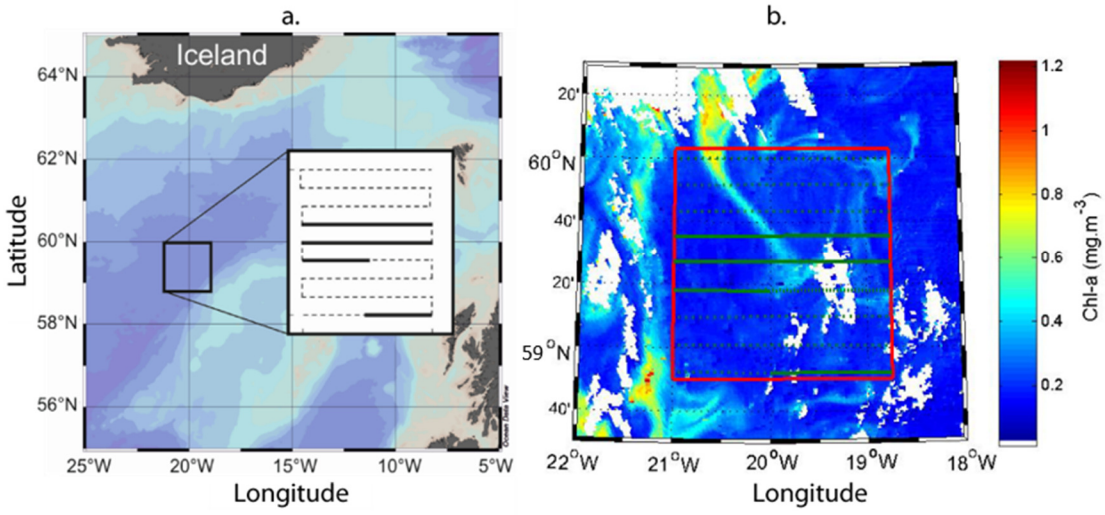

Figure 3.1: *Area covered by the Seasoar survey during the D321 cruise in 2007 (a.). Solid lines in the inset image correspond to transect legs or parts of transect legs for which simultaneous nitrate and chlorophyll-a measurements are available and used for this study. Corresponding transects are also shown in the remotely-sensed Chl-a estimates for the area (b.).*

For the purpose of reminding the reader, the following summary of the theories of phytoplankton patchiness described in Chapter 1 is given.

The first theory (Denman and Platt, 1976, Denman *et al.*, 1977) is based on the argument that the time-scale associated with turbulent motion may decrease with length-scale but the biological response time is invariant with scale. At small scales, where physical processes act fastest, the spectral slope of phytoplankton should be identical to that of physical variables such

as temperature. In contrast, at longer length-scales, the biological processes are quickest, and so patterns of spatial variability in phytoplankton can diverge from those of physical tracers. More specifically it has been predicted that there is a knee in the spectrum, not mirrored in physical variables, associated with a flattening of the phytoplankton slope at larger scales. The knee is argued to occur where biological and physical time-scales match. The second theory (Hernández-García *et al.*, 2002) takes the notion of a single biological time-scale further, arguing that it will be common to all interacting components of the planktonic ecosystem. In this scenario, the ecosystem components, whether nutrients, phytoplankton or zooplankton, are predicted to have identical spectral slopes. This theory additionally assumes that a single time-scale can describe the effect of the turbulent stirring. The third theory (Bracco *et al.*, 2009) argues that the biological time-scale associated with each constituent of the ecosystem is determined by how quickly it responds to perturbation in its environment. Consequently, zooplankton are argued to react more slowly than phytoplankton and accordingly predicted to have different spectral slopes to nutrients and phytoplankton which respond on shorter time-scales. The fourth theory (Lévy and Klein, 2004) challenges the idea of a 'cascade' of variability from large scales to small scales, a central tenet in the theories for physical turbulence, which have been used as a basis to explain power law behaviour in spectra. Although variability is still transferred to smaller scales by stirring, the upwelling of nutrients at a range of intermediate scales, particularly within the mesoscale and submesoscale, injects extra variability. The response to such localized enhancement of phytoplankton growth is ephemeral and often significantly perturbs the ecosystem relative to background conditions. A consequence is that spectral slopes for different components of the ecosystem no longer need match (Lévy and Klein, 2004, Lévy *et al.*, 2005).

Although numerous observations already exist for phytoplankton patchiness, they have proved very variable and unable to distinguish between theories. The theories can only be properly tested by simultaneously examining another component of the ecosystem that strongly interacts with and moves like phytoplankton. Comparisons with zooplankton have already been made (Mackas and Boyd, 1979, Tsuda *et al.*, 1993, Martin and Srokosz, 2002), but the motile nature of zooplankton, not taken into account by the theories, makes a phytoplankton-zooplankton comparison unsuitable for testing the above theories. Nutrients, however, are equally subject to the ambient flow, and therefore a nutrient to phytoplankton comparison, as carried out here, constitutes a strong test of the various theories.

In this chapter, the extant theories are tested using a twin-tracer approach, specifically chlorophyll-*a* (Chl-a) and nitrate data from the North Atlantic. Their spatial relationship is examined by comparing the slopes of their power spectra over the ranges (10-100 m) and (8-115 km).

3.2. Methods

3.2.1. Data

The data are from *RRS Discovery* cruise D321 which took place between the 24th July and 23rd August 2007 in the vicinity of Ocean Weather Station India (OWSI) (60°N 20°W). A 130 km by 130 km box was mapped, with parallel transects arranged in a radiator style running East to West (Figure 3.1), using SeaSoar, an undulating towed vehicle. Transects were ~14 km apart and each one took ~8 hours to survey (Pidcock *et al.*, 2013). Weather conditions together with SeaSoar mechanical problems meant that only two entire transects and two half transects were successfully sampled. SeaSoar was equipped with an SUV-6 fast response (1Hz) Ultra Violet nitrate sensor (Pidcock *et al.*, 2010). Alongside this were standard instruments such as a fluorimeter for measuring chlorophyll, and mini CTD for measuring temperature and salinity. This configuration allowed nitrate measurements to be made concomitantly with Chl-a and hydrographic measurements at a sampling rate of 1 Hz. The undulations of SeaSoar traverse the top 400 m of the water column. The 8 knot speed of the ship during transects means that profiles are approximately 4 km apart.

The data used for this study were extracted from the surface mixed layer where phytoplankton were most abundant. The mixed layer depth varied from 30-50 m. Data were used from the depth range 15 to 25 m to avoid quenching effects on Chl-a observations. A few profiles showed a significant increase in density with depth within this depth range. For these, only data shallower than the point of increase were used (see also below for further discussion). Profiles with a density difference larger than 0.1 were discarded so to minimise the presence of vertical structure in the data. Selecting only the profiles with density difference less than 0.05 did not change the results.

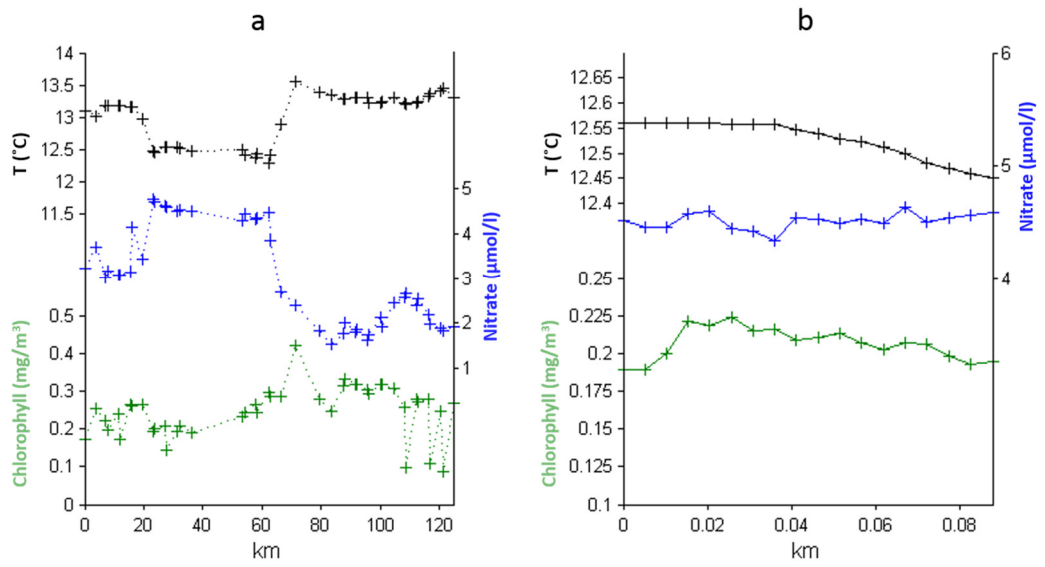

Figure 3.2: *Measurements within depth range 15-25 m for temperature T (black), nitrate NO_3^- (blue) and chlorophyll-a* Chl-a *(green) obtained along a transect. a): an example of a series of measurements, collected by the sampling vehicle from one passage through the depth range 15-25 m, used for spectrum estimation for the range 10-100 m. b): points in the graph correspond to mean values from each ascent/descent of the vehicle through the depth range used for spectrum calculation for the range 8-115 km.*

Two ranges of length-scales are investigated in this study. Data at the small scale (10-100 m) comprise clusters of 1Hz observations as SeaSoar traverses the 15-25 m depth range on each ascent and descent. Because observations are separated by ~4 m, no structure smaller than 8 m can be resolved. The time taken for SeaSoar to traverse the depth range means that these clusters of data cannot resolve structures larger than 100 m. Data at the larger spatial scale (8-115 km) arise from taking the mean value of each of the above clusters. One full undulation of SeaSoar took place approximately every 4 km, and so the larger scale dataset cannot resolve structures smaller than ~8 km. The upper limit of resolution (~115 km) is set by the length of the transects. The nature of the sampling meant that no spatial information was collected for the scales in the range 100 m to 8 km.

3.2.2. Spectral methods

Spatial spectra were estimated for nitrate, Chl-a and temperature. The contrasting sampling characteristics at small and large scales require different approaches to be taken for analysis.

At small scales (10-100 m), the traditional Fast Fourier Transform (FFT) was used. The regularity of intervals between data points in each cluster, prerequisite for the application of FFT, was

provided by the constant speed of the ship. Following results from the simulations done in Chapter 2 (Section 2.4.4.), data were additionally "whitened" using a first order difference prior to spectral estimation (Jenkins and Watts, 1968). The power spectrum of each variable was obtained by grouping the power estimates derived from all cluster groups into wavelength bins of equal width, followed by averaging (Bendat and Piersol, 1971).

At larger scales, spectral estimates were obtained using the Lomb-Scargle periodogram method (LSP) (Press *et al.*, 2007). This technique was used because of the irregular spacing of the data points resulting from the occasionally uneven nature of the vehicle's undulations. An advantage of this method is that the wavelengths for which the power is estimated can be set. Consequently power estimates for all transects could be calculated for a common set of predefined wavelengths. Such a method also avoids the need to group estimates prior to averaging. A set of wavelengths was chosen so that their logarithms were evenly spaced in log space. After visually checking for power-law behaviour for each transect, the spectrum for each variable was obtained by averaging the power of all four transects for each wavelength investigated.

The slope of the spectra was obtained by applying a linear regression to the log averaged power estimates against the log of wavelength. To give a more robust result a single regression was done for each scale range, pooling data from all transects for the larger scales (8-115 km) and from all clusters for the smaller scales (10-100 m).

Distributions for each slope were obtained by performing regressions on 10,000 data subsets generated from the full spectrum using a bootstrap routine (see Chapter 2 Section 2.4.3.). Results were unaffected when increasing the number of bootstrap generated data subsets. The uncertainty in the slope estimates (see Table 3.1) was quantified by the standard deviation of the above distributions. Analysis of the difference between spectral slopes followed a similar procedure, in this case consisting of using bootstrapping to generate a distribution for the difference between two variables' spectral slopes. All spectra were checked so to satisfy Parseval's energy conservation theorem. The statistical significance of the relative difference between two variables' spectral slope being zero was obtained by retrieving the widest 100 (1-α) percentiles (for the levels α=0.1, 0.05 and 0.01) of the 10 000 bootstrap runs for which the value zero is excluded.

3.3. Results

Examples of nitrate, Chl-a and temperature variability at small and large scales are displayed in Figure 3.2a and 3.2b, respectively. The spectra and respective slopes for both spatial scales are displayed in Figure 3.3. Both nitrate and Chl-a display a similar spectral shape often described as a 'knee' when plotted on a logarithmic scale, which is characteristic of a shift in power law behaviour. This shift is less pronounced for the nitrate spectrum (-1.26 for scales 8-115 km; -1.75 for scales 10-100 m) than for phytoplankton (-0. 50 for 8-115 km; -2.64 for 10-100 m).

For both length-scale ranges studied, nitrate and Chl-a spectral slopes are different. Distributions for the differences in slopes were obtained using a bootstrap routine (Figure 3.5). For both 8-115 km and 10-100 m ranges, the difference in slopes was significant, at the 95 % and 99 % confidence interval with mean difference of -0.75 and 0.90, respectively (Table 3.1). Further evidence of this difference is available in the spectra for each transects (Figure 3.4) where a difference is found in all four transects. Distributions of slope and slope differences are shown in Figure 3.5.

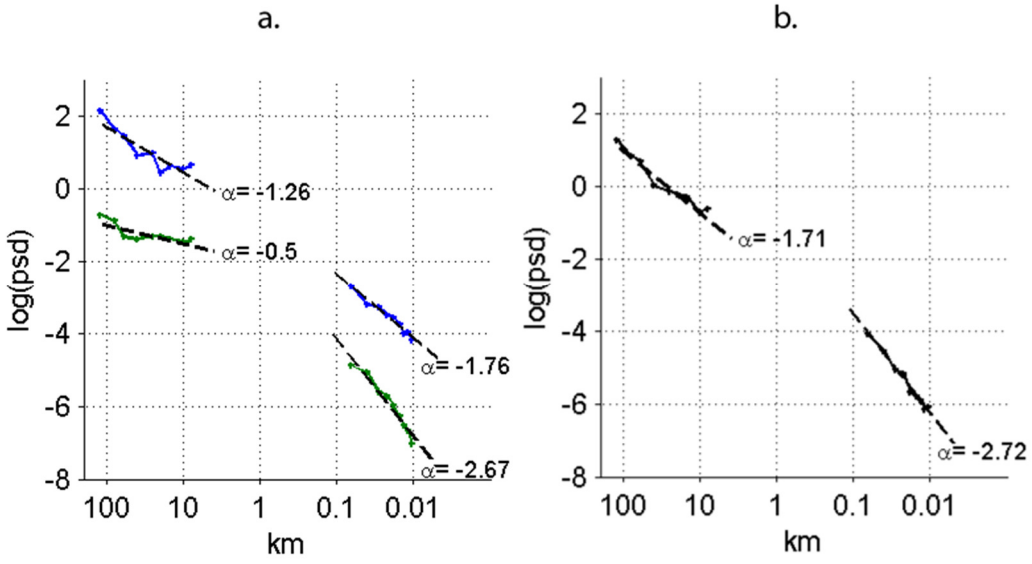

Figure 3.3: *Mean power spectral density estimates (psd) based on all 4 SeaSoar transect sections: a) for nitrate (blue), and chlorophyll-a (green); b) for temperature (black). Lines of best fit are obtained using parameters estimated using bootstrapping. Note the absence of estimates within the 0.1 to 8 km range due to the sampling strategy.*

The differences in the slopes of nitrate and Chl-a compared to that of temperature were also tested. For the range 8-115 km, a mean difference of 0.45 and 1.21 is estimated. Their distributions showed the difference to be significant at the 99% confidence interval.

Both slopes of nitrate and phytoplankton are different to that of temperature (-1.71) for the range 8-115 km. The data also reject the hypothesis of equal slopes for nitrate (-1.75) and temperature (-2.73) for the range 10-100 m. However, at these smaller scales, for Chl-a (-2.64) and temperature the difference in slopes has a distribution with mean difference of 0.09 and standard deviation of 0.22 and so a hypothesis of equal slope for temperature and Chl-a cannot be rejected.

Because of concerns about potential quenching effects on the fluorescence signal, the analysis was repeated using only night time data. The results are unchanged at scales of 10-100 m. The only significant impact is greater uncertainty in spectral slopes in the range 8-115 km. This is inevitable given the small dataset but does not affect our conclusions.

Figure 3.4: *Power spectral density estimates (psd) of all 4 SeaSoar transects sections (a, b, c and d, respectively ordered from South to North) for nitrate (blue), chlorophyll-a (green) and temperature (black). Note the absence of estimates within the 0.1 to 8 km range due to the sampling strategy.*

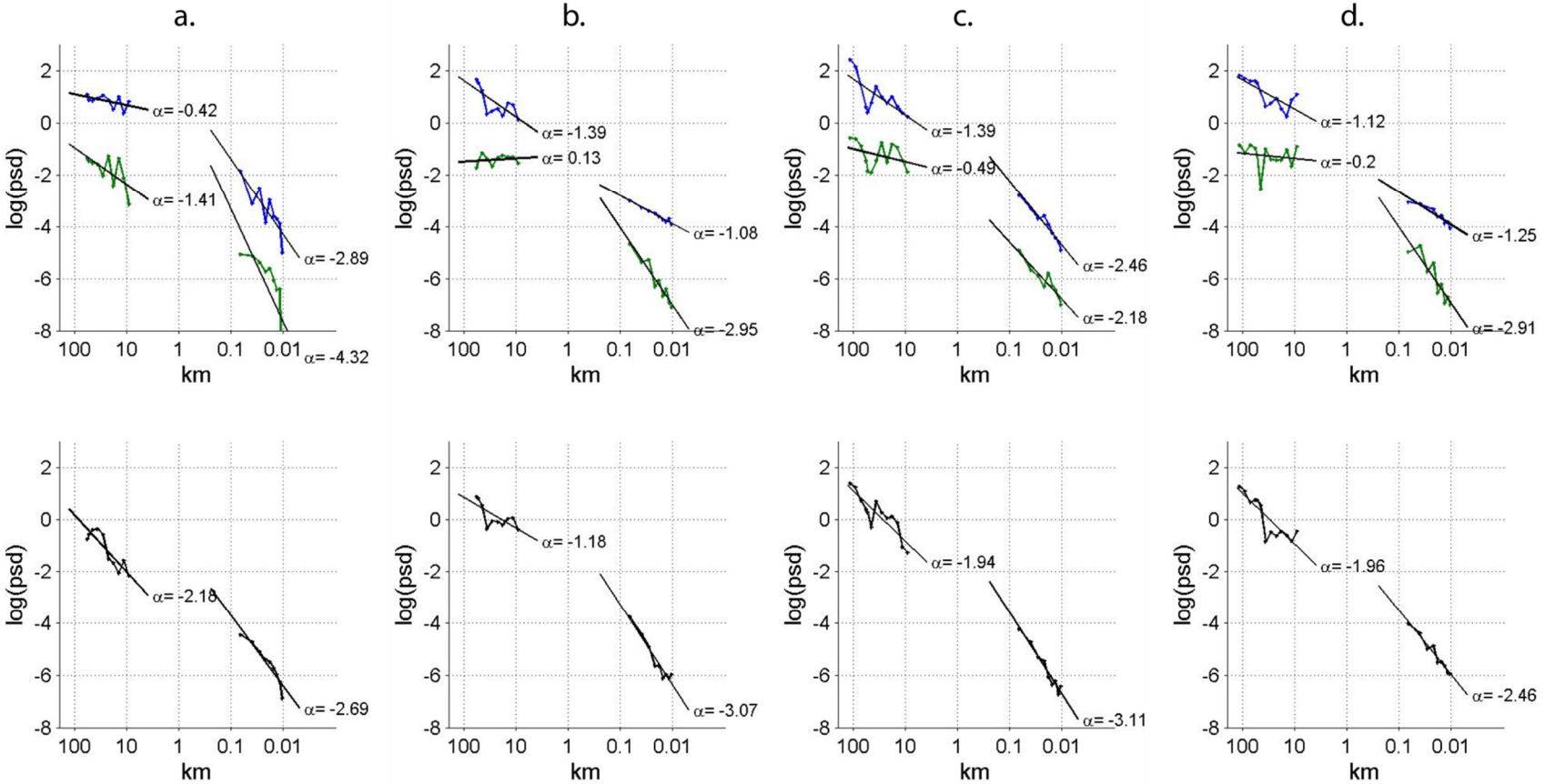

Table 3.1: *a) Spectral slope for nitrate, temperature and Chl-a, with their respective r value and standard deviation. b) Statistical properties for the distribution of the slope difference between two variables: mean and standard deviations. Distributions were obtained from 10,000 datasets generated using a bootstrap routine with 90 % randomly selected spectral estimates with replacement.*

		Range 8-115 km			**Range 10-100 m**		
	Variable	Slope (α)	Standard dev.	*r*	Slope	Standard dev.	*r*
a	Nitrate	-1.26	0.19	-0.85	-1.75	0.19	-0.96
	Chl-a	-0.50	0.24	-0.54	-2.64	0.17	-0.96
	Temperature	-1.71	0.25	-0.89	-2.73	0.15	-0.98
		Slope difference			Slope difference		
b	Nitrate-Chl-a	-0.75	0.25		0.90	0.25	
	Nitrate-Temperature	0.45	0.30		0.99	0.22	
	Chl-a-Temperature	1.21	0.24		0.09	0.22	

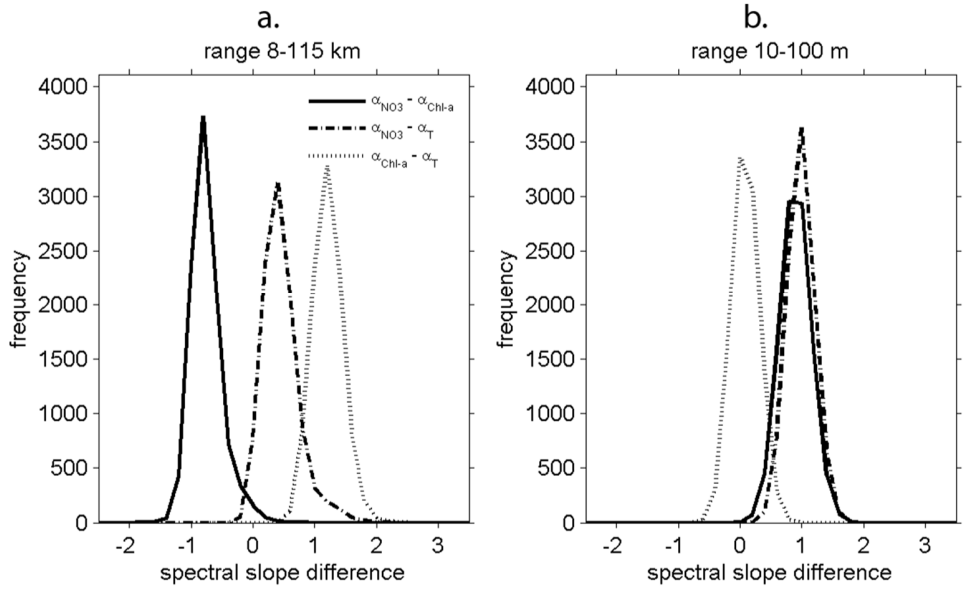

Figure 3.5: *Distribution of the difference in spectral slope between nitrate (NO_3) and chlorophyll-a (solid line), nitrate and temperature (dashed), and chlorophyll-a and temperature (dotted) for the range 8-115 km (a.) and the range 10-100 m (b.).*

3.4. Discussion

The dataset presented here is a small one, from just one location, at just one time. Nevertheless the direct comparison afforded by simultaneous measurement of nitrate and Chl-a over multiple scales allows a direct test of all four theories.

Restricting attention to Chl-a data for now, the observations initially seem consistent with the first theory, in that phytoplankton (-2.64) display a similar spectral slope to temperature (-2.73) at small scales with a relative flattening at larger scales (-0.50). For the large scale range the LSP method was used to estimate the spectrum. Two different methods were used to obtain the spectrum of phytoplankton, FFT with pre-whitening for the range 10-100 m and LSP for the range 8-115 km. In Chapter 2 (Section 2.5.2.), simulations using power-law signals with slope that could be set showed that spectral estimations using LSP had a tendency to estimate flatter slope than the original slope of the signal. Based on these simulations, it causes the knee to be more pronounced. However, the difference in slope between the two ranges of scales of 1.94 is greater than the potential error introduced by the method. The presence of the knee is therefore genuine. It is also present in the spectrum of all 4 transects. A phytoplankton spectrum with such a knee-shape has been observed previously (Denman and Platt, 1976, Denman *et al.*, 1977, Lovejoy *et al.*, 2001). This is, however, where the power of having a two tracer approach is demonstrated. If the theory does explain the relative shapes of the temperature and phytoplankton spectra then nitrate should also have the same spectral slope as temperature at the smaller scales. This is not the case, as the spectral slope for nitrate (-1.75) differs from that for both phytoplankton and temperature. The potential effect of eddies in modulating the slope of phytoplankton is raised up here. Although insufficient data is available, different slopes for the range 8-115 km are obtained between the four transects. The most southern transect (Figure 3.1) does not cross the eddies present in the survey area unlike the other three following transects. The resulting phytoplankton spectrum (Figure 3.4) shows less energy at smaller scales within that range. This is investigated further up in Chapter 6.

The mismatch in spectral slopes for phytoplankton (-0.50) and nitrate (-1.26) at larger scales means that there is no evidence to support the second theory over any of the scales sampled. An underlying assumption in the second theory is that all locations are typical, with single uniform numbers able to describe the physical and biogeochemical processes. However, there is considerable evidence that nutrient upwelling occurs frequently but intermittently at scales between 1-100 km through a

variety of physical processes (e.g. Strass, 1992, Lévy *et al.*, 2001, Allen *et al.*, 2005, McGillicuddy *et al.*, 2007, Klein *et al.*, 2008), producing localized perturbations of both flow and biogeochemistry.

Forcing at scales from 1-100 km is accounted for in the third theory, where the different components of the ecosystem react to such perturbations with their own intrinsic reaction time which consequently affects the spectral slope (Bracco *et al.*, 2009). However, in our observations the spectral slope is steeper for nitrate (-1.26) than for phytoplankton (-0.50) at larger scales but relatively shallower at smaller ones (-1.75 for nitrate and -2.64 for Chl-a). Even if it could be argued that nitrate has a different time-scale associated with it than phytoplankton it is not clear how the relative time-scales could vary with spatial scale.

Our results are consistent with the fourth theory. The simulations of Lévy and Klein (2004) show that the relative spectral slopes of components of the ecosystem can vary with time. It should be noted that we can only test this theory at the larger range of scales as their simulations do not reproduce the smaller range. Consequently a number of significant questions remain: How does intermittent forcing at the submesoscale (1-10 km), for which growing evidence exists (Callies and Ferrari, 2013), allow the relative slope for nitrate relative to phytoplankton to take different values, either side of this range? What is it about ecosystem interactions that provide an explanation for why the theory based on independent time-scales does not hold in an intermittently perturbed scenario but a theory that includes such interactions does?

Wider implication

The benefit of consistent power-law spectral behaviour would be that variability at one scale could be estimated from observations at a different scale in a straightforward manner. Current global climate models that reproduce marine biogeochemistry fail to adequately represent phytoplankton dynamics smaller than the mesoscale; effects at smaller scales are quantified by using spatial and temporal averages over a grid-cell scale. A power-law scaling in ecosystem variables could potentially provide a basis for parameterizations that implicitly capture phytoplankton dynamics at sub-grid-scale. Such a principle has already been successfully implemented in global circulation models to resolve sub-grid-scale physical processes affecting mixed layer stratification (Fox-Kemper and Ferrari, 2008, Fox-Kemper *et al.*, 2008, 2011). By analogy, bearing in mind the potential importance of the mesoscale and submesoscale for ocean primary production (Lévy *et al.*, 2012) such an approach for a description of phytoplankton behaviour in theory would present the

opportunity to improve model predictions for a relatively small computational cost. However, the only theory consistent with our results predicts continuous and significant changes in spectral slope at the mesoscale. This currently precludes such a parameterization unless the spectral slope is maintained at larger scales than the mesoscale such that it could still be estimated by a coarser model.

3.5. Conclusion

In this study we have directly compared, for the first time, spectra for nitrate, phytoplankton (Chl-a) and temperature, spanning spatial scales from 10 m to 115 km. A significant difference is observed between nitrate and phytoplankton spectral slope for the range 8-115 km and 10 – 100 m. Only the theory of Levy and Klein (2004) could explain the observed differences. A decoupling of phytoplankton and temperature spectra is observed between the two ranges, with phytoplankton slope equal to temperature for the range 10-100 m but being flatter for the range 8-115 km. This transition, commonly seen as physics dominating at small scales (10 – 100 m) and biological processes becoming influential at large ones (8-115 km), is challenged by the nitrate spectra. Under physical dominance, nitrate spectra should, like phytoplankton, be equal to temperature. As it is not, it suggests that tracers' spectral relationship are more complex to interpret.

The observations consist of one location, and therefore cannot be used to conclude that the difference between nitrate and phytoplankton spectral slope is typical. This is addressed in Chapter 5. More generally, phytoplankton scaling properties are found to vary across length-scales with the presence of a knee in the spectrum. It is not known how consistent such feature is across different regions. This is investigated in the following chapter (Chapter 4).

Chapter 4: Phytoplankton Patchiness: is the phytoplankton spectrum the same everywhere in the open ocean?

4.1. Introduction

In the previous Chapter, the focus was on the spatial relationship of phytoplankton with nitrate at a particular location in the North Atlantic. There the focus was on scales of 100 km and smaller, but nutrients influence phytoplankton patchiness on larger scales too. Nutrients are key for primary production, and their availability in the euphotic layer divides the ocean into distinctive regions or 'biomes' (e.g. Sarmiento and Gruber (2006)). Large scale physical processes such as wind stress, winter convection and Ekman transport exert a strong control on the nutrient supply into the mixed layer and delimit these regions to first order. The subpolar gyre is nutrient rich due to Ekman upwelling and relatively deep winter convection and has high levels of chlorophyll. In contrast, the subtropical gyre experiences large scale downwelling and is permanently stratified and therefore has low chlorophyll concentrations. In between, the transition region, seasonally stratified areas are replenished with nutrients by winter mixing but stocks are exhausted before the end of the summer.

This chapter addresses the question of whether these fundamental differences in biological and physical properties of the different open ocean regions affect the spatial structure of phytoplankton.

Specifically, the following hypothesis is tested in this chapter:

- Phytoplankton power spectra in different regions of the open ocean share the same properties.

To address this, *in situ* data from the subtropical gyre, the transition region and subtropical gyre obtained following the same sampling strategy, are analysed using the same methodology to allow as a rigorous comparison as possible. Note that nitrate data are not available from all regions so the focus will be on changes in the phytoplankton spectrum with region and its relationship with the temperature spectrum.

4.2. Methodology

4.2.1. Cruises and sampling information

In addition to the D321 cruise representative of the subpolar North Atlantic, for which a description was given in the previous chapter, data from the cruises D369 and D381 were used for this investigation representative of subtropical and transition regions respectively. See Figure 4.1 for their respective location.

RRS Discovery cruise D369 took place from August 9th to September 15th 2011 and sampled an area in the North Atlantic subtropical gyre centred on 26.5N, 31.00W. Three surveys using the towed vehicle SeaSoar were conducted to sample an area of approximately 150 by 150 km. Each survey took four consecutive days to complete. The dates for the surveys, denoted S1, S2 and S3, were 15th-18th August, 24th-28th August and 3rd-7th September, respectively. The surveys were carried out in a radiator style, covering the area with parallel transects of 150 km spaced by ~20 km. S1 and S2 sampled the area with transects running from East to West, starting from the South-East corner and North-West corner respectively. S3 on the other hand was oriented North-South and started in the North-West corner. For this study, a total of 6, 7 and 7 full length transects were obtained for S1, S2 and S3 respectively.

RRS Discovery cruise D381 was carried out in the Porcupine Abyssal Plain area centred on 49N, 16.5W from September 14th to October 3rd 2012 and included two SeaSoar surveys each covering a 100 km by 85 km box. The first survey (S1) had 100 km-long parallel tracks oriented East-West, the tracks during the second one (S2) were shorter (85 km) and oriented North-South.

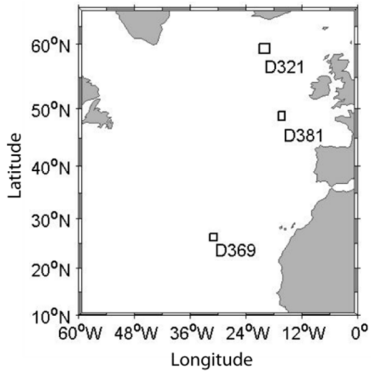

Figure 4.1: *Location of the cruises used in this investigation. They represent biogeochemically distinct regions of the open ocean: subtpolar gyre (D321), transition region (D381) and subtropical region (D369).*

With moorings occupying a central square of the survey area of size 30 by 30 km, the ship's track was slightly modified from the traditional radiator style to avoid that area (see Figure 4.2). Three days were required to complete the first survey (19th-21st September). The second started on the 23rd of September, was interrupted by a storm on the 25th September that lasted for four days and finished on the 30th September. Due to the modified layout of the surveys, a total of 6 and 3 full length transects for the surveys S1 and S2 respectively were available for this study.

4.2.2. Data selection

4.2.2.1. Subpolar cruise (D321)

A description of the data collection and spectral analysis of the D321 was given in Chapter 3. The only change for the methodology used in this chapter comes from the number of transects used for the analysis. In Chapter 3, only transects with both Chl-a and nitrate data were used. This consisted of two full and two half transects (see Figure 3.1). As nitrate is not a focus of this chapter, this restriction no longer applies. This means that four full and one half transects are available for this study (Figure 4.14).

Note that estimates of phytoplankton concentration are given using the manufacturer's calibrations. As the interest is in the slope of the spectrum rather than its magnitude this does not affect the aims of this study, assuming the usual linear calibration. Nevertheless, for simplicity, fluorimeter observations will be referred to as Chl-a throughout this chapter.

4.2.2.2. Subtropical cruise (D369)

Phytoplankton were most abundant at depth with the presence of a clear Deep Chlorophyl Maximum (DCM) and very low concentrations in the mixed layer. An example of Chl-a distribution with depth along a transect from survey S1 is displayed in Figure 4.2. The presence of the DCM is further illustrated by the histogram of Chl-a as a function of depth for each survey (Figure 4.3). The DCM distribution is centred at a depth of 120 m. The DCM displays a bimodal distribution against density for S1 and S2. S3 on the other hand is unimodal, as are all distributions against depth. Due

to the very low values no spectra for phytoplankton were calculated for the mixed layer. Instead the focus was on the DCM. Data were selected both for fixed depth and along isopycnals.

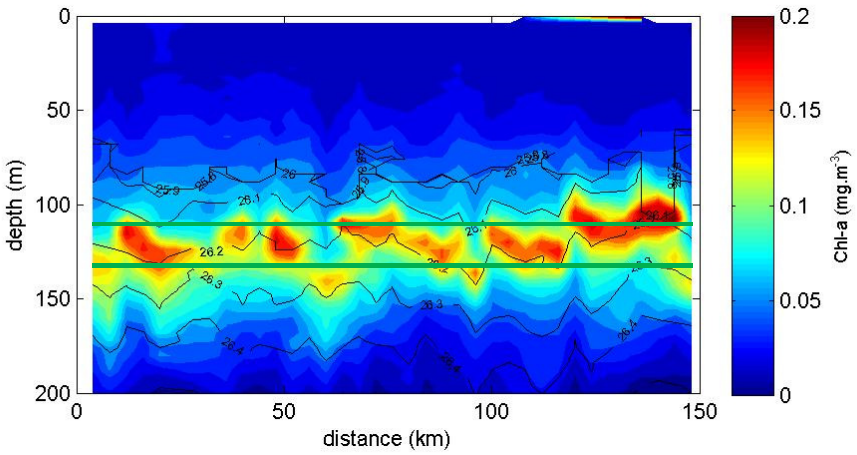

Figure 4.2: *D369 cruise Survey 1: Example of Chl-a contour plot for a transect oriented East-West. Phytoplankton vertical structure clearly displays a deep chlorophyll maximum centred at 120 m depth. Black contours show density surfaces. Two methods of data selection were used for estimating the spectrum of phytoplankton: data from along density surface 26.2 ± 0.04 kg m^{-3} and from fixed depth 120 ± 10 m (green lines).*

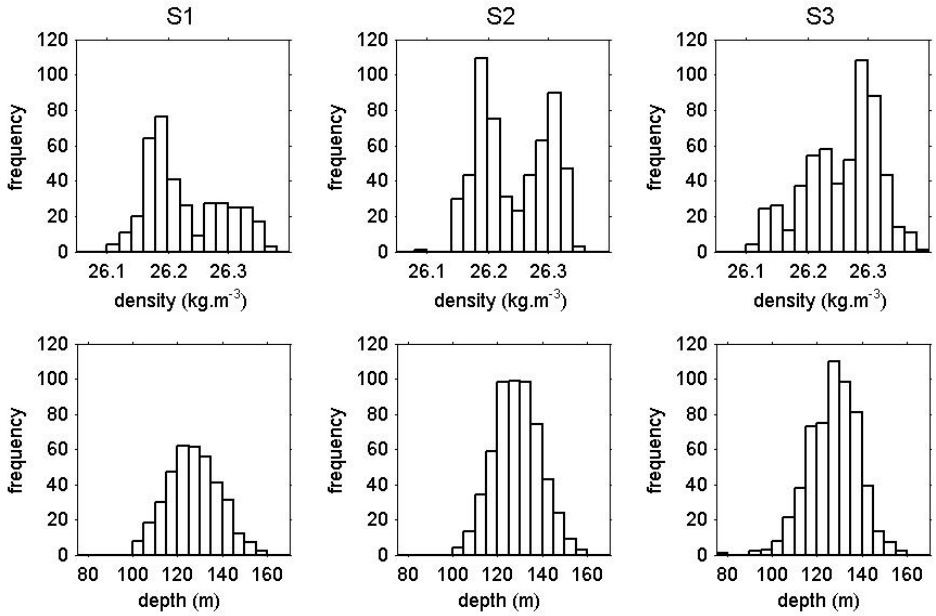

Figure 4.3*: Information on phytoplankton vertical distribution during cruise D369 in the subtropical gyre for survey S1 (left), S2 (middle) and S3 (right). Distributions against density anomaly (top) and depth (bottom) in the vicinity of the DCM are shown.*

4.2.2.3. Transition area cruise (D381)

The transition cruise displayed a more complex phytoplankton vertical structure with elements of both subpolar and subtropical cruises. The first survey (S1) showed highest phytoplankton concentrations in the mixed layer for the northern part of the survey (see Figure 4.4, legs 1, 2 and 3). The southern part displayed a DCM at a depth of approximately 40 m (see Figure 4.5). The second survey (S2) was disrupted by a storm. The Eastern part, sampled before the storm, displayed the same dual phytoplankton structure (legs 1, 2, 3, 4, 5 and 6) as in S1. The western part (legs 7, 8 and 9) sampled after the storm, displayed a homogeneous phytoplankton structure in the mixed layer. The storm perturbed the structure of the water column as evidenced by a cooler temperature and denser surface waters (see Figure 4.6). The DCM is no longer present in the southern part. Spectra were obtained for the mixed layer using data from depths 20-30 m.

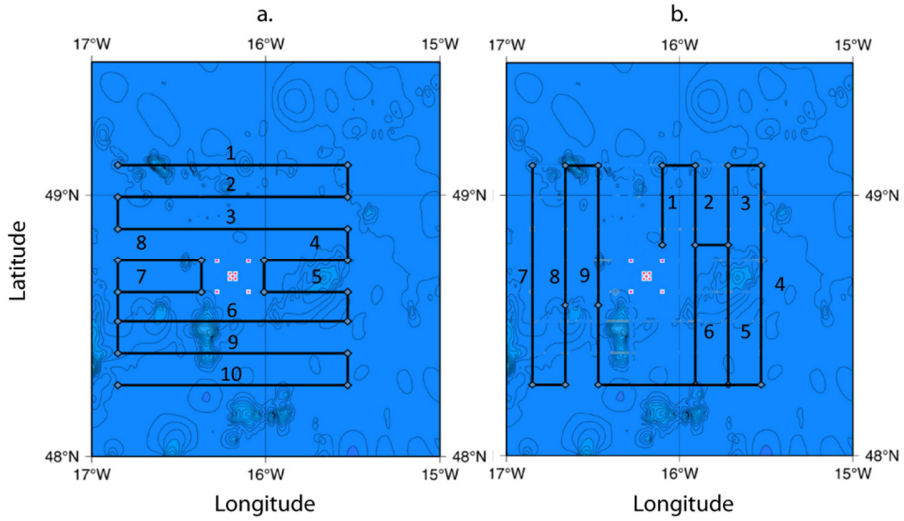

Figure 4.4: *Location and cruise tracks of Transition cruise surveys S1 (a.) and S2 (b.). Note the circumventing of the central area where moorings were installed (red squares). For S1, legs 1, 2, 3 and 6,9,10 were used to estimate the spectrum. For S2 (b.), only legs sampled after the storm were considered (legs 7, 8 and 9).*

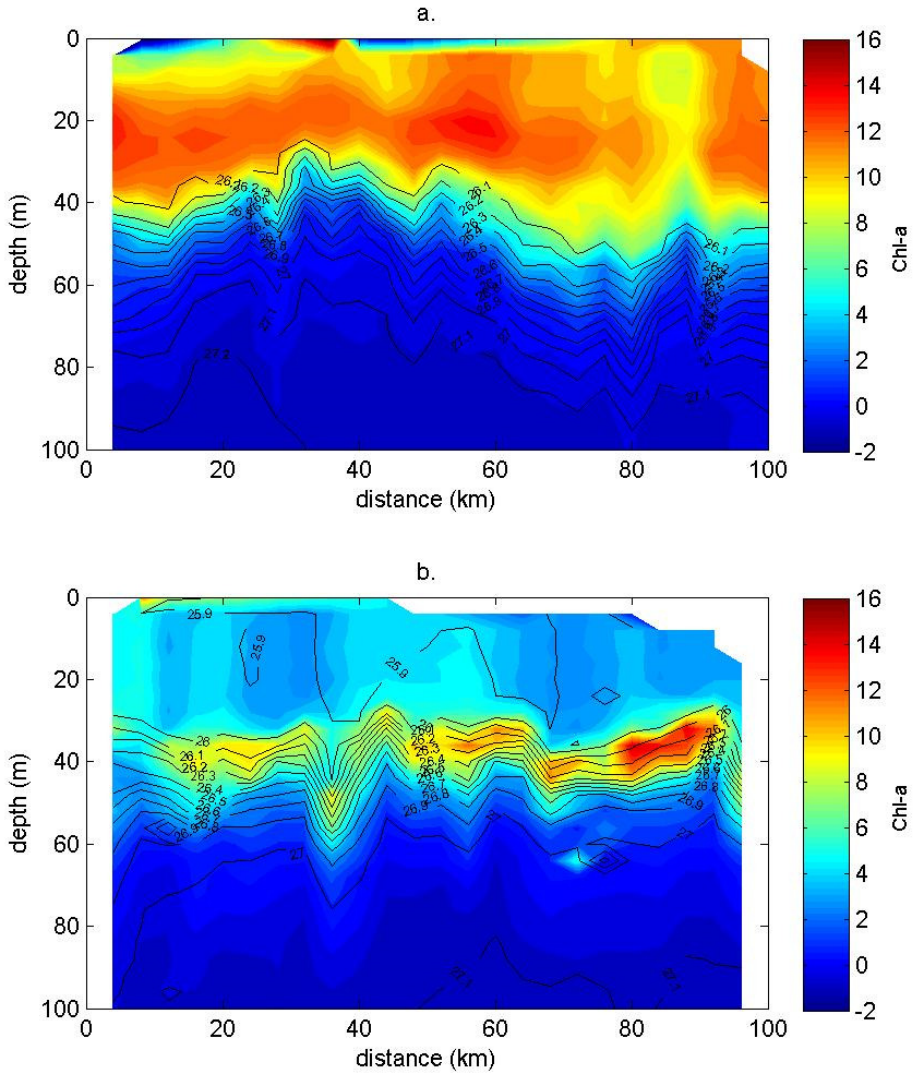

Figure 4.5: E*xamples of phytoplankton vertical structure for survey S1 of cruise D381. Highest values in the mixed layer characterises the northern half of S1 (a.). In contrast, the southern part (b.) presents a Deep Chlorophyll Maximum at around 40 m depth. Note the presence of quenching effect in the top 10 m in (a.).*

4.2.3. Estimating Power spectra

In addition to the common sampling framework of straight transects using the SeaSoar undulating sampler shared by all three cruises, it is necessary to establish a common spectral analysis procedure to make a comparison between survey areas robust. As in Chapter 3, the power spectra are calculated for two sets of range scales. For the small scale, the range was unchanged covering the 10-100 m length-scales. For the mesoscale range, the range 8 – 80 km was used instead of 8-115 km due to shorter transects in the other two cruises.. The range 8-80 km was chosen to have a range of

length-scales common to all cruises, given that each cruise had transects of different length (~120 km for D321, ~100 km and ~80 km for D381 and 150 km for D369). The upper boundary of 80 km was determined by the shortest transects studied which originated from survey S2 during the Transition cruise and was 83 km long. Transects were split into segments of 80 km with an overlap of 80% to maximize the data available. Such splitting generates 2, 4 and 5 segments for a 100 km, 130 km and 150 km transect respectively. Data from the vertical profiles for each variable studied were extracted for the targeted depth range, the spectra were then calculated using the mean values from each profile. An average spectrum for each transect is then obtained by taking the mean of all subsets' spectral estimates at each length-scale investigated. The average spectrum for the entire survey is itself the average of the transect averages. The method for obtaining the spectrum at scales 10-100 m for each survey is as detailed in Chapter3. Issues specific to the individual data sets of the several cruises are discussed next.

Subtropical cruise:

Spectra were calculated for fixed depth and along isopycnals. For fixed depth, data in all three surveys were selected for a depth range of 120 ± 10 m i.e. centred on the DCM (Figure 4.2). The 20 m span was chosen to maximize the number of data points without introducing significant vertical structure in the phytoplankton or temperature measurements. Spectra were also calculated for depth ranges 120 ± 5 m and 120 ± 20 m for comparison. Spectra using data from 120 ± 10 m for scales 8-80 km were indistinguishable from those using data from 120 ± 5 m. However, selecting data for depth range of 120 ± 20 m generated a dataset with clusters spanning over 300 m of horizontal data. Although this only slightly affected results for the range 8-80 km, it significantly affected the shape of the spectra for the small range scale with unrealistic results showing a drop of energy for the range 100-300 m. 120 m ± 20 m data were therefore discarded.

For fixed density, data were selected for the density anomaly ranges 26.20 ± 0.04 kg m^{-3}, 26.20 ± 0.04 kg m^{-3} and 26.30 ± 0.04 kg m^{-3} for S1, S2 and S3 respectively. In addition, for S2 the spectra for density range 26.30 ± 0.04 were also estimated due to the presence of a second peak in the DCM distribution (Figure 4.3). The range of density anomaly of 0.08 kg m^{-3} was determined so that the depth interval of the selected data did not exceed 25 m and had mean 20 m like the depth interval of data selected for fixed depth (120 ± 10 m).

Transition cruise:

For S1, two data sets were extracted from the survey. For the northern part, data were selected only along legs 1, 2 and 3, within the mixed layer depth for depths of 20 m ±5 m. Data for the southern part (legs 6, 9 and 10), however were selected along the isopycnals corresponding to 26.2 ± 0.2 kg m^{-3}. Transects 4, 5, 7 and 8 were not considered because too short. For S2 only post storm data were analysed. Pre-storm legs were not long enough except for leg 4. Leg 4 was not considered because it displayed a Chl-a vertical structure different to those of the post-storm legs. Data were extracted from depths 25 m ±5 m. This is deeper than S1 to be further away from quenching effects.

4.3. Results

4.3.1. Subtropical region

4.3.1.1. Biological and physical landscape

The three surveys of subtropical cruise (D369) spaced over 4 weeks provide a series of snapshots of the biological and physical landscape of the area over that time as is illustrated by the Chl-a and temperature contour plots of Figures 4.7, 4.8 and 4.9. A number of changes occur over the course of the cruise. Potential temperature shows that an eddy moved westward through the survey area. This anticyclonic eddy (Zubkov, 2012) occupies the majority of the area in S1. By S2 it only occupies half of the area and is nearly outside of the area by S3. The passage of the eddy is associated with a shift in DCM distributions (Figure 4.4). S1 displayed a unimodally distributed DCM centred around waters of density anomaly 26.19 kg m^{-3}. In S2 the DCM became bimodal with a second peak developing around density anomaly 26.3 kg m^{-3} corresponding to the values outside the eddy. The first peak eventually disappears with DCM becoming unimodal again but centred around 26.3 kg m^{-3} instead.

A clearer understanding of the DCM bimodal distribution for S2 can be obtained from Figures 4.7 and 4.8 which display phytoplankton concentrations for density surfaces 26.2 kg m^{-3} and 26.3 kg m^{-3} respectively. Two non-overlapping plankton populations appear along the two density surfaces. One lying along the density surface 26.2 kg m^{-3} (Figure 4.6) in the western part of the area and one along density surface 26.3 kg m^{-3} in the eastern part (Figure 4.7). Such a divide in plankton structure

is not distinguishable when using data from fixed depth (Figure 4.8) indicating the importance of light.

4.3.1.2. Estimation of spectrum using data from fixed depth

Across the three surveys, phytoplankton consistently display a knee in their spectrum illustrating a shift in power law behaviour between the ranges 8-80 km and 10-100 m (Figure 4.10). This is the same shape that characterised the phytoplankton spectrum in the subpolar cruise (D321). The variability for the range 10-100 m does not change appreciably across surveys with slope -3.53 ± 0.07, -3.52 ± 0.05, -3.59 ± 0.06 for S1, S2 and S3 respectively. Flatter slopes are observed for the range 8-80 km as well as some variability across surveys with slopes -0.36 ± 0.11, -0.83 ± 0.09 and -0.73 ± 0.13 for S1, S2 and S3 respectively. The steepening of the spectrum between S1 and S2 is caused by a drop in variability at the 8km length-scales end of the range rather than an increase at the 80 km end.

The temperature spectrum also displays a knee across the three surveys. Like phytoplankton, the temperature spectrum has similar behaviour for the range of scales 10-100 m with slopes -2.73 ± 0.07, -2.76 ± 0.05 and -2.98 ± 0.06, and displays more variability for the range 8-80 km with slopes -1.30 ± 0.11, -1.37 ± 0.11 and -0.98 ± 0.14 for S1, S2 and S3 respectively.

Note that for the range 8-80 km, the largest change in phytoplankton spectrum occurs between S1 and S2 with the slope varying from -0.36 to -0.83, whilst for temperature spectrum this large change happens between S2 and S3 with the slope varying from -1.38 to -0.99.

Despite the variability observed in the slope steepness at the range 8-80 km, the phytoplankton-temperature relationship remains unchanged across the three surveys. Phytoplankton display a steeper spectrum than temperature for the range 10-100 m but a flatter one for the range 8-80 km. The difference is significant at the 99% confidence interval for all surveys and all ranges with one exception: for S2 for the range 8-80 km there is a difference of 0.27 ± 0.18 (Table 4.1) so there is not sufficient evidence to reject the hypothesis that the slopes are the same. Average spectra using all 3 surveys maintains these trends with the phytoplankton spectrum (-0.63 ± 0.06) flatter than temperature (-1.21 ± 0.07) for the range 8-80 km and steeper at scales 10-100 m with slopes -3.54

± 0.03 and -2.83 ± 0.03.respectively. The spectra for the entire cruise are obtained from averaging the estimates at each length-scale of all transects from S1, S2 and S3 (20 in total).

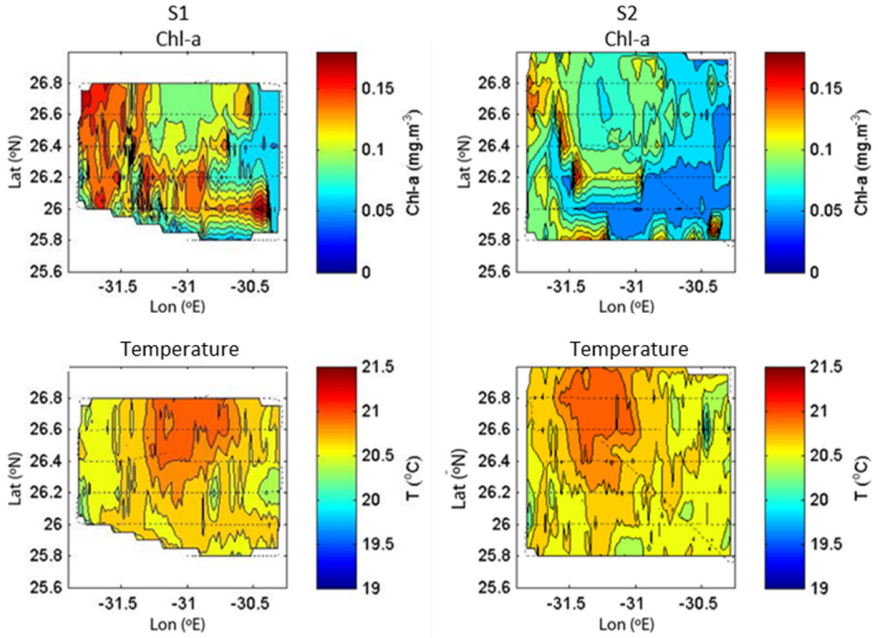

Figure 4.6: *Horizontal contour plots of S1 and S2 on cruise D369 for Chl-a (top) and potential temperature (bottom) along density surface 26.2 kg m^{-3}. The cruise tracks are overlaid as black dashed lines.*

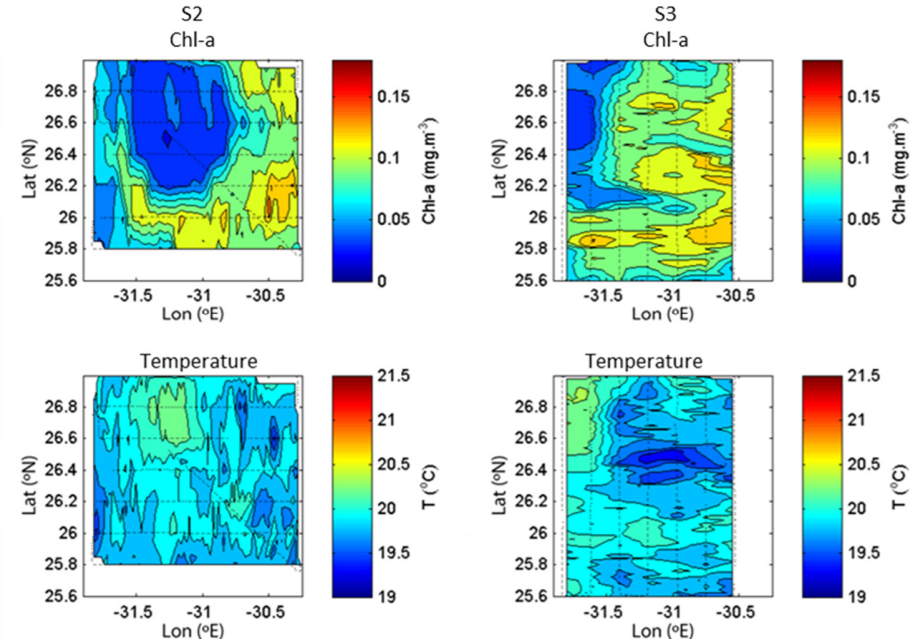

Figure 4.7*: Horizontal contour plots of S2 and S3 on cruise D369 for Chl-a (top) and temperature (bottom) along density surface 26.3 kg m^{-3}. Note the change in sampling direction between S2 and S3. The cruise tracks are overlaid as black dashed lines.*

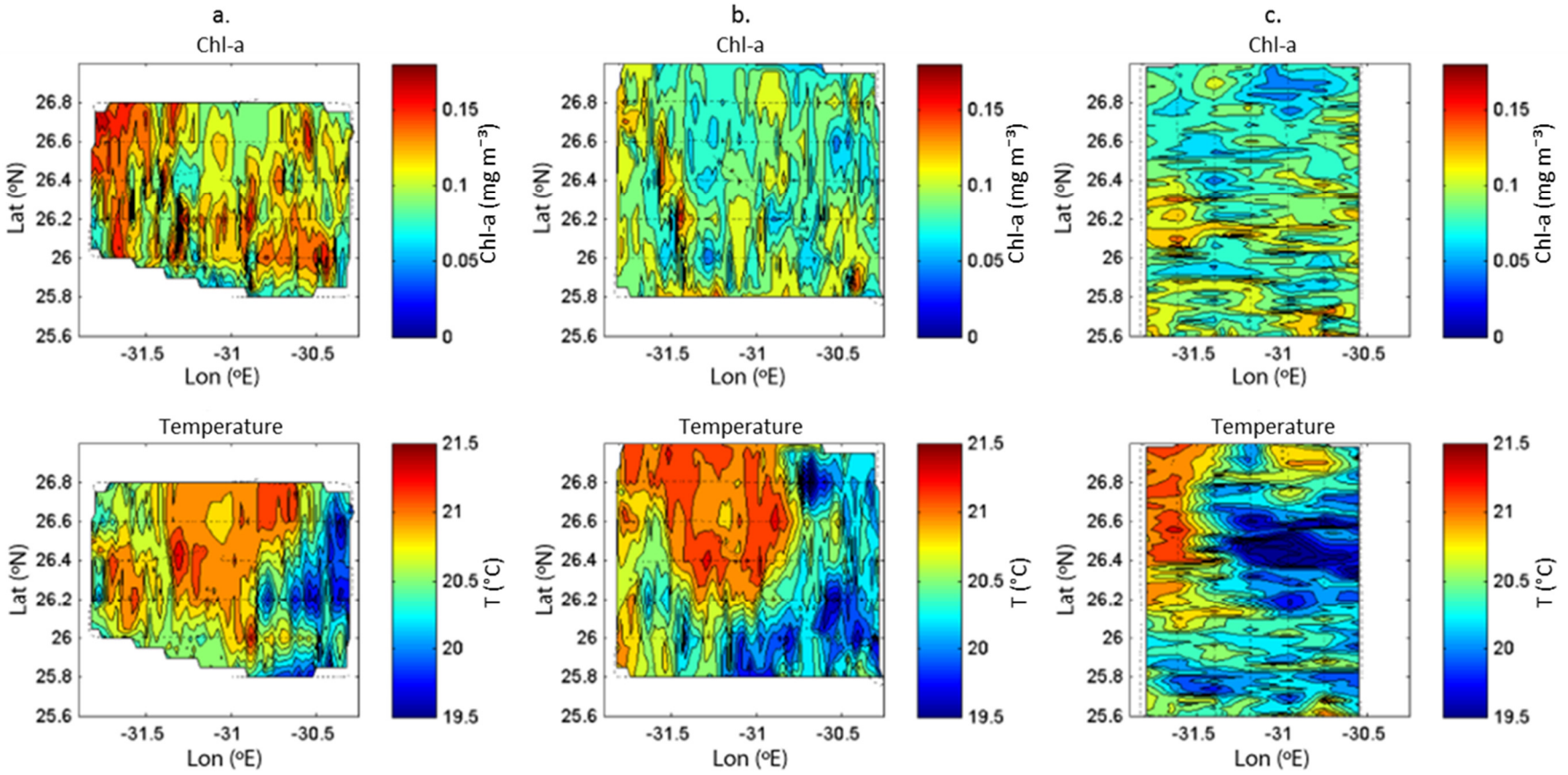

Figure 4.8*: D369, contour of Chl-a measurements (top) and potential temperature (bottom) for S1 (a.), S2 (b.) and S3 (c.) for a fixed depth of 120 m ± 10 m.*

Table 4.1:*Spectral slopes and their uncertainties for phytoplankton and temperature for the surveys S1, S2 and S3 of cruise D369 in the subtropical gyre. Results shown are for data from fixed depth 120 ± 10 m. The difference between phytoplankton and temperature slopes was also calculated. Spectral slopes using spectra averaged over the whole cruise were also estimated.*

D369	Slope	8-80 km	10-100 m
S1	Chl-a	-0.36 ± 0.11	-3.53 ± 0.07
	temperature	-1.30 ± 0.11	-2.73 ± 0.07
	difference	-0.94 ± 0.16	-0.80 ± 0.10
S2	Chl-a	-0.84 ± 0.09	-3.52 ± 0.05
	temperature	-1.37 ± 0.11	-2.76 ± 0.05
	difference	0.53 ± 0.14	-0.76 ± 0.07
S3	Chl-a	-0.71 ± 0.13	-3.59 ± 0.06
	temperature	-0.98 ± 0.14	-2.98 ± 0.06
	difference	0.27 ± 0.18	-0.62 ± 0.08
average of S1, S2, S3	Chl-a	-0.63 ± 0.06	-3.54 ± 0.03
	temperature	-1.21 ± 0.07	-2.83 ± 0.03
	difference	0.58 ± 0.10	-0.71 ± 0.05

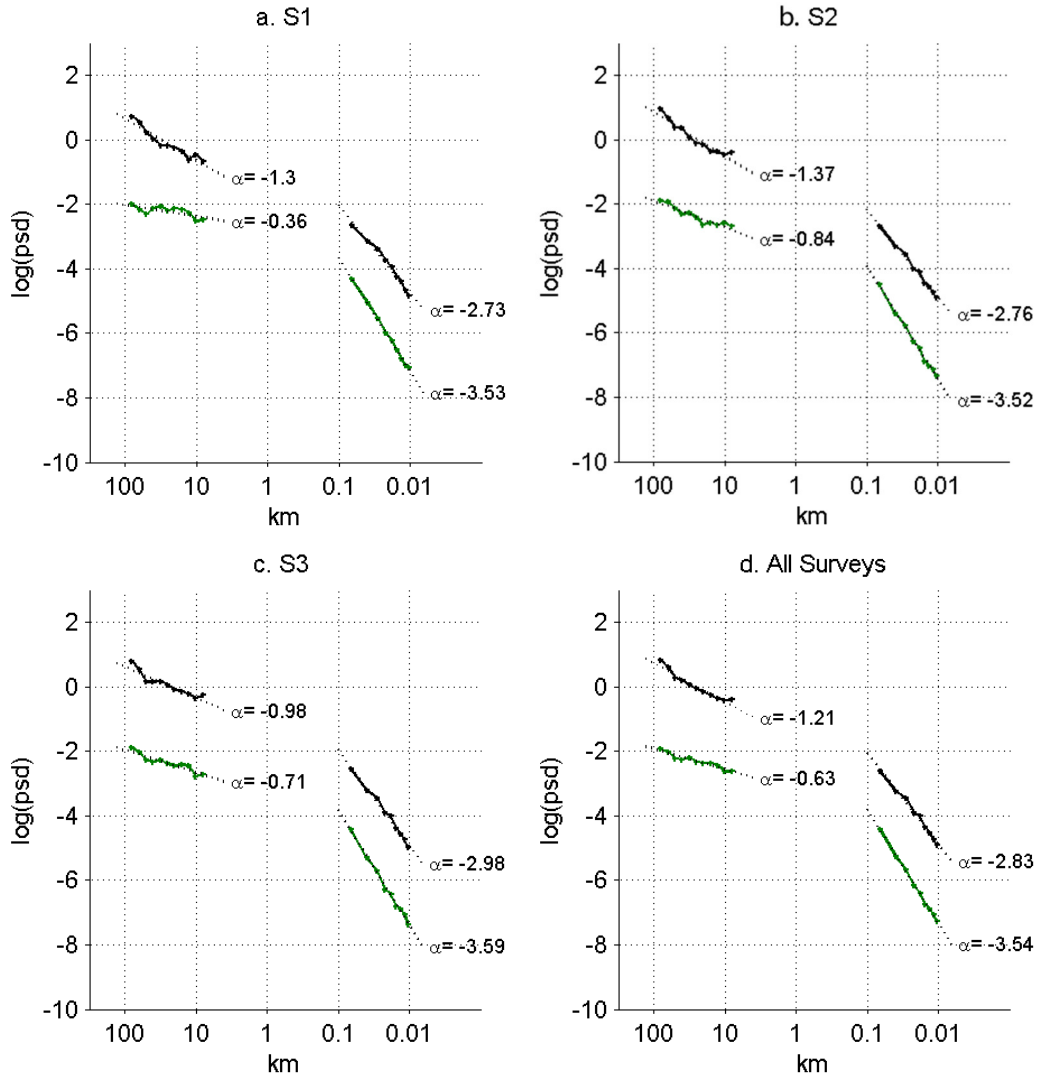

Figure 4.9: *Power spectrum of Chl-a (green) and temperature (black) for surveys S1 (a.), S2 (b.) and S3 (c.) using data from depth of 120±10 m on cruise D369.Spectra for the entire cruise were also calculated (d.).*

4.3.1.3. Estimation of spectrum using data along density surfaces

Like spectrum obtained from fixed depth data, the spectra of phytoplankton on density surfaces consistently display a knee with slopes for the range 10-100 m steeper than for 8-80 km for all three surveys. Equally, little variation was observed at small scale with slopes of -3.37 ± 0.10 and -3.39 ± 0.08 for S1 and S2 along density surface 26.2 kg m^{-3} respectively, and -3.00 ± 0.07 and -3.16 ± 0.06 for S2 and S3 along density surface 26.3 kg m^{-3}. For the range 8-80 km, steeper slopes are observed than for the spectra obtained from fixed depth data. For density 26.2 kg m^{-3}, the slope changes from -0.98 ± 0.13 to -1.49 ± 0.17 between S1 and S2. For density 26.3 kg m^{-3}, it changes from -1.78 ± 0.10 to -1.43 ± 0.12 between S2 and S3. Note also the difference in slope in S2 along different density surfaces.

The phytoplankton-temperature relationship however differs compared to results using data from fixed depth. For the range 10-100 m, the phytoplankton spectral slope is steeper than temperature for spectra on depth or density surface. However, for the range 8-80 km, for all three surveys, phytoplankton spectral slope cannot be distinguished from temperature slope using data from a density surface. Differences of 0.16 ± 0.17 for S1 along 26.2 kg m^{-3}, -0.10 ± 0.23 for S2 along 26.2 kg m^{-3} and -0.12 ± 0.19 for S3 along 26.3 kg m^{-3} are found (Table 4.2). The only exception is the case of S2 along 26.3 kg m^{-3} which shows slopes significantly different with a difference of -0.50 ± 0.19. Like spectra for data from fixed depth, the largest change in slope for phytoplankton occurs between S1 and S2 with slopes of -0.98 and -1.48 respectively. The largest change in slope for temperature also occurs between S1 and S2, from -1.14 to -1.39, unlike data from fixed depth where the greatest change took place between S2 and S3.

Table 4.2: *Same as Table 4.1 but for data from along density layers instead.*

D369	Data	slope	8-80 km	10-100 m
S1	26.2 ± 0.04 kg m^{-3}	Chl-a	-0.98 ± 0.13	-3.37 ± 0.10
		temperature	-1.14 ± 0.14	-2.77 ± 0.06
		difference	0.16 ± 0.17	-0.60 ± 0.10
S2	26.2 ± 0.04 kg m^{-3}	Chl-a	-1.49 ± 0.17	-3.39 ± 0.08
		temperature	-1.39 ± 0.15	-2.78 ± 0.05
		difference	-0.10 ± 0.23	-0.61 ± 0.08
S2	26.3 ± 0.04 kg m^{-3}	Chl-a	-1.78 ± 0.10	-3.00 ± 0.07
		temperature	-1.27 ± 0.17	-2.84 ± 0.05
		difference	-0.50 ± 0.19	-0.16 ± 0.08
S3	26.3 ± 0.04 kg m^{-3}	Chl-a	-1.43±0.12	-3.16 ± 0.06
		temperature	-1.32±0.13	-2.98 ± 0.05
		difference	-0.12 ± 0.19	-0.18 ± 0.07

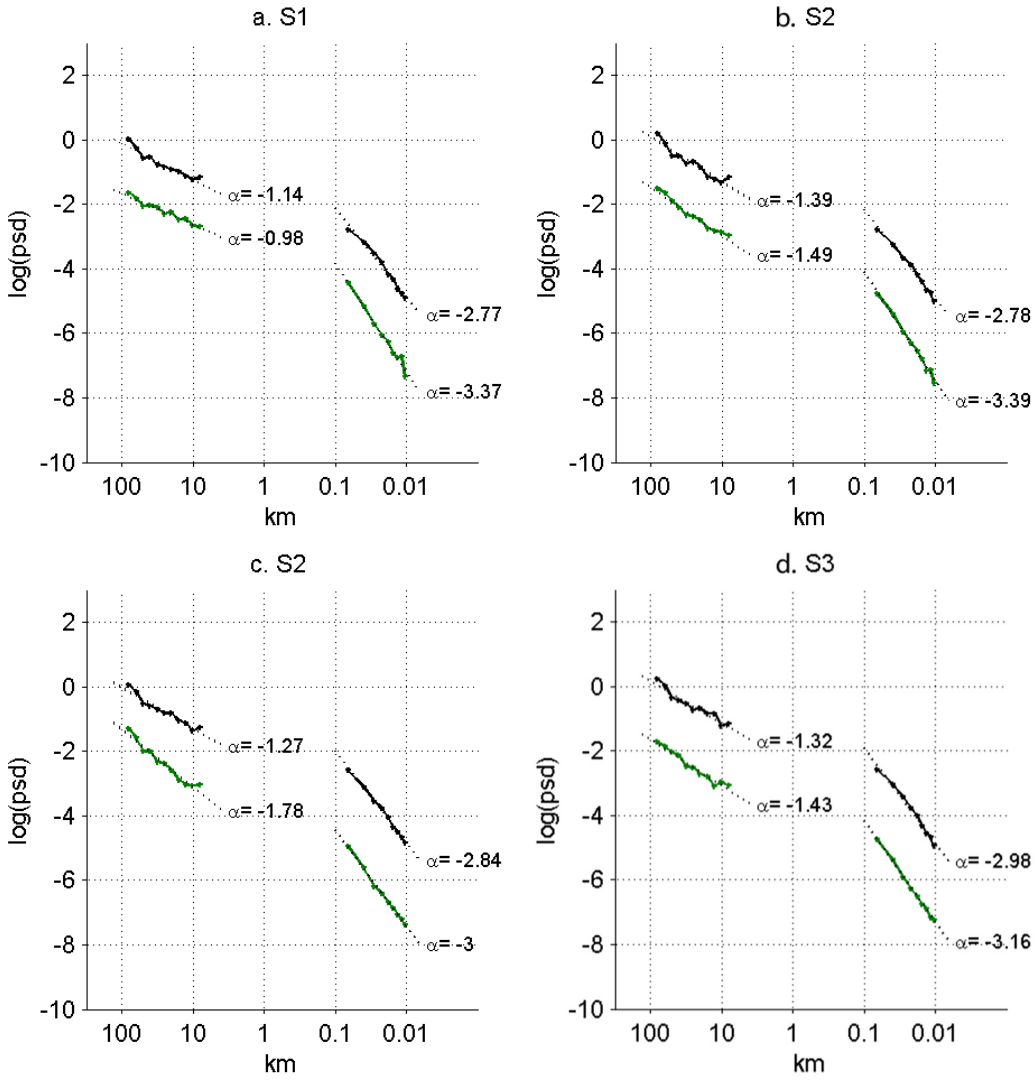

Figure 4.10: *Power spectrum of Chl-a (green) and temperature (black) for S1 (a.) and S2 (b.) for data from along density layer 26.2 kg m^{-3}, and S2 (c.) and S3 (d.) along density layer 26.3 kg m^{-3} for cruise D369.*

4.3.2. Transition region

As described earlier, for the transition cruise (D381) the first analysis uses data for the mixed layer. It consists of the northern part of the data from S1 (3 legs) and the western part of S2 (3 legs) (see Figure 4.4). The second analysis uses data from along a density surface. It includes the southern three legs of S1 where a DCM is observed.

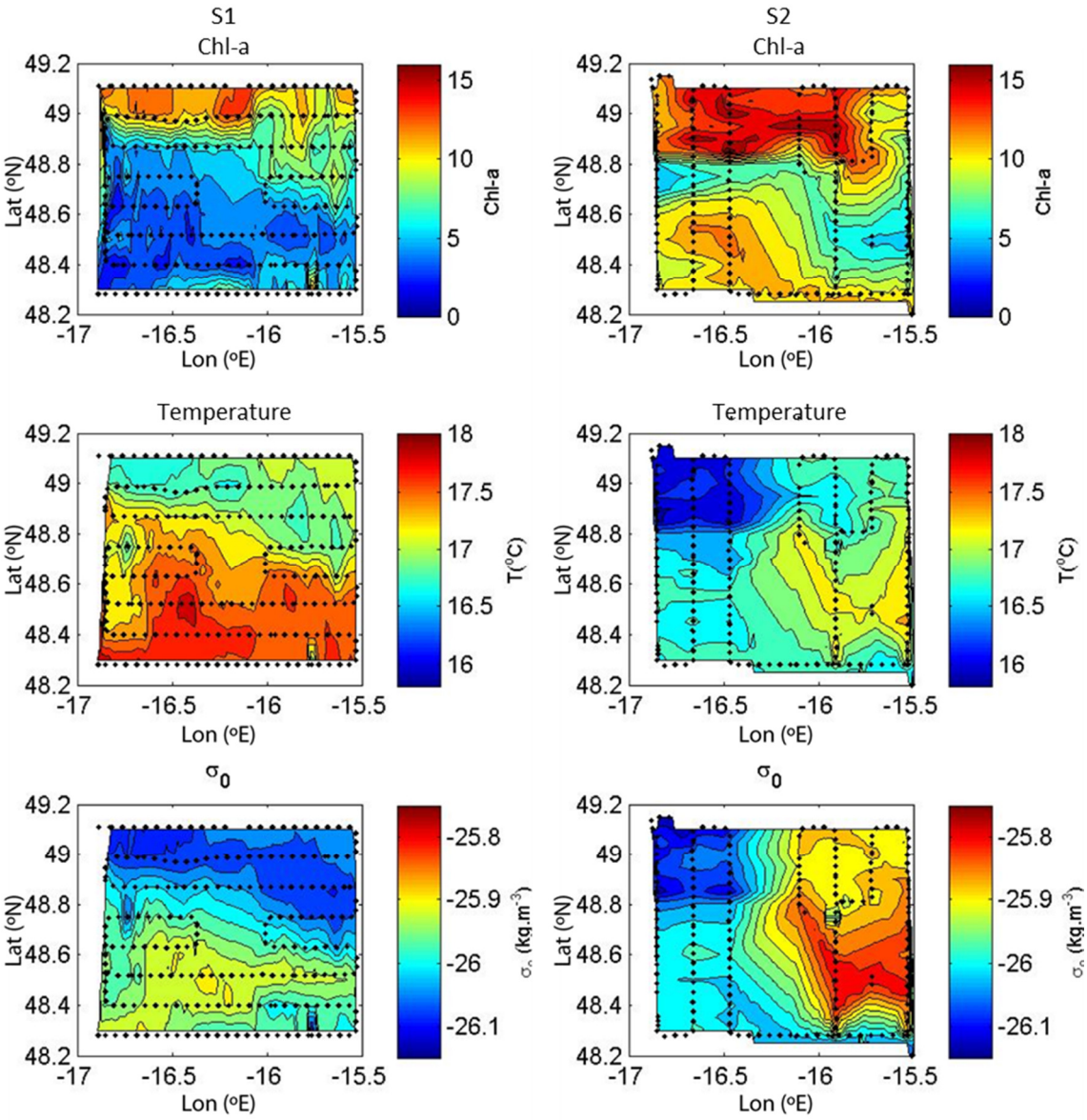

Figure 4.11: *Contour plots of phytoplankton abundance (top), potential temperature (middle) and density anomalies for depth range 20 m ±5 m for survey S1 (left) and S2 (right) of D381. Note that manufacturer's values were used for the phytoplankton measurements.*

4.3.2.1. Mixed layer depth

The storm occurring midway through survey S2 disrupted the sampling of the area. The western part of the area was sampled after the storm. Denser and colder waters occupy that part of the area compared to the pre-storm part to the East and to waters sampled during survey 1 (Figure 4.6). Combined with the deepening of the density gradient, these observations indicate a vertical mixing of surface waters with deeper ones induced by the storm. Further evidence of vertical mixing of the storm can be observed in the concentrations of phytoplankton that were

homogeneous in the mixed layer post-storm unlike previously observed in survey 1 where it displayed a DCM to the South and the eastern part of S2.

For both S1 and S2, the spectra of phytoplankton are consistent with the knee shape seen in the subpolar and subtropical regions (Figure 4.12). The spectral slopes at large scales (8-80 km) are significantly different between the two surveys. The phytoplankton spectra is steeper for S2 (-1.57 ± 0.21) than for S1 (-1.23 ± 0.26). A more pronounced steepening is observed in temperature with slopes of -1.48 ± 0.16 for S2 and -1.14 ± 0.30 for S1. Changes in spectra for both variables are associated with variability being introduced at the larger scale end of the range.

At small scales phytoplankton spectral slope changes little between S1 (-2.71 ± 0.23v) and S2 (-2.44 ± 0.46) unlike temperature for which a significant flattening from -3.04 ± 0.17 to -2.28 ± 0.32 is observed (Table 4.3). This change of steepness in temperature spectra at small scale is the most abrupt recorded for all three cruises.

Both S1 and S2 have spectra for temperature and phytoplankton that are indistinguishable at the range 8-80 km. At the small scale range (10-100 m), temperature is steeper than phytoplankton in S1, with a difference of 0.34 ± 0.21, and becomes flatter in S2, with a difference of -0.16 ± 0.36. This change is mainly resulting from the strong flattening of temperature spectrum between the two surveys.

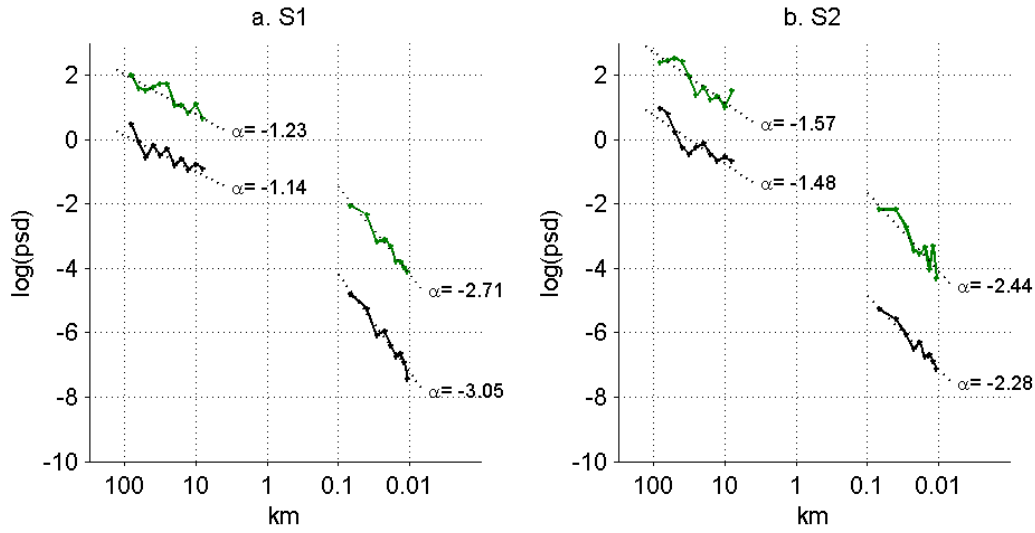

Figure 4.12*: D381, spectra of Chl-a (green) and temperature (black) using data from the mixed layer at fixed depth 15-25 m for S1 (a.) and 20-30 m for S2 (b.). Deeper depth was selected for S2 (25-35 m) to be further away from quenching effect.*

4.3.2.2. Along density surfaces

Spectra for the southern part of the survey S1 display a clear knee with values of -1.04 ± 0.44 for the range 8-80 km and -3.12 ± 0.11 for the range 10-100 m for phytoplankton. The temperature spectrum displays the same slope (-1.06 ± 0.23) for the range 8-80 km (Figure 4.13) but is flatter for the range 10-100 m (-2.75 ± 0.09). Large uncertainties are observed for phytoplankton slope (0.44) for the range 8-80 km. A significantly larger amount of variability is observed for temperature for the range 10-100 m compared with the case for fixed depth in the northern part, with more than two order of magnitude difference.

Table 4.3: *Spectral slopes and their uncertainties for phytoplankton and temperature for the surveys S1, S2 of D381. The difference between phytoplankton and temperature slopes was also calculated. Two estimates were made for S1. Data from depth 15-25 m from were used for legs 1,2 and 3 (see Figure 4.4). As legs 6, 9 and 10 displayed a Deep Clorophyll Maximum, spectra were also calculated from data along density layer 26.2 ± 0.2 kg m^{-3}.*

D381	Data	slope	8-80 km	10-100 m
S1	15-25 m	Chl-a	-1.23 ± 0.26	-2.71 ± 0.23
		temperature	-1.14 ± 0.30	-3.05 ± 0.17
		difference	0.09 ± 0.25	0.34 ± 0.21
S2	20-30 m	Chl-a	-1.57 ± 0.21	-2.44 ± 0.46
		temperature	-1.48 ± 0.16	-2.28 ± 0.32
		difference	-0.08 ± 0.29	-0.16 ± 0.36
S1	26.2 ± 0.2 kg m^{-3}	Chl-a	-1.04 ± 0.44	-3.12 ± 0.11
		temperature	-1.06 ± 0.23	-2.75 ± 0.09
		difference	0.03 ± 0.57	-0.37 ± 0.15

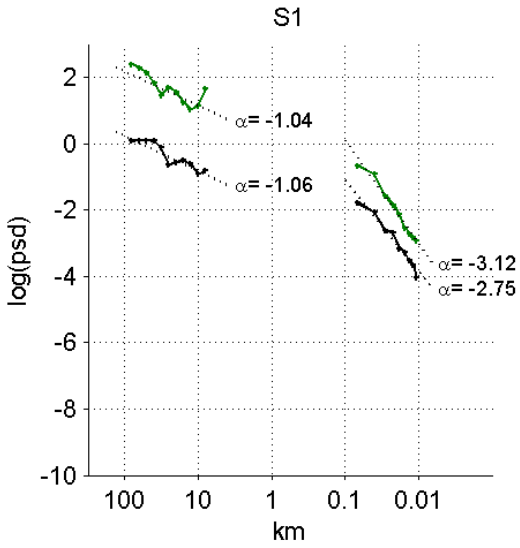

Figure 4.13: *D381, spectra of Chl-a (green) and temperature (black) using data at the bottom of the mixed layer for S1 along density 26.2 kg m^{-3}. Leg 6, 9 and 10 were used for the spectral estimation.*

4.3.3. Subpolar region

Relative to Chapter 3, for the subpolar cruise (D321) temperature and phytoplankton slopes have changed slightly due to the larger data set used and smaller range of length-scale studied (Figure 4.14). Compared with the results of Chapter 3, phytoplankton spectral slope changed from -0.50 ± 0.24 to -0.63 ± 0.26 for the range 8-80 km, but remained similar at -2.67 ± 0.13 (-2.64 ± 0.17 in Chapter 3) for the 10-100 m range. The temperature spectrum flattened with the slope of -1.71 ± 0.25 changing to -1.48 ± 0.30 for the range 8-80 km, and steepened from -2.73 ± 0.15 to-3.38 ±0.20 for the range 10-100 m. Slopes for temperature and phytoplankton for scales 10-100 m are no longer undistinguishable, with a difference of -0.74 ± 0.22. For scales 8-80 km, temperature (-1.48) remains steeper than phytoplankton (-0.63).

Like for the subtropical and transition cases, the phytoplankton spectral slope shows a shift between the two length ranges. For both ranges, the temperature spectrum is steeper than phytoplankton, a case not encountered in the other cruises.

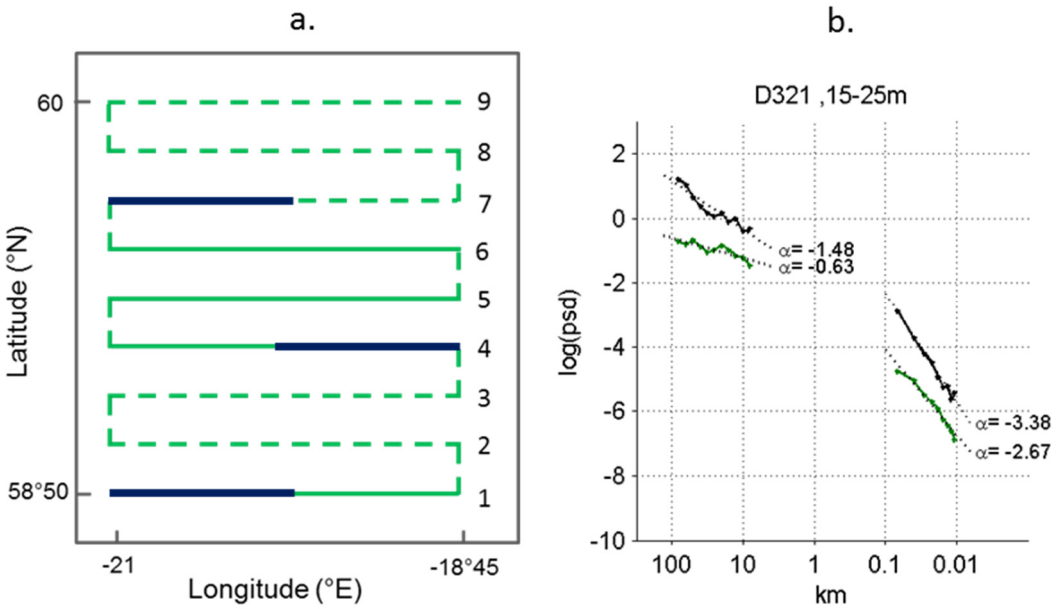

Figure 4.14: *D321 survey tracks (a.) used for calculating the spectra (b.) of Chl-a (green) and temperature (black) for a fixed depth of 15-25 m. Tracks represented in solid lines were used for the estimates. Dark blue consists of the extra data not used in Chapter 3.*

Table 4.4: *Spectral estimates and their uncertainties for phytoplankton and temperature for the cruise D321. The difference between phytoplankton and temperature slopes was also caluclated.*

	Data	slope	8-80 km	10-100 m
D321	15-25 m	chla	-0.63 ± 0.26	-2.67 ± 0.13
		Temp	-1.48 ± 0.30	-3.38 ± 0.20
		difference	-0.88 ± 0.35	-0.74 ± 0.22

4.4. Discussion

Are the phytoplankton spectral properties identical in all open ocean regions?

In Chapter 3, the phytoplankton power spectrum was estimated for an area of the North Atlantic subpolar region. It revealed a spectrum with a 'knee' shape. The hypothesis tested in this chapter is that the properties of the phytoplankton spectrum are consistent for all regions of the open ocean despite their contrasting bio-physical environments. In addition to the subpolar

gyre, the Chl-a power spectra were calculated for areas in a subtropical region and the transition area between subpolar and subtropical regions.

The results show that for all three regions phytoplankton share the same power spectral shape resembling a 'knee' in loglog-space. For the range 8-80 km, spectral slopes are consistently flatter than those for the range 10-100 m. This is also true for the spectrum of temperature. Selecting data for a fixed depth or along a density surface for cases presenting a Deep Chlorophyll Maximum does not remove the presence of the knee in the spectrum.

It was mentioned in the methodology chapter (Chapter 2 Section 5.2) that the method used for the range 8-80 km (Lomb Scargle periodogram) showed a tendency to under-evaluate the spectral slope particularly in cases for which the original slope was steeper than -2. No surveys here display slopes for phytoplankton or temperature spectra steeper than -1.79 for the range 8-80 km. Therefore, according to the findings of Chapter 2, the slopes calculated from the *in situ* data should not suffer from significant under-estimation.

Differences in slopes between the two ranges of length-scales vary between 0.87 and 3.17 for phytoplankton spectra. For temperature spectra, the differences range between 0.80 and 1.90. These differences are larger than the over-estimation errors of the LSP method for signals with slope flatter than -2. For slopes $-2<\alpha<-0.5$, the LSP method estimates flatter slopes than the true signal with error 0.22 (Chapter 2 Section 5.2.). It can be concluded that a change in power law behaviour between the ranges 8-80 km and 10-100 m is a property that is common to all phytoplankton spectra of the regions studied.

Even though the overall shape of the spectrum is a robust feature, the phytoplankton spectral slope shows significant variability. This is true for both scale ranges. For instance phytoplankton slope values between -0.36 and -1.79 for the range 8-80 km are found. For the range 10-100 m, slope values vary between -3.39 and -2.44. Furthermore, the relationship with temperature spectrum is also inconsistent with cases for the range 8-80 km of phytoplankton being flatter (D369 S1), equal (D381 S1) or steeper (D369 S2) than temperature. The same occurs for the range 10-100 m.

From these findings a number of questions arise. Following the observed variability in the phytoplankton slope, are the differences observed a result of regional variability or is the slope changing in time?

Is the strongest variation in slope temporal or regional?

A stronger version of the hypothesis, that the phytoplankton spectral slope would be identical for all regions, cannot be supported given the different slope values observed. The advantage of cruises having multiple surveys and located in different regions of the open ocean is that it also allows a preliminary examination of whether the variability is temporal or regional.

Quantifying the variations of the phytoplankton slope over time-scales of days to weeks is important before evaluating whether regional differences exist. This cannot be quantified robustly using only the 2 to 3 consecutive surveys discussed in this chapter but they can at least give an indication of the level of temporal variation that can be expected.

Results from D369 in the subtropical region for which three consecutive surveys were made over 4 weeks during the summer indicate that phytoplankton spectra display significant variability in slope for the range 8-80 km (Figures 4.10 and 4.11). The slope changed from -0.36 ± 0.11 to -0.84 ± 0.13 to -0.71 ± 0.13 when selecting data for a fixed depth. Variations in slope were also found when using data along a density surface instead (from -0.98 ± 0.13 for S1 to -1.49 ± 0.17 for S2 along 26.2 kg m^{-3}, and from -1.78 ± 0.10 for S2 to -1.43 ± 0.12 for S3 along 26.3 kg m^{-3}). For the 10-100 m range, the spectrum of phytoplankton displays little variation across surveys with values centred around -3.2 using data along density surfaces and -3.5 using data for fixed depth. The slope is always steeper than that of the temperature spectrum.

Short time-scale variations are also present for the transition area (D381) with slopes varying from -1.23 ± 0.26 to -1.57 ± 0.21 for scales 8-80 km. The storm may be the driver behind the change in slope. But given that storms happen frequently, such change may provide an explanation for temporal variability. Extra variability compared to S1 is introduced in the S2 spectra of both temperature and phytoplankton at large scales of the 8-80 km length-scale range.

The evidence of temporal variations in slope raises further questions that will need to be investigated. It is important to know if short time-scale variations in phytoplankton slope are consistent across regions or if they vary regionally. How much phytoplankton vary may be a defining property of the phytoplankton spectrum. Characteristic traits in phytoplankton for a region may be found in the manner that they evolves over time. Also, are variations in slope over a short period e.g. a month, the same throughout the year or do different periods of the year exhibit different levels of variability?

Given the apparent magnitude of temporal variability, it is difficult to determine whether phytoplankton spectra present regional differences on the basis of such a small number of measurements. The mean phytoplankton slope for D369 (-0.63) is the same as for D321 for the range 8-80 km. The phytoplankton average spectrum of the transitional area has a steeper slope (-1.43) for the same range. Many more surveys from each of the regions are needed to conclude that differences in estimated means are statistically robust. Obtaining an understanding of the phytoplankton slope variability over both space and time requires the use of other types of data. For instance, models provide high resolution data in time (order of days) that span over large spatial (basin) and time-scales (multi-year). It may be a valuable tool to overcome such limits and obtain an idea of the magnitude of the temporal variability relative to the difference in slope between regions. This is investigated in Chapter 5.

Figure 4.15: *Spectra of Chl-a for each the 7 transects of survey S3 in the subtropical area (cruise D369 using. data obtained along density surface 26.3 kg m^{-3}. Transects were sampled from West to East (see Figure 4.7). Spectra of Chla from the first 3 transects traversing the eddy are shown in red (a to c) and those from the transects further East and outside the eddy in blue (d to g). Spectra of temperature are shown in black.*

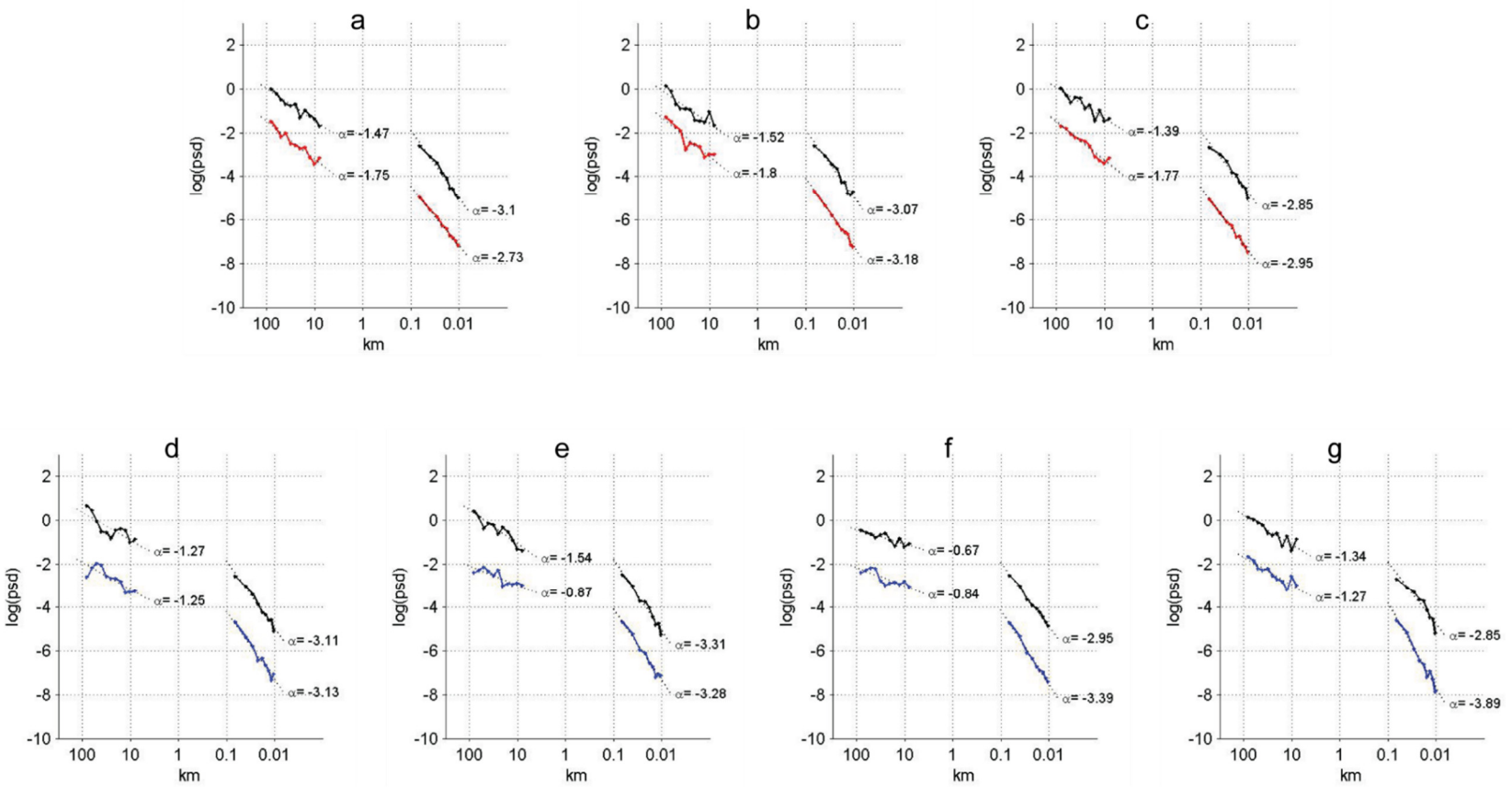

How big an area is it necessary to sample to accurately measure the slope in the range 8-80 km? (and 10-100 m?)

The subtropical surveys show significant variability in phytoplankton spectral slope between surveys. The area surveyed experienced the crossing of an eddy. Its signature is clearly visible in the phytoplankton field (Figure 4.7). For example, S2 shows low concentrations of phytoplankton within the core of the eddy and higher ones at its margin. The position of the eddy within the survey area and the number of transects affected by its presence may impact the estimated phytoplankton slope value for the survey.

The layout of the transects allows for the eddy contribution to be investigated. Transects in S1 and S2 traverse the eddies whilst for S3 some do not. The clearest example comes from S3 for data obtained along density surface 26.3 kg m^{-3} (Figure 4.7). The 7 North-South transects are carried out beginning with the one furthest West. Only the first 3 transects cross the core of the eddy. They display steeper phytoplankton slopes (-1.75, -1.79 and -1.76) than the following four transects outside the eddy (-1.25, -0.87, -0.84 and -1.28) (Figure 4.15). The same steepening of spectra for transects crossing eddies is observed for data from fixed depth.

With eddies being both ubiquitous in the ocean and exerting an influence on phytoplankton patchiness, even if the interest is a specific length range (e.g. 8-80 km) the choice for the survey area size may influence the final slope estimation. If multiple surveys of the same area over a period greater than the time needed for an eddy to pass through cannot be achieved, then sampled areas should include a larger number of eddies so that their location within the area does not bias the results. This is only possible with larger areas. The problem is that ship based surveys cannot sample larger areas. It takes approximately three days to map 130 km by 130 km area. Surveys mapping a larger area, and therefore taking longer, would not be able to capture the physical and biological environments before they change. The data is therefore not 'synoptic' because it contains not on spatial but also temporal information.

Whether variability in phytoplankton slope estimated for an area of ~130 km x130 km is representative of the true phytoplankton variability at those scales cannot be properly tested using the data studied here. Satellite data, which provide synoptic snapshots of Chl-a over large areas, may be more suited to study this question. The effect of the size of the area surveyed on the phytoplankton slope estimate is evaluated using satellite data in Chapter 6.

Measuring patchiness at depth: at fixed depth or along density surfaces?

Variability induced by internal waves is potentially present when using data from a fixed depth below the mixed layer. With horizontal mixing occurring along isopycnals, data points selected for fixed depth are retrieved from different density layers. If phytoplankton are more uniform with density than depth, potentially because nutrient contours typically follow density surfaces, data from a fixed depth may, for example, result in the selection of high phytoplankton concentration data points from the DCM alongside lower concentration ones from neighbouring density surfaces. As internal waves have a wavelength of around 0.1-10 km, the induced variability affects the higher end of the 10-100 m range and the lower end of the 8-80 km. This would cause the phytoplankton slope to flatten for the range 8-80 km and steepen for the range 10-100 m. This may explain the relatively flatter phytoplankton slopes obtained for data from fixed depth compared to slopes obtained with data from along isopycnals for the range 8-80 km. Although measuring patchiness along isopycnals would avoid the introduction of vertical spatial variability into horizontal spectra the example shown here (D369) demonstrates a case where phytoplankton are better correlated with depth than density, potentially indicating light control, and so taking density surfaces would also create what might be considered as artificial variability at small scales. The issue of how best to quantify spectra at depth is therefore an open question. The rest of the thesis will focus on surface spectra to address the questions raised on spectral slope variability.

4.5. Conclusion

This chapter found that the knee shape of the phytoplankton spectrum is common to all the regions of the open ocean investigated in this study. However it has also shown that the spectrum may display significant variability in slope for both the scale 8-80 km and 10–100 m. This is best illustrated by the summary figure 4.16 which shows a clear shift in slope values between the two spatial ranges but also the presence of variability in slope within each range, particularly at the mesoscale. The spatial and temporal limitations associated to *in situ* surveying prevent from determining the source and robustness of this variability. These will be explored in subsequent chapters.

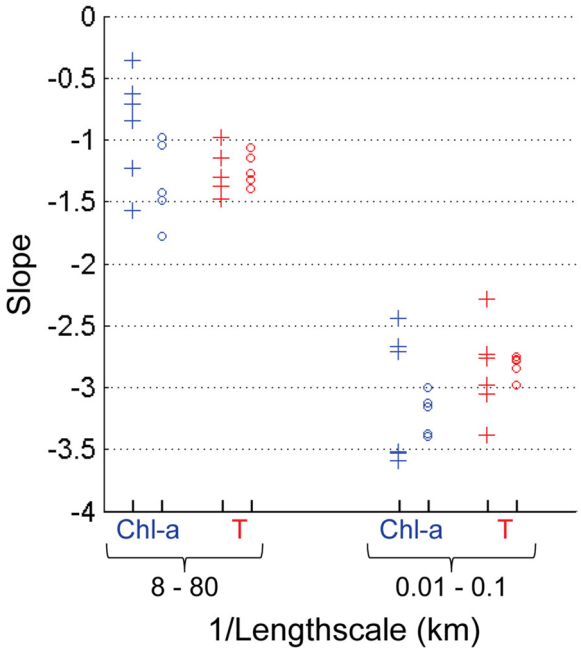

Figure 4.16: *Summary of spectral slopes for Chl-a (blue) and temperature (red) obtained from all 3 cruises (Subpolar, subtropical and transition region) for the range of length-scales 8-80 km and 10-100 m. Slopes obtained using data from fixed depth and along a density surface are shown with crosses and circles, respectively.*

Chapter 5: Temporal variability in spectra

5.1. Introduction

The scaling properties of phytoplankton spatial variability have been examined in the previous Chapters (3 & 4) using *in situ* observations. This revealed the presence of power-law behaviour in phytoplankton spectra for all areas investigated. However, significant differences in spectral slopes of phytoplankton were found for both different areas and times. For example, phytoplankton slope values more than doubled in a matter of days at one location.

The time and space limitations of *in situ* sampling make it difficult to explore further the extent of such variability. The use of a model to complement field data is particularly attractive as this allows questions to be raised such as: how is the phytoplankton slope modulated over time? How does this vary with location? The model of Levy et al. (2012b) is used for this investigation. Although the model is an idealised representation of the North Atlantic, it has the advantage of having a high spatial (1/54°) and temporal (2 days) resolution, both necessary characteristics for this study.

This chapter therefore uses this model's output to explore variability in spectral slopes. More specifically, the following hypotheses are addressed in this chapter:

- Phytoplankton spectral slopes vary significantly over time-scales of days.
- Temporal variations over a period of months exceed variations in slope between regions.
- There is a difference in nitrate and phytoplankton spectral slope which is consistent in time.
- There is a seasonal pattern in phytoplankton spectral slopes.

5.2. Methodology

5.2.1. Data description

To investigate the above hypotheses, a high resolution idealized model of the North Atlantic is used. This model resolves the scales of interest at a basin scale, something not currently achievable by global biogeochemical models. The physical model is the primitive equation ocean model NEMO (Nucleus for European Modelling of the Ocean) (Madec, 2008) forced by analytical zonal wind and buoyancy forcings. The model simulates a double gyre ocean basin representative of an idealized version of the North Atlantic basin. The domain is a closed rectangular basin of size 3180 x 2120 km with a constant depth of 4000 m centred at 30°N and rotated by 45°. In total, 30 layers constitute the vertical structure of the model, varying in thickness from 10 to 20 m in the upper waters to 300 m at bottom. The atmospheric physical forcing generates a strong jet which runs diagonally across the domain separating a warm subtropical gyre from a cooler subpolar gyre.

The LODyC Ocean Biogeochemical System for Ecosystem and Resources biogeochemical model model (LOBSTER) (Lévy *et al.*, 2001) is embedded within the physical model, describing the interactions and evolution of six biogeochemical variables: phytoplankton, zooplankton, detritus, semi-labile dissolved organic matter, nitrate and ammonium. The model is spun up for 50 years. Data for the last four are used in this study. For each year, data are obtained at a two-day interval.

Numerical solutions for the ocean dynamics are obtained with a resolution of 1/54°. The effective resolution of the model is of order 10 km which still captures mesoscale features and their feedback on the system. Solutions for the biogeochemical model were obtained using the physical solutions downgraded to 1/9° resolution. The loss of the finest scales does not alter the passive tracers' solutions (Lévy *et al.*, 2012). More details can be found for the physical solutions in Lévy *et al.* (2010) and for the biological system, including downscaling, in Lévy *et al.* (2012).

Regions investigated

As it is motivated by Chapter 4, this study uses three study areas that replicate the setting of the *in situ* investigation. Areas of size 350 km by 350 km are investigated in the subpolar gyre, the inter-gyre transition area and subtropical gyre of the idealised model basin. Their locations are displayed in Figure 5.1.

The subpolar region in this idealised model is defined as the region with annual Chl-a mean values higher than 0.3 mg m^{-3} (Figure 5.1) (Lévy *et al.*, 2014). Within this region, the box is selected sufficiently north to be within the highest mean nitrate concentration to be analogous to the location of D321 cruise (60°N, 20°W) which is within the highest mean nitrate concentration of the north east Atlantic (Sarmiento and Gruber, 2006).

The subtropical region consists of the area with annual Chl-a mean values lower than 0.15 mg m^{-3}. A model area analogous to the location of the D369 cruise was chosen based on low chlorophyll concentrations for the summer period from August 9th to September 15th corresponding to the time of the cruise. The area lies within the 0.1 mg m^{-3} Chl-a contour (Figure 5.3).

The transition area lies within the 0.15 and 0.3 mg m^{-3} Chl-a boundaries. The area is located on the eastern side to correspond to the D381 cruise location in the Porcupine Abyssal Plane site (49N, 16.5W).

Surface data are analysed for all three areas selected. In the subpolar region, ocean colour data for the area and year of the D321 cruise (2007) show a typical phytoplankton seasonal cycle with a pronounced spring bloom occurring in April-May and an autumn bloom in September-October (Figure 5.2a). The model annual phytoplankton cycle for the selected region reproduces the same qualitative features of the phytoplankton cycle observed in the ocean colour data (Figure 5.2d). However, the spring and autumn blooms are more pronounced in magnitude. They also occur earlier (March-April) for the first, and later (October-November) for the second creating a longer period of low phytoplankton concentration in the summer period.

For the transition region, the qualitative features of the phytoplankton cycle are once again reproduced (Figure 5.2 b and e). The model spring bloom occurs earlier than in the ocean colour data for the year (2012) and location of the D381 cruise. The magnitude of the model phytoplankton peak is lower than observed.

For the selected area in the subtropical region, unlike *in situ* observations, model output for phytoplankton did not display a deep chlorophyll maximum (DCM). Rather, homogeneous concentrations down to 70 meters depth were observed with a sharp decrease below. Given the absence of a DCM, only surface model data were investigated. A comparison with ocean colour data for the region covered by cruise D369 nevertheless indicates that the model reproduces the qualitative features observed in the phytoplankton seasonal cycle (Figure 5.2 c and f).

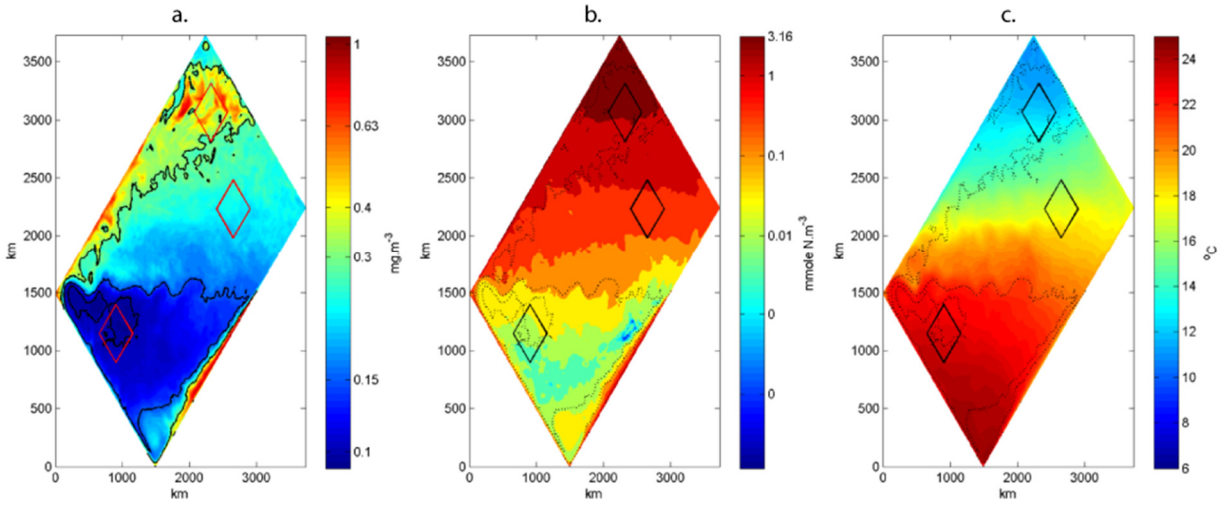

Figure 5.1: *Model annual mean chlorophyll concentration (a.), nitrate concentration (b.) and surface temperature (c.). Annual average chlorophyll concentrations were used to identify survey areas characteristic of subpolar (top), transition (middle) and subtropical (bottom) regions. Contour lines represent the 0.1, 0.15 and 0.3 mg m^{-3} phytoplankton concentrations used to delimit the regions.*

5.2.2. Spectral analysis

The spectra for temperature, nitrate and phytoplankton are calculated in this chapter. For consistency with the *in situ* analysis, a one dimensional spectral analysis technique is used. However, as the dataset presented has evenly spaced data, the Fast Fourier Transform was chosen rather than the Lomb-Scargle periodogram. The boxes surveyed consist of areas of 32 by 32 grid cells. 32 transects of 32 data points were therefore used for estimating the spectrum for each variable. The interval between data points corresponds to the pixel size of 11 km. Data for each transect were pre-whitened by taking the first order difference before calculating the power spectra. The spectral estimates were subsequently reddened by multiplying the estimates by the squared inverse of the wavenumber (see Chapter 2) before the slope was calculated.

Note that the slopes obtained for *in situ* covered the ranges of length-scales 8-80 km and 10-100m. The latter was not studied here as it is well below the model resolution. Spectral estimates were calculated for the range 30-150 km. Estimates between 22 km and 30 km length-scale were discarded due to a sharp drop off in spectral power being consistently observed across the three variables. The upper limit was increased to give a similar range of scales to *in situ*. The mean power spectrum for the area is obtained by averaging the 32 estimates from each transect at each wavenumber studied. A linear regression was fitted to the logged mean spectral estimates and logged wavenumbers to obtain the slope of the spectrum.

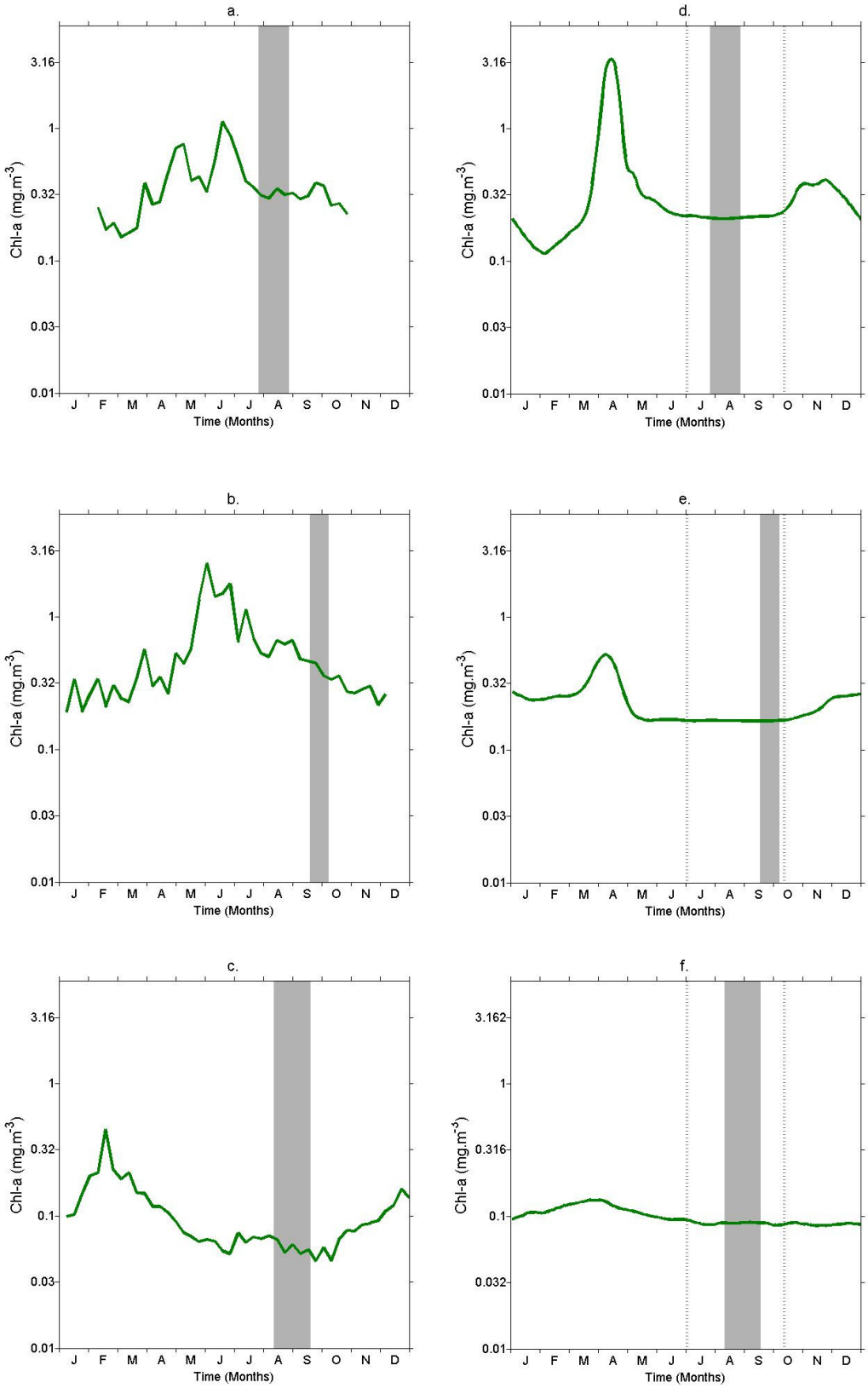

Figure 5.2: *Seasonal cycle in chlorophyll concentration as a proxy for phytoplankton abundance for satellite observations for the years in which each of the cruises in Chapter 4 took place (left) and model (right) at three sites: subpolar (a. and d.), transition (b. and e.) and subtropical (c. and f.) regions. For each site, the relevant cruise period (see Chapter 4) is marked in grey. The common period used for the analysis is delimited by dotted lines. The satellite data are 8 day composites with 4 km resolution of a 5 degree box around the in situ survey areas.*

5.3. Results

5.3.1. Hypothesis 1: Phytoplankton spectral slopes vary significantly over time-scales of days

In Chapter 4, the cruise with greatest number of surveys (D369 in the subtropical region) revealed that the slope of phytoplankton could vary from -0.36 to -0.83 during a period lasting 6 weeks. Is such a large change due to genuine fluctuations in slope over a relatively short amount of time or a consequence of uncertainties arising from sparse data? The above hypothesis can be tackled using model output for which such limitations are absent.

The period of time studied for the selected area in the subtropical region corresponds to the six week period of the cruise (9th August-15th September).

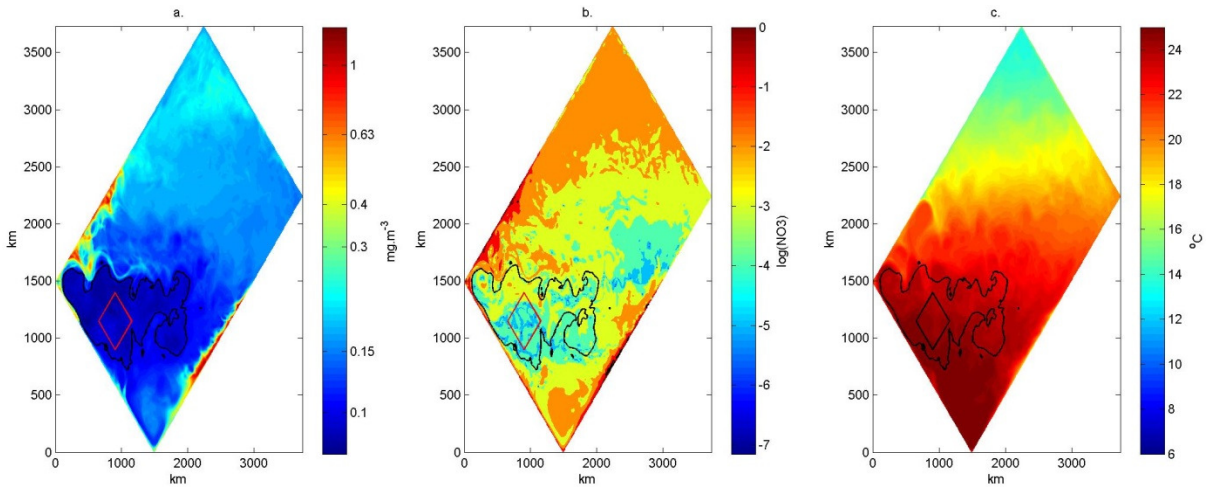

Figure 5.3: *Average phytoplankton concentration (a.), nitrate concentration (b.) and surface temperature (c.) for the period corresponding to cruise D369 (August 9th to September 15th) to the subtropical North Atlantic. The overlaid box corresponds to the area selected for this study to represent the subtropical region. The contour line represents the 0.1 mg m^{-3} of phytoplankton concentration line for the cruise period.*

Spectral slopes for phytoplankton were calculated and plotted against those from *in situ* observations using data from a fixed depth (Figure 5.4). Differences clearly exist between model and *in situ* results. Model phytoplankton spectral slopes for this period vary between -2.52 and -3.71. This is much steeper than results from observations for which slopes of -0.36, -0.83 and -0.73 were found. Differences are addressed in the Discussion Section 5.4. However, given such differences it is difficult to directly compare slope variability observed *in situ* with that found in the model.

A comparison of the variation in slope, between model output and *in situ* observations, can be attempted by normalizing their respective dispersion. This can be done using the coefficient of variation which is the ratio between the standard deviation (σ) to the mean (μ) of a distribution of sample values (here the slope values). It quantifies the extent of variability of the sample values in relation to the mean and therefore allows variability for data with different means to be compared.

For the model output slope estimates, the coefficient of variability (CV) can easily be estimated. With a mean slope value of -3.17 and a standard deviation of 0.33, the CV equals to 0.10. For the *in situ* data, too few observations are available to estimate the standard deviation and therefore obtain a robust CV estimate. An alternative approach can nevertheless be used. If it is assumed that the CV for phytoplankton slopes is well captured by the model, both *in situ* and model output CVs should be equal. In that case, the CV of the model can be used to estimate the variability in slope that should be expected for *in situ* observations. More specifically, predicted variability for *in situ* observations is calculated by assuming that $CV_{in\ situ}=CV_{model}$ and rearranging the formula for CV as follows:

$$CV_{in\ situ} = \frac{\sigma_{in\ situ}}{\mu_{in\ situ}} = CV_{model}$$

$$\Rightarrow \sigma_{in\ situ} = \mu_{in\ situ}.CV_{model}$$

Note that it is assumed that a good estimate of the mean slope for *in situ* observations can be found with 3 values only. The mean *in situ* phytoplankton slope being equal to -0.64 and the CV of the model estimate equal to 0.10, the predicted standard deviation of *in situ* slope observations is calculated to be 0.07.

Slope values for *in situ* observations are -0.36, -0.73, -0.83 with mean -0.64. If slopes are considered to be normally distributed with standard deviation of 0.07, this would mean that only one estimate (-0.73) lies within the 95% confidence intervals or two (-0.73 and -0.83) within the 99 % interval. Note the 95 % and 99 % confidence intervals correspond to 2 and 3 standard deviations either side of the mean value. To first order, this would indicate that the variability observed *in situ* is greater than that predicted by the model. This would also suggest that the model may underestimate the short term temporal variability of phytoplankton slope.

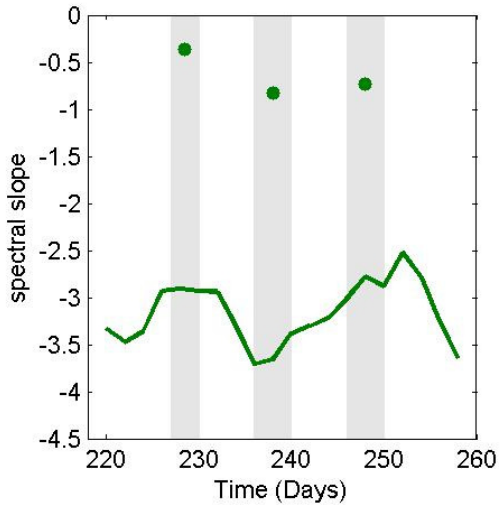

Figure 5.4: *Comparison of phytoplankton spectral slope estimates over the course of the summer for in situ (green dots) and model (green line) for the subtropical area.*

5.3.2. Hypothesis 2: Temporal variations over a period of months exceed variations in slope between regions

Analysis of *in situ* observations in Chapter 4 indicated that short term variability in phytoplankton spectral slope could be significant relative to regional differences but data are too sparse to be certain. Once again, a model allows a more thorough examination of this.

All three cruises were carried out during the post-bloom summer period (Figure 5.2). This study focuses on a period of time in the summer which encompasses all three cruise periods. It was also chosen to be as long as possible within the post-bloom low phytoplankton concentration conditions of the three regions. The period studied spanned 100 days from the 1st July (Julian Day 182) to 9th October (JD 282).

The hypothesis is tackled from two perspectives. First, I test whether there is any statistically significant difference in slope between the regions given the temporal variability at each site. Second, I explore whether any difference could be reliably diagnosed in practice given the practical limitations of sampling *in situ*. To test the sensitivity of the results to the period of time, the analysis is initially done for the whole summer but then repeated for a shorter period of a month. Finally, the robustness of any regional difference in the context of temporal variability in slope is examined over the longer period of a year.

5.3.2.1. Variability of phytoplankton over the summer

The spectral slope of phytoplankton was calculated for each of the three regions for the 100-day summer period, Figure 5.5. The mean slope for phytoplankton differs across the regions (Table 5.1) with mean slopes of -2.63, -2.85 and -3.40 found for the subpolar, transition and subtropical areas respectively.

The slope distribution for each region (Figure 5.6) shows that slopes for the subpolar area are the least variable with a standard deviation of 0.33 compared to the transition (0.42) and the subtropical (0.45) regions.

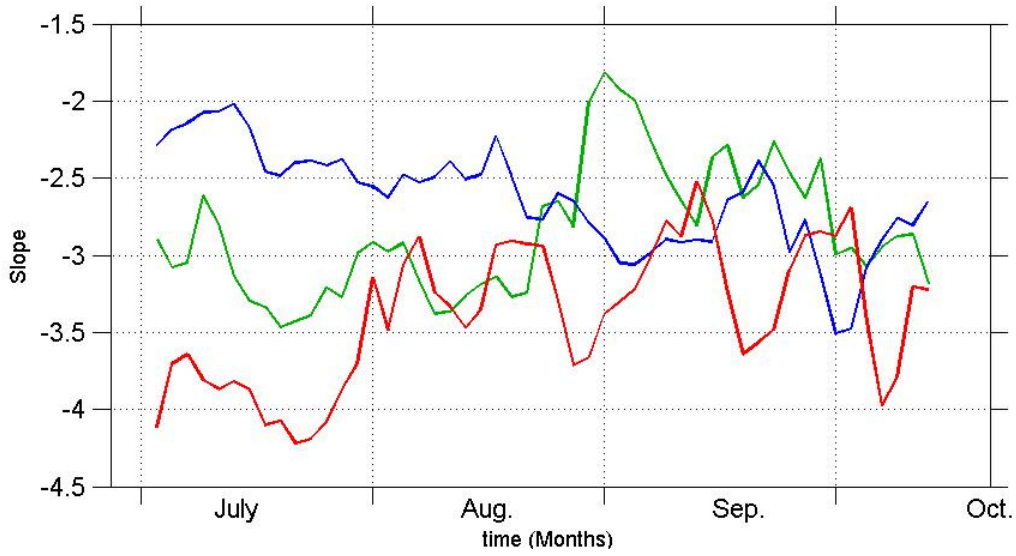

Figure 5.5: *Model phytoplankton spectral slope time series for the subpolar (blue), transition (green) and subtropical regions (red) over the course of the summer.*

Given the slope fluctuations for each regions, the significance of the differences in mean slope between regions can be tested. There are differences with confidence intervals of 0.22 ± 0.08, 0.55 ± 0.09 and 0.77 ± 0.08 between the mean slopes of subpolar and transition regions, transition and subtropical regions, and subpolar and subtropical regions respectively. The corresponding 95 % confidence intervals are [0.07:0.37], [0.38:0.72] and [0.62:0.92] respectively. Despite the temporal variability over the summer period the results therefore reject the hypothesis that the regions display equal means at the 95 % confidence interval. Nonetheless, the large standard deviations of the slope distributions for all three regions illustrate the extent of short term variability in the slope time series.

To test how well an *in situ* study could detect the observed differences in slope between regions, three 30-day long periods, or 'cruises', from within the 100 day summer period, each sampling one area, were compared. The cruise start date is different for each cruise but otherwise chosen randomly. To mimic the *in situ* studies discussed in Chapters 3 and 4, three phytoplankton slope estimates are taken from each cruise. These samples are taken on day 5, 15 and 25 of the cruise period. The mean slope is calculated from the 3 values for each cruise and then the differences in the mean slopes between regions recorded. The experiment is run 10,000 times to build a distribution of the differences.

The experiment shows significant differences are observed in the phytoplankton slope between the different regions. The distributions of differences have mean and standard deviation of 0.17 ± 0.40, 0.68 ± 0.35 and 0.51 ± 0.44 between subpolar and transition area, subpolar and subtropical area, and transition and subtropical area respectively. The experiment indicates that using such strategy for sampling the different regions, it is not possible to capture reliably the regional differences in phytoplankton slope. In all cases, the hypothesis of the regions having a mean slope difference equal to zero cannot be rejected at the 90 % confidence interval or higher.

Table 5.1 : *Summary of spectral slope statistics for phytoplankton for the period July 1st to October 9th. The mean slope, standard deviation (SD) and standard error (SE) are recorded.*

Region	Mean Slope	SD	SE
Subpolar	-2.63	0.33	0.0462
Transition (PAP)	-2.85	0.42	0.0588
Subtropical	-3.40	0.45	0.0630

The choice of period for this study was justified by the fact that the *in situ* surveys (Chapters 3 and 4) did not occur at the same time and together spanned the 100-day period. However, the relationship between slopes of different regions varies across this period. Despite them possessing statistically different means, the time series of the slopes for the subpolar, transition and subtropical area display periods of overlap (Figure 5.5), particularly from mid-August onwards. This suggests that the choice of time-scale used to study regional differences may influence the results and that different behaviour may occur on a smaller time-scale. The

question of whether regional differences in slope are apparent over smaller time-scales is therefore investigated next.

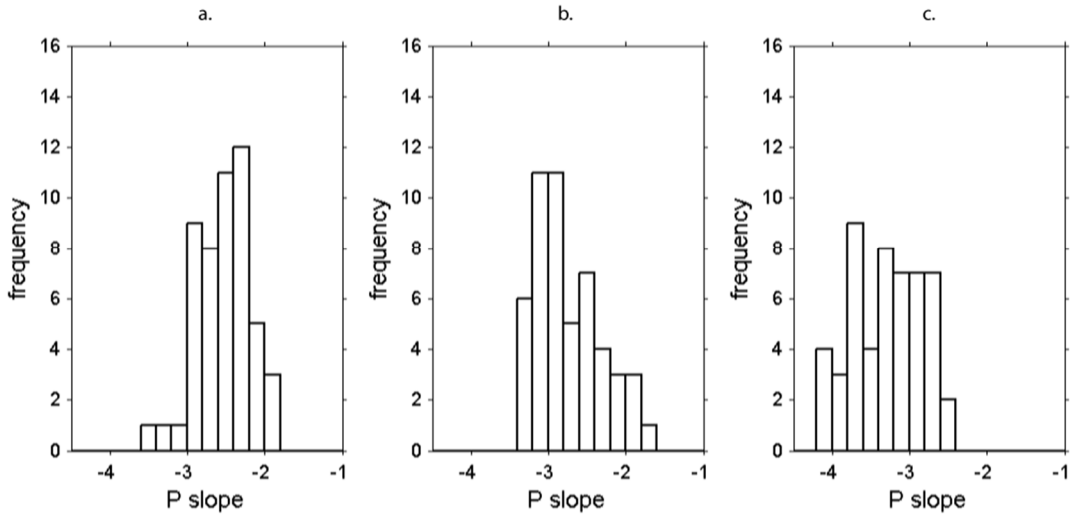

Figure 5.6: *Histogram of phytoplankton slope values for the subpolar (a.), transition (b.) and subtropical region (c.) over the course of the summer.*

5.3.2.2. Monthly variations of phytoplankton slope over the summer

Over these smaller time-scales, the regional spectral slopes are once again calculated. As in the previous sub-section, I first determine whether significant differences exists between regions and secondly, whether these differences can be captured by cruises collecting only three samples within the monthly period. The three cruises are now constrained to cover the entire month. Within the cruise/month, three samples are chosen at random. Only samples obtained at least six days apart are considered to make the selection comparable to *in situ* sampling.

Table 5.2: *Monthly estimates for the mean and standard deviation for the phytoplankton spectral slope for the summer months and the different regions. Mean and standard deviations are obtained from the 15 measurements available in each month given the 2 model output every 2 days.*

	July	**August**	**September**
Subpolar	-2.30 ± 0.18	-2.58 ± 0.17	-2.89 ± 0.27
Transition	-3.12 ± 0.25	-2.92 ± 0.47	-2.44 ± 0.29
Subtropical	-3.88 ± 0.27	-3.24 ± 0.28	-3.08 ± 0.33

Table 5.3: Mean d*ifferences and standard deviations in phytoplankton slope between the three regions investigated for the months of July, August and September.*

	July	**August**	**September**
Subpolar-transition	0.82 ± 0.08	0.34 ± 0.13	-0.49 ± 0.10
Subpolar-Subtropical	1.58 ± 0.08	0.66 ± 0.09	0.19 ± 0.11
Transition -Subtropical	0.76 ± 0.10	0.32 ± 0.14	0.63 ± 0.11

Results for the mean slope of each month and standard deviation are shown in Table 5.2. In July, mean slopes of -2.30 ± 0.18, -3.12 ± 0.25 and -3.88 ± 0.27 are observed for the subpolar, transition and subtropical region respectively. The difference between regions are all significant at the 99 % confidence interval (Table 5.3) with differences and standard deviation of 0.82 ± 0.08, 1.58 ± 0.08, 0.76 ± 0.10 between subpolar and transition area, subpolar and subtropical area, and transition and subtropical area respectively. For July, the cruises successfully distinguish the differences in slope between the regions. Differences of 0.80 ± 0.12, 1.56 ± 0.15 and 0.76 ± 0.17 are obtained when comparing subpolar and transition area, subpolar and subtropical area and transition and subtropical area (Table 5.4). Cruises obtained the correct relationship in each of the 10,000 simulations done.

For August, slopes of -2.58 ± 0.17, -2.92 ± 0.47 and -3.24 ± 0.28 are observed for the subpolar, transition and subtropical area respectively. Differences in slope reduce to 0.34 ± 0.13, 0.66 ± 0.09 and 0.32 ± 0.14 between subpolar and transition area, subpolar and subtropical area, and transition and subtropical area respectively. They however remain significant at the 95 % confidence interval. The cruises are successful in capturing the difference. Between subpolar and transition (0.29 ± 0.22), for 90 % of cases the correct relationship was measured. For the difference between subpolar and subtropical regions, the correct relationship was obtained on 100 % and 95 % of cases respectively.

In September, a slope difference between regions of -0.49 ± 0.10, 0.19 ± 0.11 and 0.63 ± 0.11 was observed between subpolar and transition area, subpolar and subtropical area, and transition and subtropical area respectively. Differences are significant except between subpolar and subtropical (0.19 ± 0.11).

In conclusions, there exist significant differences in slope between regions. However levels of short term variability are such that only mean differences larger than 0.5 are significant. Cruises are nevertheless able to capture such differences with only 3 estimates.

Table 5.4: *Differences in phytoplankton slope between the three regions investigated for the months of July, August and September using cruise style surveying. Mean and standard deviation for slope difference obtained from the distributions generated by running 10,000 simulations are given. The percentage in bracket corresponds to the portion of measurements that correctly estimated the difference between regions.*

	July	**August**	**September**
Subpolar-Transition	0.80 ± 0.12 (100%)	0.29 ± 0.22 (90%)	-0.47 ± 0.19 (100%)
Subpolar-Subtropical	1.56 ± 0.15 (100%)	0.66 ± 0.14 (100%)	0.17 ± 0.17 (80%)
Transition -Subtropical	0.76 ± 0.17 (100%)	0.37 ± 0.23 (95%)	0.64 ± 0.19 (100%)

5.3.2.3. Monthly variations of phytoplankton slope over an entire year

The mean and standard deviation for phytoplankton spectral slope were calculated for each month for the entire year for each of the three regions (Figure 5.7) to evaluate regional differences over the course of the year.

Monthly mean slopes show statistically significant differences between the three regions. These were largest for the summer months. The consistently large intra monthly variability (Figure 5.8), of on average 0.39 in the subtropical area, 0.31 in the transition area and 0.26 in the subpolar area, means that only differences in mean slope of more than 0.23 can be distinguished robustly.

Using only three surveys for measuring the regional differences generates larger uncertainties for the mean difference. As a results, the correct sign of the difference between regions could be robustly obtained only for regions with monthly mean difference larger than 0.5.

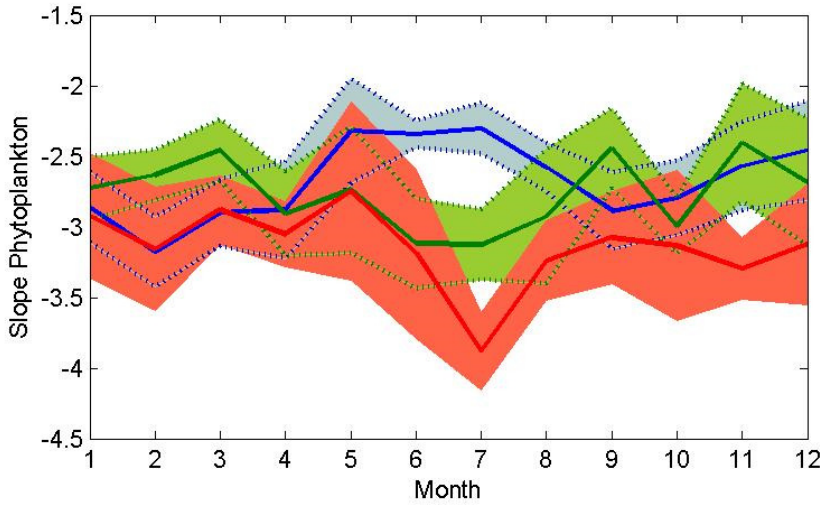

Figure 5.7: *Model monthly mean phytoplankton slope estimates for the subpolar (blue), transition (green) and subtropical area (red). Intervals delimited by one standard deviation either side of the mean are given in shaded colour.*

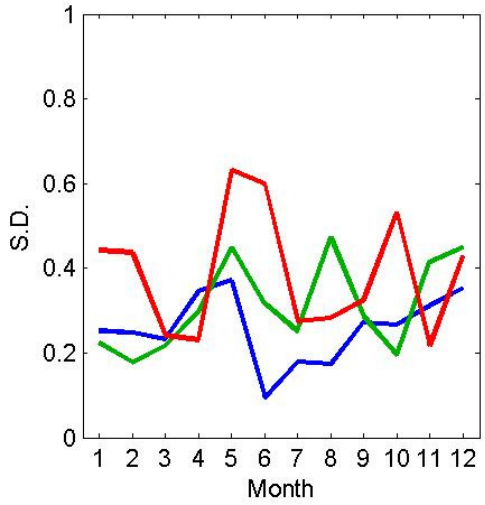

Figure 5.8: *Comparison of inter-monthly variability in phytoplankton spectral slopes for the subpolar (blue), transition (green) and subtropical area (red). The variability is represented by the standard deviation (SD) obtained from the slopes values in each month.*

5.3.3. Hypothesis 3: There is a difference in nitrate and phytoplankton spectral slope which is consistent in time

Chapter 3 evaluated the nitrate (N) and phytoplankton (P) spatial relationship in the subpolar gyre for one short period of 3 days in one year. A difference of -0.64 was measured between nitrate and phytoplankton spectral slopes i.e. nitrate was steeper. Previous sections of this chapter highlight the variable nature of phytoplankton spectral slope, and the question of how this affects the nitrate-phytoplankton relationship is now addressed; in particular how

representative the observed nitrate-phytoplankton (N-P) spectral relationship is of the relationship between the two variables on longer time-scales. Model output allows us to investigate this question given that there are too few *in situ* data to do so. Two steps are required. First, the consistency in the model difference is explored throughout the relatively stable summer period. If the difference is not consistent during this period then the hypothesis is disproven. Second, the similarity in the difference in N and P slopes for the model and *in situ* estimates is assessed. The cruise took place during the summer, a period of low chlorophyll concentrations caused by the nutrient depletion of surface waters (Figure 5.4). The study aims at evaluating the nitrate-phytoplankton slope relationship for conditions similar to those of the cruise. The model displays an extended summer period of low chlorophyll concentration, so the analysis covers the 82-day period from the 29th of June to the 17th of September. The period is shorter than for the previous study because it does not have to include periods from other cruises.

Figure 5.9 displays the spectral slopes calculated for nitrate and phytoplankton over the course of that period. A clear difference is apparent between slopes calculated from *in situ* observations and those obtained from the model. The model slopes are steeper than those for *in situ* data with model spectral slopes varying between -2 and -3 to first order. Note that the *in situ* spectra for nitrate and phytoplankton have slopes of -1.29 and -0.65 respectively. By way of comparison to a non-biological tracer, steeper slopes are also found for model temperature compared to *in situ*.

Nevertheless, the focus of this hypothesis is on the difference between the spectral slopes of nitrate and phytoplankton rather than their absolute values. Slopes of model phytoplankton and nitrate are similar over the studied period. Cases of both phytoplankton and nitrate slope being steeper arise (Figure 5.9). However, the phytoplankton slope is steepest for 83 % of the period. This means that the sign of the difference is only consistent with *in situ* observations for 17% of the period.

The nitrate-phytoplankton slope difference (Figure 5.10) confirms this picture. A mean difference of 0.12 with a standard deviation of 0.21 is measured. In contrast, a difference of -0.64 with standard deviation of 0.27 was observed for *in situ* (Chapter 3). Based on a normal distribution with mean 0.12 and standard deviation 0.21, a negative N-P spectral slope in the model would occur in 28 % of cases.

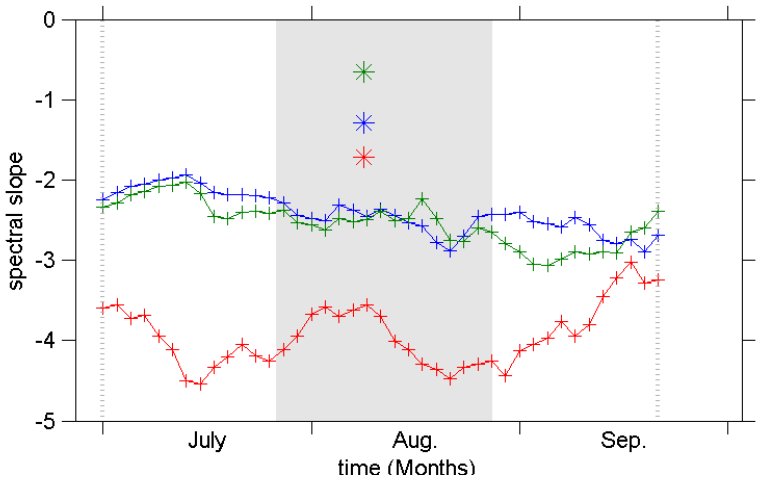

Figure 5.9: *Model slope variation for nitrate (blue), phytoplankton (green) and surface temperature (red) from the subpolar region over the course of the summer. The grey band delimits the period of the D321 cruise. The blue, green and red dots are the in situ nitrate, phytoplankton and temperature slope estimates respectively.*

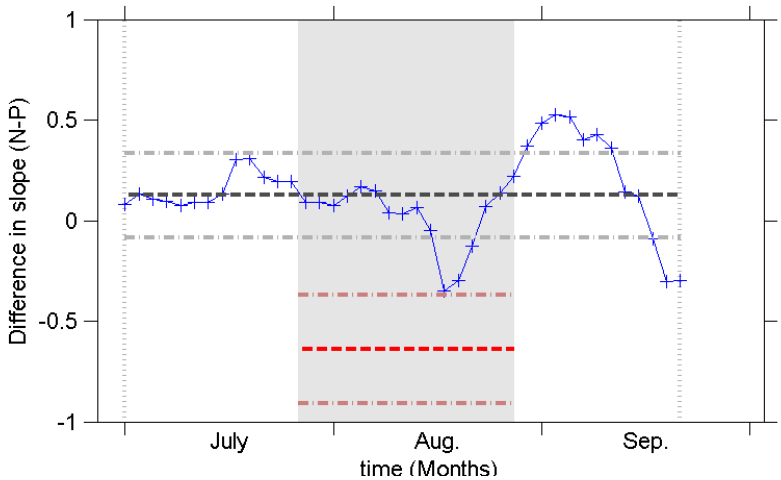

Figure 5.10: *Difference in slope for nitrate and phytoplankton (N-P) over the summer period (vertical grey dotted lines with cruise period marked as solid grey band). Horizontal black and grey dashed lines represent mean and standard deviation for the model respectively. Red lines represent the in situ N-P slope difference from D321 with its associated standard deviation.*

Large variations from the mean are observed in the second half of August and September. Figure 5.10 shows that within an interval of two weeks, between mid- August and early September, the N-P slope changes sign from being strongly negative (-0.34) to strongly positive (0.54) to strongly negative again. It is therefore clear that not only can the difference in slopes for N-P vary significantly in time, it can also do so on the same short time-scales as the individual slope values.

Figure 5.10 also illustrates, by overlaying *in situ* results, that no slope difference for the model lie within one standard deviation of the *in situ* mean. Assuming that the distribution of differences in slopes is normally distributed, the statistical significance of the difference

between *in situ* and model distributions for the slope difference can be estimated: the mean difference is estimated as $\mu = 0.12 + 0.64 = 0.76$ and the standard deviation as $\sigma = \sqrt{0.27^2 + 0.21^2} = 0.34$, using the results from Chapter 3. *In situ* distributions are different at the 95 % confidence level but equal means cannot be rejected at the 99 % confidence level. Although this only represents a simple test and only a small amount of *in situ* data are available, the results suggest that such a large difference between the slopes of phytoplankton and nitrate *in situ* is not representative of the overall N-P slope relationship for this region in the model during the summer.

5.3.4. Hypothesis 4: There is a seasonal pattern in phytoplankton spectral slopes

In previous sections it was shown that the phytoplankton slope exhibits significant temporal variability on time-scales of the order of days and months. Here the focus is on whether there is also variability on an annual time-scale. Because of differences between regions, time series for the subpolar, transition and subtropical area are first studied individually. Inter-annual patterns are also investigated later to examine the robustness of any seasonal signal.

5.3.4.1. Subpolar

For the subpolar area, Figure 5.11a indicates the presence of a pattern in both the time series of the phytoplankton slope and the monthly variability in the slope. During the month of January, February and March, slope values are centred around -2.95, with mean monthly slopes of -2.86, -3.18 and -2.90 respectively. The monthly variability in slope (Figure 5.8) also remains constant with standard deviations of 0.25, 0.25 and 0.23 respectively.

Appreciable changes in the spatial distribution of phytoplankton start to develop during the month of April and May with the phytoplankton spectrum reaching its flattest slope, with a value of -1.78, by mid-May. During that period larger variations develop with values of 0.31 and 0.37 for April and May respectively. The flattening of the slope is echoed in the monthly means with values of -2.88 and -2.32 for April and May respectively. A period with flatter slopes and lower variations follows until August. Monthly means of, -2.34, -2.30 and -2.57 are measured for June, July and August respectively. The following three months display the lowest variability of the year with values of 0.09, 0.18 and 0.17 respectively. The end of the year, from September to December shows steeper values and larger monthly variability.

Results from the three following years exhibit the same patterns (Figure 5.12). In particular patterns in monthly variability are clearly apparent and consistent across the four years (Figure 5.13). The pattern describes a seasonal cycle with a spring peak in monthly variability during April-May followed by a significant drop across the summer and another peak in autumn during October-November.

A seasonal cycle is also present in the nitrate slope time series (Figure 5.11a). The cycle is coincident with the phytoplankton seasonal cycle. It displays a flattening during the spring bloom of a larger magnitude (from -3.44 to -1.06) followed by a more gradual flattening over the summer.

Periodicities of a time series can be extracted using spectral analysis. Such analysis was done on the time series for each region. For the subpolar region, in each of the four year time series a peak was found for frequencies of 1/180 day^{-1} with a smaller one at 1/360 day^{-1}. The nitrate spectral slope time series (Figure 5.11) follows a similar cycle. For the year both N and P data are available, their slope time series are highly correlated and have the same periodicities at 1/180 day^{-1} and 1/360 day^{-1}. The spectrum of the nitrate time series displays however more variability at the two peak frequencies. These peaks support the presence of a seasonal cycle. This cycle is dominated by the spring bloom. However, the higher peak for the nitrate slope timeseries being at frequency 1/180 day^{-1} also shows the importance of the autumn slope changes in setting this seasonal cycle.

5.3.4.2. Subtropical and transition areas

The time series of the phytoplankton slope in the subtropical area does not display a seasonal cycle. Variability is more marked on a shorter time-scale. Monthly variability in slope has standard deviation of 0.39 which is the largest for the three areas, with values of 0.31 and 0.26 for the transition and subpolar area respectively. Similar to the subpolar area, the phytoplankton slope displays periods of larger and smaller variability (Figure 5.8). The benefit of having four years of data is that what can appear as no particular structure using only one year, is given more importance when reproducing in other years. For all four years, lowest variability is found for the summer period (5.13c). A seasonal signal is also not seen in the nitrate slope time series.

No particular patterns appear in the time series of phytoplankton and nitrate slope for the transition area (Figure 5.11). Also, comparison of time series of different years shows that no

interannual relationship exists in the timing of the variations observed. As a consequence, the average of the four years cancels most of these variations out which results in a mean signal close to white noise (Figure 5.12).

Figure 5.11: *Time series of model phytoplankton spectral slope for the subpolar (a.), transition (b.) and subtropical region (c.). Four consecutive years are represented: year 1 in red, year 2 in green, year 3 in blue and year 4 in orange. Average time series from the four years are displayed in black. Individual plots for each year are available in the Appendix A5.1 to this chapter***.**

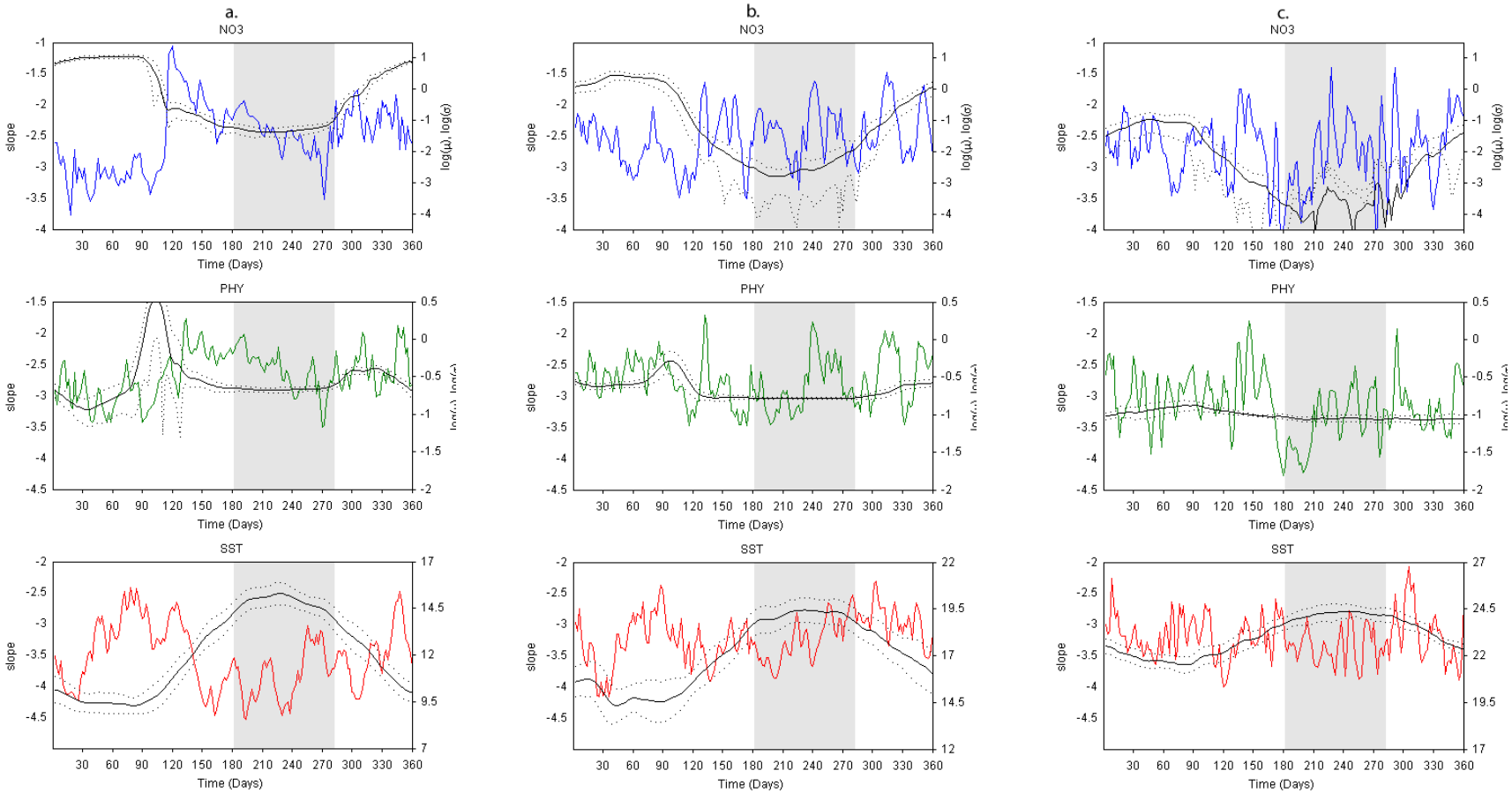

Figure 5.12: *Annual cycle of spectral slope for nitrate (blue), phytoplankton (green) and temperature (red) for the*

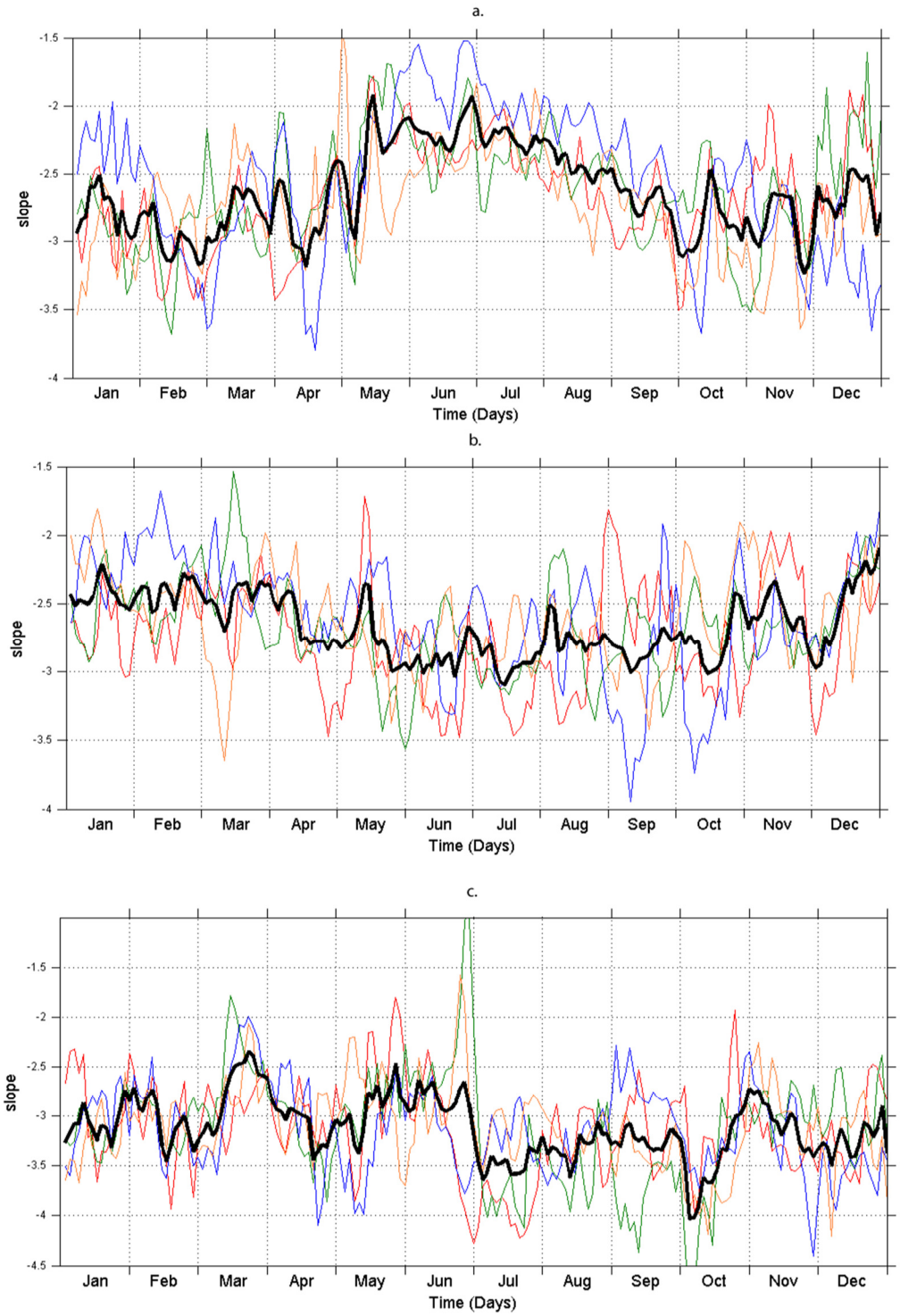

subpolar (a.), transition (b.) and subtropical regions (c.). Mean annual concentration ± standard deviations for the area are overlaid in black solid and dotted lines respectively

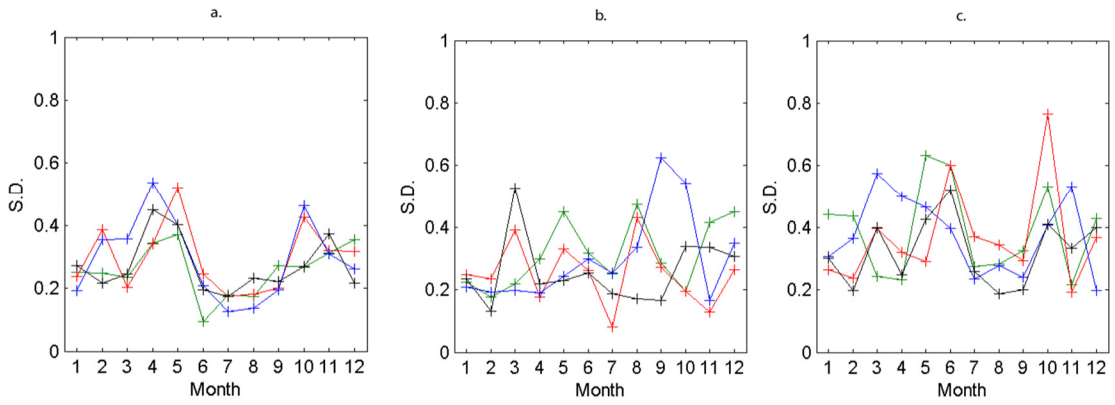

Figure 5.13: *Model intra monthly slope variability for the subpolar (a.), transition (b.) and subtropical region (c.) for the four consecutive years studied.*

For the subtropical region, under spectral analysis of the time series the periodicities were weaker and also varied from year to year. For year 1 and year 3 variability was the largest for a frequency of 1/72 day^{-1}. For year 2 and year 4 it was for a frequency of 1/360 day^{-1}. The second largest was also inconsistent with 1/120 day^{-1}, 1/72 day^{-1}, 1/51 $day^{-1}$and 1/45 day^{-1} for year 1 to 4 respectively. The time series of the transition area only showed a weak peak in periodicity for a frequency of 1/360 day^{-1}. As stated earlier, the periodicities in one year did not appear in another and vanished in the averaged time series for the 4 years.

5.3.4.3. Phytoplankton slope relation to bloom

In the subpolar area, the springtime flattening of slope, present in every year, occurs around the time of the phytoplankton bloom. The more precise timing of the flattening relative to the peak in phytoplankton abundance, and what causes the flattening can be examined a little more deeply.

The period of the spring bloom corresponds to a period of strong biological activity. Phytoplankton concentrations increase rapidly over a matter of weeks consuming nutrients which consequently decay rapidly (Figure 5.14). Such changes in concentrations may affect the spatial distribution of phytoplankton and nitrate. Increasing concentrations of phytoplankton can introduce variability into the phytoplankton spectrum at a variety of scales. Equally, as concentrations decrease, the variability in the spectrum decreases. The issues of where in the spectrum this variability is introduced and lost and how this affects the spectral slope are now investigated.

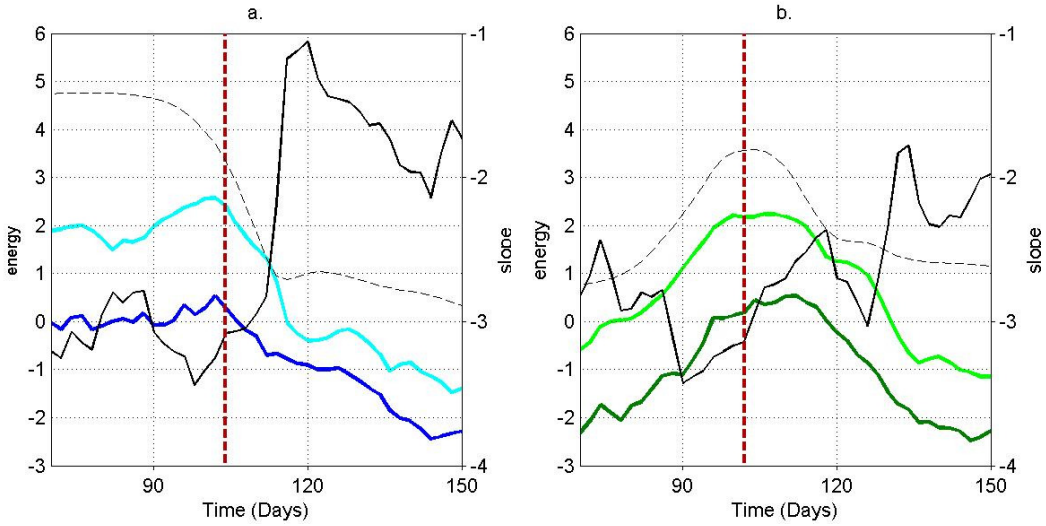

Figure 5.14: *Model spectral slope variation for nitrate (a.) and phytoplankton (b.) over the course of the spring bloom for the subpolar region for the 1st year of the four studied. Slope and mean concentration time series are represented in solid and dashed black lines respectively. The phytoplankton concentration maximum is marked with a dashed red line. The energy levels in the spectrum at 130 km length-scale (light blue/green) and 30 km length-scale (dark blue/green) are also shown.*

Given the power-law nature of the spectra, only a measure of the variability at either end of the length-scale range is necessary to study changes in slope. In this study, the length-scales 30 km and 130 km were used to represent the small and large scale respectively. In Figure 5.14 the slope and the mean concentrations for nitrate and phytoplankton are overlaid. Spring time series for phytoplankton for the other years are displayed in Figure 5.15. For each year the time of the maximum phytoplankton concentration is also identified.

For year 1, the start of the flattening of the nitrate spectral slope precedes the phytoplankton concentration peak by six days. A large change in nitrate spectral slope occurs from -3.44 at day 98 to -1.06 in twenty two days. Nitrate variability is steady before the bloom peak, but the flattening in slope is associated with a loss of variability at both large and small scales. The flattening is caused by a larger drop in variability at large scale relative to small scale.

In contrast, the phytoplankton slope starts flattening as levels of variability are still increasing in the spectrum, because variability is increasing faster at small scales than large. Despite some short term variability, it continues flattening as variability levels start dropping. Two periods for which the phytoplankton slope flattens can be distinguished. The slope starts flattening fourteen days before the phytoplankton maximum (day 90) for a period of thirty days from a slope of -3.43 to -2.36. Slopes then steepen for eight days to -3.03. The second period of flattening, starting at day 126 lasts eight days to reach the flattest slope of the annual cycle of -1.78 at day

134. The first period corresponds to one when variability is largely increasing or stable. The second corresponds to a period when variability is decreasing.

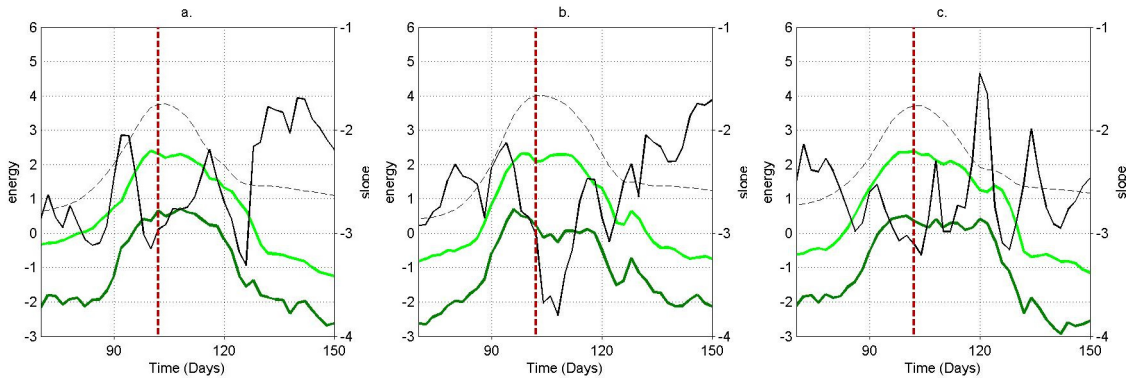

Figure 5.15: *Model spectral slope variations for phytoplankton for year 2 (a.), 3 (b.) and 4 (c.) over the course of the spring bloom for the subpolar region. Slope and mean concentration time series are represented in solid and dashed black lines respectively. The phytoplankton concentration maximum is marked with a dashed red line. The variability in the spectrum at 130 km length-scale (light green) and 30 km length-scale (dark green) is also shown.*

Nitrate model output were not available for the following three years and therefore spectral slopes could not be obtained. The emphasis for these years is therefore examining the flattening of the phytoplankton slope relative to the bloom peak. Unlike in year 1, in years 2, 3 and 4, the flattening process starts after or around the phytoplankton peak in concentration and only at the moment variability starts dropping in the spectrum. For year 1, the flattening started fourteen days before the phytoplankton maximum whilst variability in the spectrum was still increasing.

However, the three years display significant differences (Figure A5.1). In year 1, the slope transits from being steep on average for January to March to being flat during June, July and August. In other years, the spring period of flattening is interrupted by a long period of significant steepening (year 2 and 4). Others display a less noisy signal (year 1 and 3). The clearest period of flattening in slope occurs during year 3 starting from day 106 (mid-April) to 146 (end-of May) from slope -3.68 to -1.74 but even this is interrupted by periods of steepening.

The increase and decrease of variability at large and small scale is not symmetric about the phytoplankton maximum concentration even though the peak in variability coincides with the peak in abundance. The increase in variability is near smooth while the decay shows episodic injections, for instance at day 120 in year 4 or day 124 for year 3. Such jumps in variability explain

some of the random noise observed in slope. While it might be tempting to interpret the delayed peak in large scale variability in year 4 after one at small scale on day 120 as a cascade of variability to other scales, in other cases (e.g. year 3, ~day 128) such peaks are coincident at both scales. In summary, there is no consistent flattening in spectral slope after the spring peak in phytoplankton concentration.

5.4. Discussion

A fundamental question to phytoplankton patchiness studies and one at the heart of this thesis is whether the spectrum displays universal scaling properties. In this chapter, it is shown using a model that the spectrum displays significant variability over temporal scales of days to weeks and that this variability can also exceed changes in slope between regions. Variability occurs over many temporal scales with important changes in slope over time-scale of weeks, months and a year. There is some evidence for a seasonal pattern in the subpolar region but generally there is no clear cause of such variability. Furthermore, variability was also shown to be present in the relationship of slopes for phytoplankton and nitrate. Therefore, from the point of view of the model, universal properties in the phytoplankton spectrum do not exist.

This variability is now discussed progressing through the different time-scales that are involved. First, variability over time-scales of days is discussed, followed by time-scales of months and a year.

In this study, model results indicate that significant short term variability, on time-scales of days to weeks, exists in the time series of phytoplankton spectral slope. Limited information on variability over such scales is available *in situ*. A comparison of slopes between model prediction and *in situ* estimates showed model estimates to be significantly steeper (Section 5.3.1.). Because model slopes are steeper than *in situ* ones, the variations in spectral slopes from the model over time are greater in absolute values than *in situ* but are smaller using relative ones as shown by the coefficient of variation.

Potential reasons contributing to the difference in steepness between *in situ* and model may come from the data originating from different depths. *In situ* slopes are obtained with data below the mixed layer which will have potential influences like light and internal waves that are not present in surface estimates. This is illustrated in Chapter 4 where results show differences

in variability depending on whether data are retrieved along density surfaces (to remove internal waves) or for fixed depth (to keep the effect of light more constant).

Nevertheless, this cannot explain on its own the difference between *in situ* and model slopes because *in situ* measurements from other regions obtained from within the mixed layer are also flatter than model estimates (Figure 5.9). Furthermore steeper spectra in the model are obtained for all variables studied.

Such levels of temporal variability in slope have consequences for *in situ* results. It is shown that unless a sufficient number of slope measurements are made, results may not be representative of the spatial distribution of phytoplankton for the region sampled. Furthermore, it is also shown that these short term variations are different across the year and for different geographic locations. Therefore, future *in situ* studies may require a different number of slope measurements over the cruise duration depending on the region and time of year being investigated to obtain the same degree of accuracy in their slope estimates. For instance, in the subpolar area different levels of monthly variability in slope are observed during the spring and summer time (Figure 5.13). Variability in slope changes by a factor of two between the two periods. A larger number of samples is required when investigating the patchiness in spring compared to summer.

The danger of under-sampling for *in situ* studies also impacts on their ability to effectively compare patchiness of phytoplankton between different regions. The model shows that when three slope measurements are made over a one month period, only regional differences in slope larger than 0.5 can be distinguished. Furthermore, this is in the case that the same months are being sampled. In the case of the *in situ* study in Chapter 4 where the 3 cruises cover the entire summer, a geographical comparison is difficult due to the time window being too large.

Ship surveying is however not practical to investigate variations of phytoplankton patchiness over time-scales of several months due to cost. Satellite data allow variability over such longer time-scale to be investigated and this is studied in the next chapter (Chapter 6). Other alternatives can be developed too, such as collecting Chl-a data using mooring arrays like the OSMOSIS project (http://www.osmosis.ac.uk). For this project the two sets of moorings organized in concentric squares allow variability at different length-scales to be captured which can be used to derive a partial spectrum. This array was only instrumented for physical variables though. More on the method and another option of using gliders are discussed in Chapter 7.

However, the potential high frequency of such measurements over periods of months would allow variability over time-scales of months to a year to be investigated.

The model also indicates that variability in the phytoplankton spectral slope may be present over longer time-scales with regions displaying seasonal patterns. Results suggest that in the subpolar region, the steepness of the slope may vary with season, possibly linked to the seasonal cycle of phytoplankton concentration. A significant flattening starting around the phytoplankton concentration spring peak and developing over the month of April and May is observed in the four years investigated (Figure 5.12 and 5.15). Peaks of monthly variability in slope are also recorded during months of highest biological activity (Figure 5.13) such as during the spring and autumn bloom. Seasonal patterns are not present in all regions. However, provided sufficient cloud free data are available, the existence of these patterns can partially be tested with ocean colour data (Chapter 6). Other alternatives to explore include using ships of opportunity as a mean to collect Chl-a data via a flow through system fitted onboard that continuously samples the surface water. As they follow commercial routes on a regular basis across the year, a large amount of data can potentially be collected containing both sufficient spatial resolution to measure the mesoscale and sufficient spatial and temporal coverage to capture seasonal trends at the regional scale. Such alternatives are discussed (Chapter 7).

The temporal trends in phytoplankton slope variations may also be analysed from the perspective of the nitrate-phytoplankton spectral slope relationship. Results show that nitrate and phytoplankton slope variations can show coincident changes but there is only evidence in the subpolar region. Over short time-scales, model results however show that the difference in their slope can vary significantly, with slopes for nitrate and phytoplankton being equal, nitrate being steeper or flatter within a period of a month (Figure 5.10). However, currently only a small number of cases exists for which nitrate and phytoplankton have been measured simultaneously at the high resolution necessary to study the mesoscale. Furthermore, model results suggest that a large number of measurements are necessary, and that therefore when only one measurement of the relationship is made, like in Chapter 3, it cannot be considered representative for the region.

The model additionally highlights the intricate relationship between interacting biogeochemical variables. For instance, the flattening of phytoplankton slope during the spring bloom in the subpolar region (Section 5.3.4.1.) is preceded by a flattening of the nitrate slope of even greater magnitude over the same period. The nitrate spectrum flattens as a result of a larger drop in variability at larger scale relative to small scale. One interpretation for the loss of variability at

large scale may be by the role played by the winter convection in driving the initial spatial variability at large scale. Consumption of winter stocks by phytoplankton removes variability at large scale but as it is doing so, the transfer of variability to higher trophic levels is taking place. Turbulence will also cascade the variability to smaller scales. In contrast, changes in variability at smaller scales display a smaller amplitude. This may be explained by them being driven by submesoscale dynamics which are relatively more constant in introducing variability across the year compared to winter convection. Organising cruises around that time of year rather than in the summer like in Chapter 3 and 4 may consist of a more strategic time to understand those mechanisms.

5.5. Conclusion

In this chapter the variable nature of phytoplankton patchiness across time and geographical regions has been studied using an idealized model. Temporal variability is present across a variety of time-scales of days, months to a year. In the case of the subpolar region, there is some evidence that this variability has a seasonal signal. Regional differences in slope also exist but no strong seasonal signal is found for the subtropical and transition areas. From a model perspective, there is no evidence for universal properties in the phytoplankton spectrum. The next chapter explores whether this can be corroborated using satellite data.

Chapter 6: Can remotely-sensed ocean colour bridge *in situ* limitations in phytoplankton patchiness studies?

6.1. Introduction

The *in situ* observations analysed in Chapters 3 and 4 indicate how variable the characteristics of phytoplankton patchiness may be. With the data being sparse and sampled at different locations and at different times of year, it is not possible to determine, based on *in situ* data, whether this variability is spatial or temporal. Models do not have these problems, but while they provide considerable insights, particularly for relationships with other parts of the ecosystem such as nutrients, these results must be interpreted with caution because of the discrepancies models share with the available *in situ* observations (Chapter 5).

Satellites provide global coverage of the oceans, with phytoplankton mapped at approximately 1 km resolution. They offer the advantage of providing data that are synoptic, cover vast regions and are available all year round. Except for the problem of clouds, satellite data therefore present major advantages for evaluating temporal and spatial variation in the slope of phytoplankton. Despite this, no direct comparison of simultaneous satellite and *in situ* data derived estimates of phytoplankton spectra exists. The question of 'How consistent are satellite and *in situ* phytoplankton slope estimates?' therefore needs to be answered.

Another issue with *in situ* surveys is that physical features such as eddies have a size relatively large compared to the size of such survey areas, which are typically around 100 km by 100 km. Often only one or two of these features can be captured within one survey. Yet eddies are known to influence the phytoplankton field and spectrum. For instance in Chapter 3, transects from surveys crossing eddies had a phytoplankton spectrum that was different to those that did not. The question therefore is whether such small *in situ* survey areas are large enough to give a robust estimate of the spectrum at regional scale. Understanding whether sub-regional variability exists in the phytoplankton spectrum is essential to be able to quantify other variability such as the changes in the spectrum for one region over time. The reduced area of the North Atlantic represented by the idealised model analysed in Chapter 5 does not lend itself to such a study. Satellite data, however, provide an ideal means to assess this.

The model analysis in the previous chapter did, however, provide considerable insight into temporal variability in spectral slopes. In particular, there was an indication that there may be a seasonal cycle in phytoplankton slope for the subpolar gyre. Satellite records provide a means to test this, and its possible link to the annual cycle of phytoplankton abundance, observationally.

In summary, the following hypotheses are tested in this chapter:

- Satellite and *in situ* data are consistent for the study of phytoplankton patchiness.
- Phytoplankton spectral slope is insensitive to how an area is mapped
- Satellite data show seasonal cycles in spectral slope.

6.2. Methods

The satellite data used for this chapter consist of daily 1 km resolution ocean colour from the MODIS satellite. The areas investigated were chosen so that a comparison with *in situ* results (Chapters 3 and 4) could be made. They consist of areas covered by the cruises D321 in the subpolar North East Atlantic around the Ocean Weather Station India (60°N 20°W) and D381 in the Porcupine Abyssal Plain in the inter-gyre transition region (49°N, 16.5°W). Satellite and *in situ* data are consistent in providing observations of Chl-a for use as an index for phytoplankton abundance. Low surface phytoplankton abundance in subtropical regions (see, for example, Chapter 4) make remotely sensed data for these regions not suitable for quantifying phytoplankton patchiness. Satellite data from enlarged areas, of up to 400 km by 400 km, located in the vicinity of these sites were also used to address the first two hypotheses.

The presence of a seasonal cycle in the phytoplankton spectral slope is also investigated with satellite data for just the subpolar and the transition regions, for the same reason. The area with coordinates 15°W-28.5°W, 54°N-60°N was investigated for the subpolar region, an area extended to the South-West of the D321 cruise (60°N 20°W). For the transition area, it was the area with coordinates 15°W-28.5°W, 44°N-51°N, an area extending to the West of the D381 area (49°N, 16.5°W). Their positions were chosen so as to remain within the subpolar and transition regions, yet provide better temporal coverage. The ocean colour data used were daily 1 km resolution pictures from the year 2007 from the 5th April (Julian Day (JD) 95) to the 22nd July (JD 203). Note that data outside these times were very sparse due to cloud cover and so analysis of

seasonal variation is confined to this window. Subsets of approximately 400 km by 400 km within these areas were used for the analysis. The subsets were chosen as the areas with least cloud coverage over the period investigated.

Calculating spectra

To be consistent with the rest of the thesis, a one dimensional spectral method was applied to the satellite data. The MODIS data provided by NEODAAS (see Acknowledgements) are on a regular grid with pixels equidistant in degrees. This corresponds to a constant 1 km resolution in the latitudinal direction. In the longitudinal direction the pixel size in kilometres decreases with cosine of latitude, from 1 km at the Equator. Transects are extracted from the grid in both the latitudinal or longitudinal direction. For each transect, data were the given latitude and longitude coordinates of their pixels. Distance in degrees between the data points was then used to calculate distance in kilometres. A direct consequence is that although transects in the longitudinal direction have equally spaced data points, the interval between data points changes with latitude with transects from higher latitudes having a smaller interval. For instance, a transect at the equator has data points separated by 1 km whilst at 60^{o}N the interval is 0.5 km. In contrast, all transects taken in the latitudinal direction have the same interval of 1 km between data points. To avoid selecting data duplicated during the processing and gridding of the data by NEODAAS, transects at least 5 km apart are selected.

Despite the regular spacing of data pixels, spectra were evaluated as in Chapter 3 and 4 using the Lomb-Scargle periodogram method. This was due to the presence of clouds which at times caused the data to be unevenly spaced. The spectrum of phytoplankton was estimated for the length-scale range 8 to 130 km to be consistent with the *in situ* analysis in Chapters 3 and 4. Only transects with at least 80 % of cloud free data were considered. Transects longer than 130 km were split into segments each 130 km long and overlapping by 50 % whose spectra were then combined to decrease uncertainties in the slope estimates (see Chapter 2).

For the comparison of satellite data with D321 *in situ* data only transects coincident with the cruise were extracted. In this case the combined spectrum was calculated using the mean variability at each wavenumber to be consistent with the *in situ* method. Elsewhere, as datasets with a larger number of segments were studied (up to 300 segments), the median variability at each wavenumber was used instead. Doing so eliminates the effect of occasional outliers (not present in the D321 data) which, with a power-law signal, can significantly modify the slope

estimate when using the mean. A slightly modified bootstrap routine was therefore used, using median rather than the mean for calculating the average spectrum. For each instance in the bootstrapping, 90% of estimates were randomly selected (allowing repetition) from all the estimates obtained with all the 130 km segments and the average spectrum obtained by selecting the median value of the variability for each length-scale. The slope and its uncertainty were obtained by taking the mean and the standard deviation of the bootstrap generated probability distribution for the slope.

Simultaneous satellite SST data were also investigated but concerns over artefacts resulting from processing of the data by NEODAAS (see Figure 6.1b) led to them being discarded.

6.3. Results

6.3.1. Hypothesis 1: Satellite and *in situ* data are consistent for the study of phytoplankton patchiness

In order to test this hypothesis, we need an instance in which both satellite and *in situ* data exist simultaneously. Fortunately D321 offers the opportunity to quantify the differences in the phytoplankton spectrum between *in situ* and satellite derived data. Figure 6.1a shows an ocean colour image from MODIS taken on August 6th 2007, during the time of the D321 survey (5th -7th August). The red box corresponds to the area sampled during cruise D321, with the solid green lines representing the cruise tracks along which *in situ* Chl-a measurements were made. The dynamical features, most strikingly the two counter-rotating eddies that form the dipole, are clearly observable in the colour image. A coincident picture was not available for the D381 cruise.

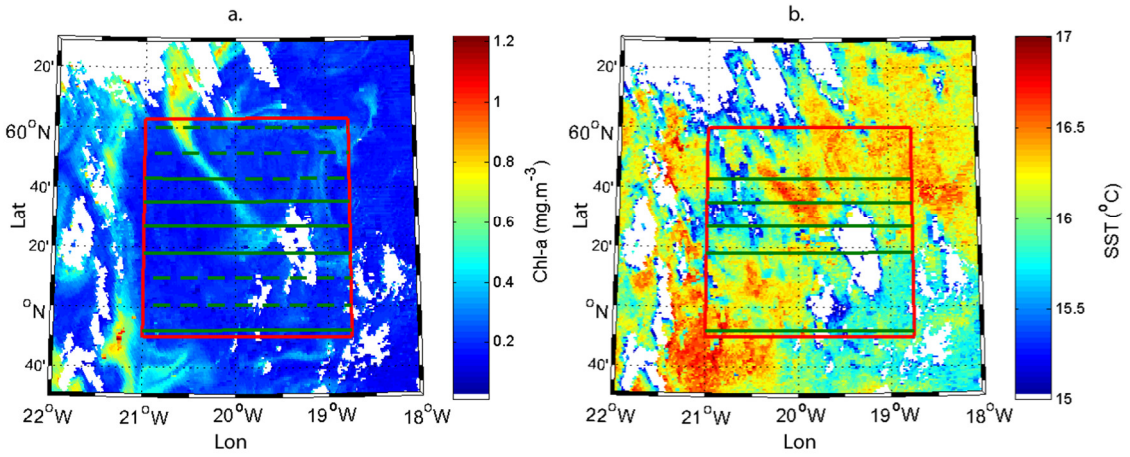

Figure 6.1: *Snapshot of the MODIS satellite image taken on the 6th of August 2007: Chl-a (a.) and SST (b.). The red box bounds the area surveyed during the D321 cruise. The green lines indicate the location of the transects planned for the survey. Solid lines correspond to the in situ transects successfully sampled for which Chl-a estimates are available. The dashed lines are those that could not be sampled on D321. Both solid and dashed transects are used for the satellite data spectral analysis. Note the blurring and elongated features in b) which led to SST data being discarded.*

Data for Chl-a along each marked transect can be seen in Figures 6.2a and 6.2b for *in situ* and satellite measurements, respectively. The satellite captures the main features observed in the *in situ* Chl-a data: the amplitude and position of the major peaks in each transect are similar to *in situ* transects. Less variation is observed at small scale in the satellite data, however. This is illustrated by smaller Chl-a changes between neighbouring data points when around the 0.2 mg m^{-3} concentration.

Figures 6.2c and 6.2d show the spectral estimates for each transect. Overlaid are the mean spectrum and line of best fit used for calculating the slope. The slope of the satellite phytoplankton spectrum has a value of -1.23. It is steeper than the *in situ* estimate (-0.72 – see Chapter 3). Levels of variability at large scale for the satellite and the *in situ* spectra are equivalent. In contrast, confirming the visual impression, variability at smaller scales is lower in the satellite spectrum, particularly at length-scales smaller than 25 km. This is why a steeper slope is found for the satellite spectrum. A potential explanation for this discrepancy comes from the differences in the data collection process which will be discussed later on. Despite the discrepancy in energy levels at small scale, the ability of the satellite data to reproduce the patterns seen in the phytoplankton data gives us confidence to use it to address the second and third hypotheses, with the awareness that it might over-estimate slope.

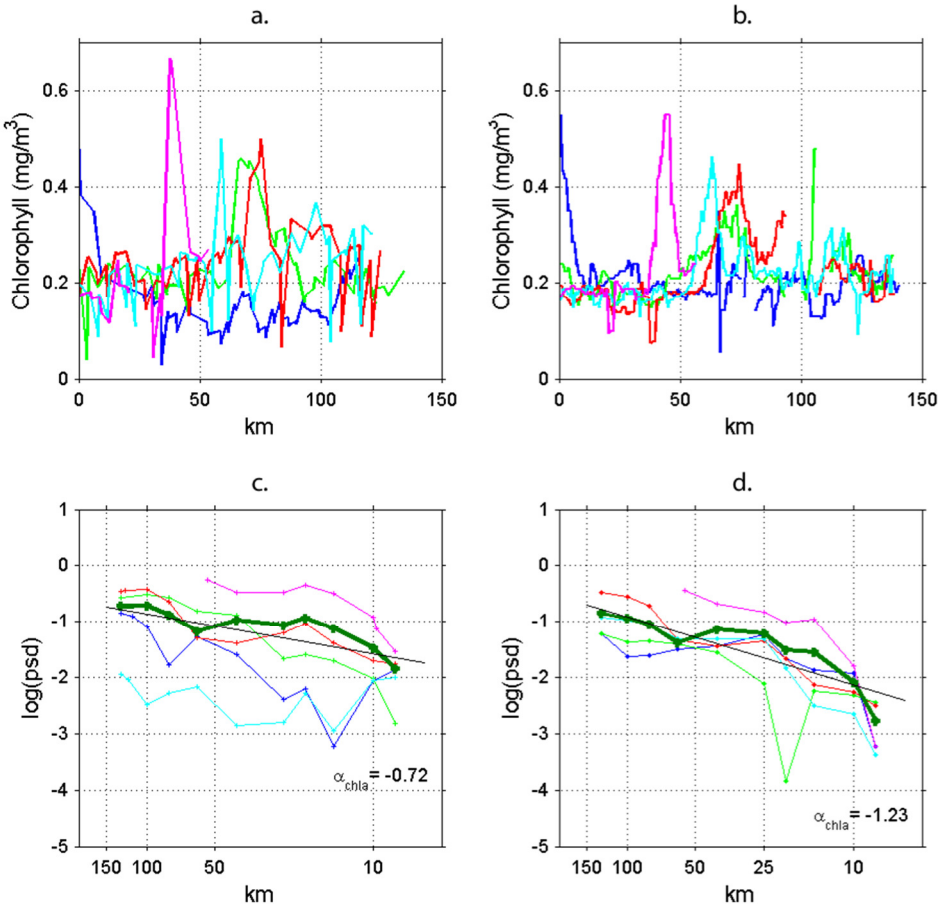

Figure 6.2: *Chlorophyll-a time series for the D321 area obtained with in situ (a.) and satellite data (b.). The gaps in the satellite data time series are due to cloud coverage. The corresponding respective spectral estimates are shown in (c.) and (d.). The different colours correspond to the time series and power spectra of the different transects carried out during the cruise. The mean spectra are shown in bold green.*

6.3.2. Hypothesis 2: Phytoplankton spectral slope is insensitive to how an area is mapped

The advantage of having satellite data available for the exact time and location of the survey is that alternative scenarios for the cruise location and sampling method can be investigated. For instance, what would the spectrum of phytoplankton be had all transects been successfully sampled? Or, would the spectrum be the same if the choice of orientation had been from North to South rather than East to West? More generally, given the element of randomness present when it comes to choosing a survey location, another point worth investigating is what the phytoplankton spectrum would look like if another location in the vicinity of the D321 area was sampled instead. The hypothesis is therefore tackled via four questions.

6.3.2.1. Question 1: Does the number of transects matter?

In the previous section the phytoplankton spectrum was calculated with satellite data using only transects matching those successfully sampled *in situ*. These consisted of only four and a half of the nine transects originally planned (See Figure 6.1). Figure 6.3a shows the mean phytoplankton spectrum obtained from satellite data using the 9 transects of what would have been the complete survey. The slope of the spectrum, -1.35 ± 0.14, is steeper than that obtained with the incomplete survey using satellite data (-1.23 ± 0.19) but the two are undistinguishable given the uncertainties. However, the uncertainty in the slope is reduced with a standard deviation of 0.14 compared to 0.19 for the incomplete survey (Figure 6.4). By effectively doubling the number of transects, the uncertainty in slope is decreased by ~30 %.

The confidence interval, which is bounded by one standard deviation of the power estimates either side of the mean for each wavenumber band in Figure 6.3, is seen to vary with length-scale. The shape of the confidence intervals may give the impression that the power spectra do not follow a power-law. A closer look at the individual spectrum of each transect (see Appendix A6.1) indicates that this is not the case and that variability in slope steepness between the transects creates the curved shape of the uncertainty envelope.

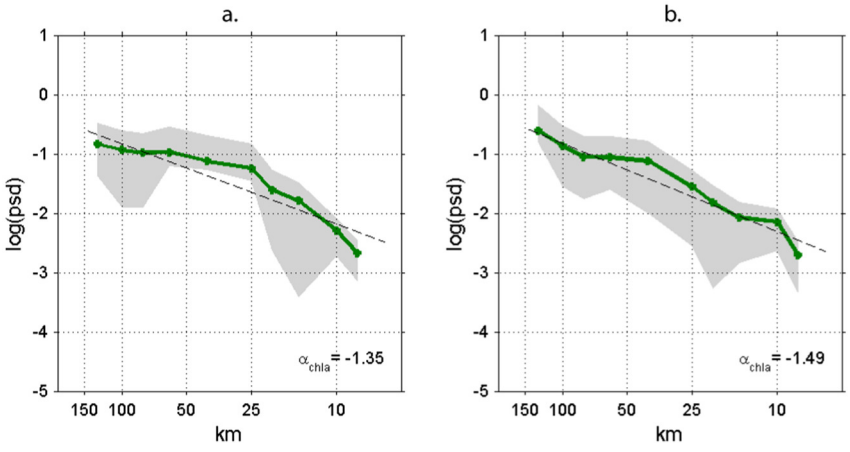

Figure 6.3: *Average spectra obtained from satellite data for the D321 area using all 9 East-West transects originally planned for the in situ survey (a.) and for the same area using 9 North-South transects instead (b.).*

6.3.2.2. Question 2: Does the direction of transects matter?

Figure 6.3b displays the phytoplankton power spectrum resulting from when the survey is conducted North-South instead of East-West, once again using 9 transects. The slope is steeper

(-1.49 ± 0.16) than that obtained from data sampled in the East-West direction (-1.35 ± 0.14) but not significantly given the uncertainties. Uncertainties in the slope, however, remain similar (Figure 6.4). Using a t-test, a mean difference of 0.14 is measured with standard deviation of 0.071. Although a difference in the mean exists there is not sufficient evidence to reject the hypothesis that the means are not equal. The same applies when comparing N-S slope results with E-W results for the 4.5 transects that were actually sampled; the differences are not significant at the 95 % confidence interval (Figure 6.4). In this case, with a study area of such small size, the direction of sampling impacts little on the value of the mean slope estimate.

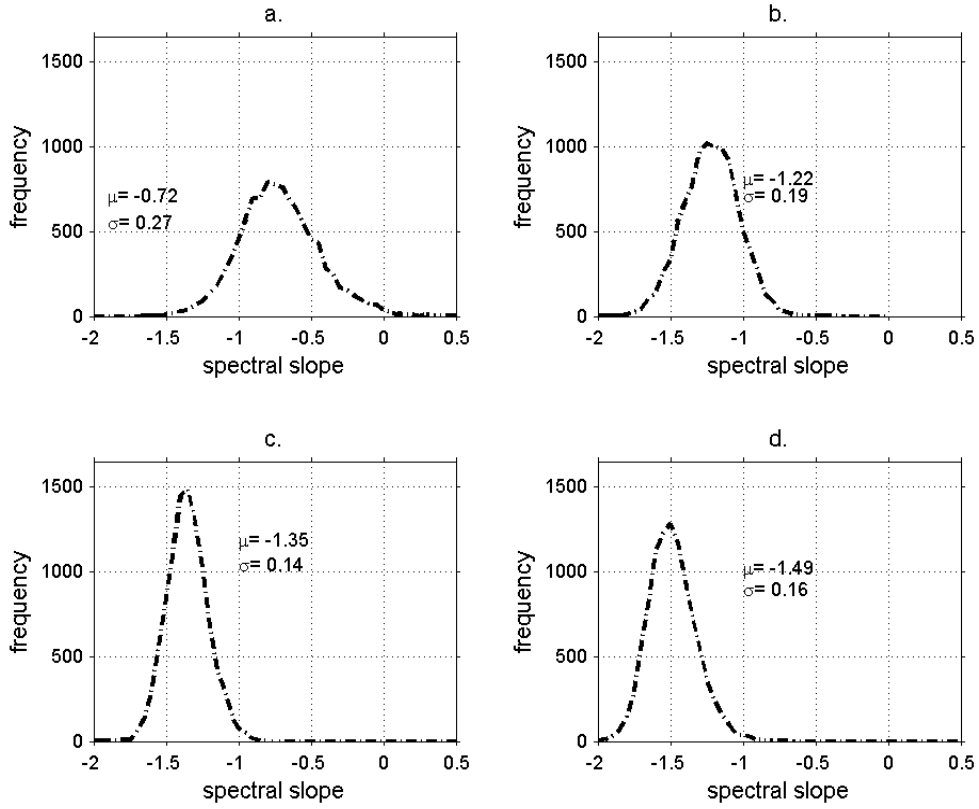

Figure 6.4: *Slope distributions for phytoplankton spectra obtained for the D321 area using in situ observations (a.) and a series of satellite data sets (b. to d.): case using 4 East-West transects corresponding to ones sampled in situ (b.); case of full area surveyed with 9 East-West transects (c.) and case of full area surveyed with 9 North-South transects (d.).*

6.3.2.3. Question 3: How sensitive is the slope to the choice of location of the survey?

To evaluate this question, an area extended from that covered by the D321 cruise has been investigated. The satellite picture data are extracted (Figure 6.5) from the same day as the previous study (Figure 6.1) but instead covering the area with coordinates 57.1N-61N ,23.5W-15W i.e. approximately 400 km by 400 km centred on the original survey area. This area was divided into subset areas of size 130 km by 130 km to match the size of the D321 survey area. An overlap of 50 % between subsets was used for both the latitudinal and longitudinal direction. By overlapping, a larger number of subsets are generated (30) improving the estimation of the mean slope (see Chapter 2).

The spectrum of phytoplankton was estimated for each box using 9 equidistant transects oriented East-West. As in Section 3.2.1., 19 subset areas were affected by the presence of clouds. Those with cloud cover exceeding 30 % (in this case, four) were discarded. However, for subsets with less than 30 % cloud cover, only transects with at least 80 % of cloud free data were considered in the mean spectral estimation.

Figure 6.6 shows the distribution of the slopes obtained for the 26 subsets. Slope values ranged between -0.95 and -1.94 with a mean slope of -1.46. The uncertainty in the slope also varied between subsets, from 0.11 to 0.44 with a mean uncertainty of 0.20. The largest uncertainties were recorded for subsets with the least number of transects (Figure 6.6) consistent with Section 3.2.1. In total, 5 subsets have only 5 or less transects (minimum of 3) and all but one of these display variability in spectral slope in excess of 0.23 (Further details on the slope value, uncertainty and number of transects used for each of the 30 subsets is available in Appendix A6.2). Significant regional variability therefore exists in estimates of the phytoplankton slope when using a method replicating *in situ* sampling. Results from a single survey may therefore not be representative of the patchiness at regional scale.

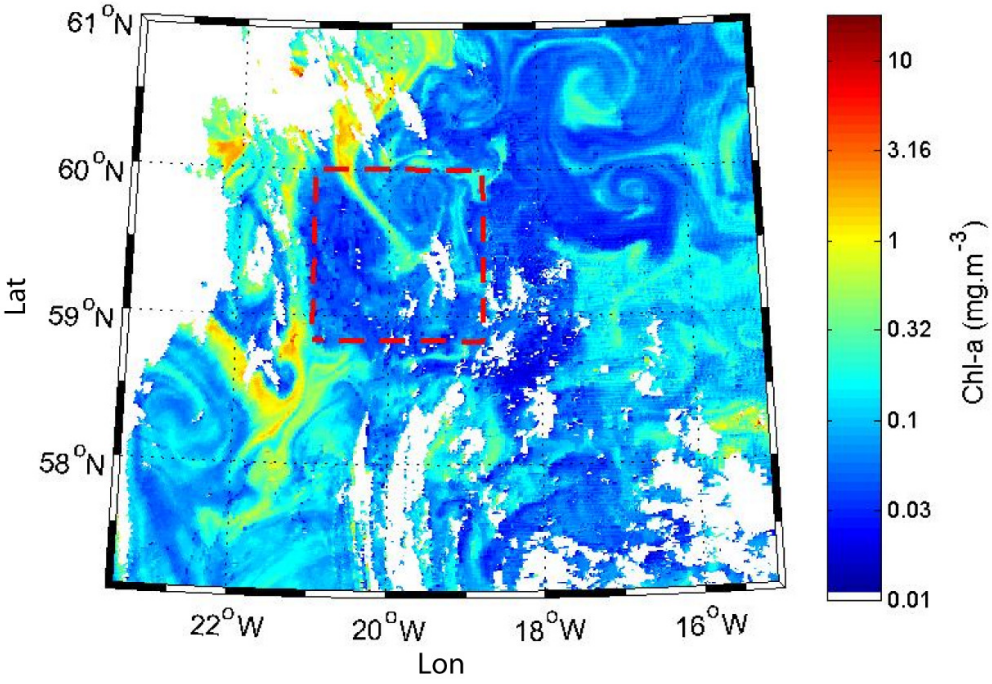

Figure 6.5: *Ocean colour satellite image captured by MODIS. The area shown is used for comparing the spectrum of phytoplankton from the D321 survey area (red box) to that of the wider region.*

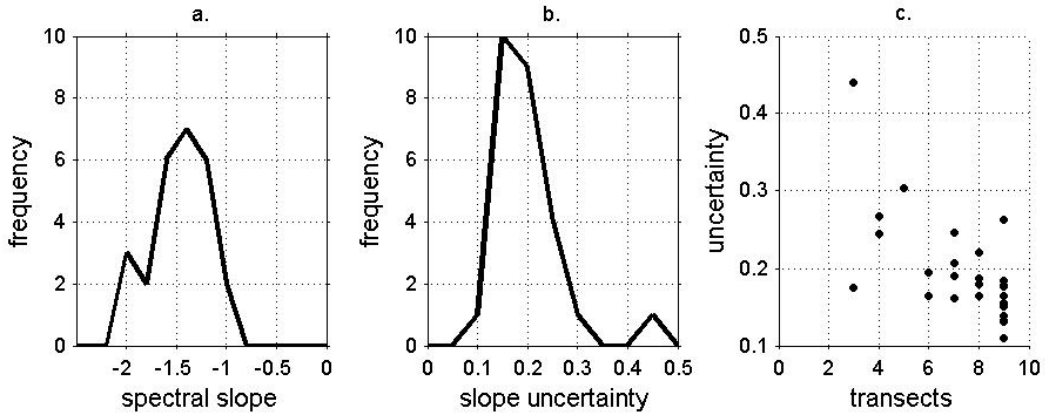

Figure 6.6: *Distribution of the phytoplankton spectral slope (a.), its uncertainty (b.) and uncertainty plotted against number of transects in each survey (c.). Results are obtained from the satellite data displayed in Figure 6.5 using subsets of size 130 km by 130 km. The mean of the slope is α=-1.45 and the mean uncertainty 0.20.*

6.3.2.4. Question 4: Are spectral slope and its variability a function of box size? Or Does the size of the sampling box matter?

The variability displayed in the spectral slope of phytoplankton across the different 130 km by 130 km subsets in the previous section raises the question of whether such small areas are the optimal size for quantifying the spectrum of a region. Even if the interest is in scales up to 130 km, does a larger area need to be sampled to get a more accurate estimate of the spectrum at scales 130 km and less?

In addition to a survey area of size 130 km by 130 km, survey areas of dimension 200 km, 260 km, 325 km and 400 km (in the same region used to address Question 3) are now used to evaluate the spectrum. The spectrum was estimated for the same range of length-scales (8-130 km) as before. The sizes of the survey areas were chosen to be able to split the transects within them into 130 km segments overlapping by 50 %. By overlapping survey areas by approximately 50 %, 30, 9, 4 and 4 subsets were available for the 130 km, 200 km, 260 km and 325 km sized survey areas. To have 4 subsets of size 325 km obliged a larger overlap between subsets. For obvious reasons, only one set could be used when using the 400 km survey area. Within survey areas, transects were taken along latitudinal lines. For transects longer than 130 km, transects were subdivided into segments of 130 km overlapping by 50 %.

Two cases were investigated: the first using a constant separation between transects of 13 km (as for *in situ)*, the second using a constant number of 9 transects. This was done to evaluate the effect of both using a larger area and a larger number of transects on the slope variability and uncertainty. With the first method, increasing the box size increases the number of transects from 9 for a box of 130 km to 119 for a box of 400 km. Therefore both increased area and increased number of transects influence the outcome. The second method controls the number of transects to better highlight the effect of survey area size. Results for fixed separation distance and fixed number of transects are shown in Figures 6.7 and 6.8 respectively.

Fixed distance: Figure 6.7a shows that mean slope remains nearly constant with box size, with values of -1.43, -1.41, -1.51, -1.48 and -1.58 for boxes of side 130 km, 200 km, 260 km, 325 km and 400 km respectively. The significant variability in slope observed for survey areas of size 130 km reduces for larger areas investigated (Figure 6.7a). Additionally, the size of the survey area affects both the uncertainty in slope and the variability in this uncertainty (Figure 6.7b). For survey areas of dimension 130 km a mean uncertainty of 0.19 with maximum values attaining 0.30 is observed. Mean uncertainties decrease to 0.096, 0.083, 0.066 and 0.058 for box of size 200 km, 260 km, 325 km and 400 km respectively (Figure 6.7b).

Nevertheless, it is not possible to say whether the reduction in slope uncertainty with increasing box size is the result of an increase in the area surveyed or the number of transects.

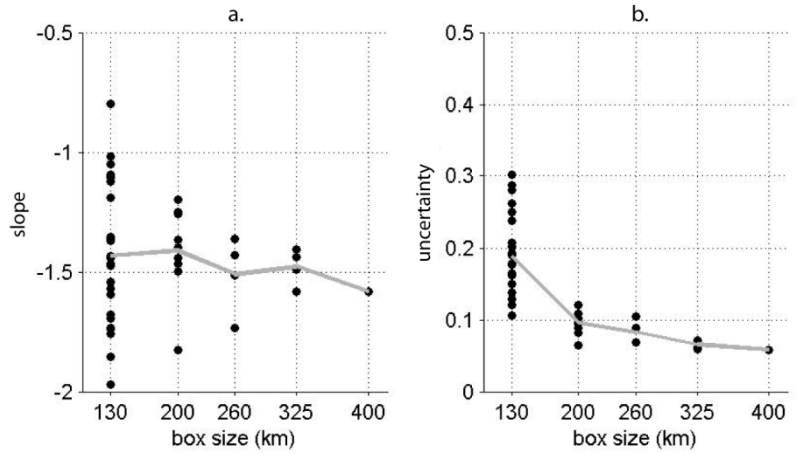

Figure 6.7: *Comparison of phytoplankton spectral slope estimates (a.) and uncertainties (b.) as a function of survey area size. Each data corresponds to one survey area within the 400 km x 400 km region displayed in Figure 6.5. Transects in each box used are separated by 13 km.*

Fixed number of transects: Results for the mean slope and the variability of the slope estimates do not change compared to the experiment with fixed intervals (compare Figures 6.7 and 6.8). However, the uncertainty associated with each slope value increases due to the smaller number of transects used. Slopes for survey area sizes of 200 km, 260 km, 325 km and 400 km have uncertainties of 0.118, 0.122, 0.116 and 0.092 respectively. Although the number of transects was held fixed, bigger survey areas yield more 130 km segments. The number of segments does not affect the mean slope (Figure 6.8c). As expected, the uncertainty decreases as the number of segments increases (Figure 6.8d).

A coarse attempt to evaluate the influence of the number of segments on the uncertainty levels is made here. The uncertainty in slope values obtained with 9 segments (only 13 estimates were used because others had segments lost due to cloud cover) has a mean of 0.161. Assuming that each subset is an independent sample and originating from the same slope distribution, the uncertainty s should decrease when more segments are used. It should follow the relationship $s = \sigma/\sqrt{n}$, where σ is the original standard deviation of the slope distribution and n the number of samples or segments. Using results obtained with 9 subsets, σ can be estimated to be $\sigma = s.\sqrt{n} = 0.161 \text{ x } 3 = 0.482$.

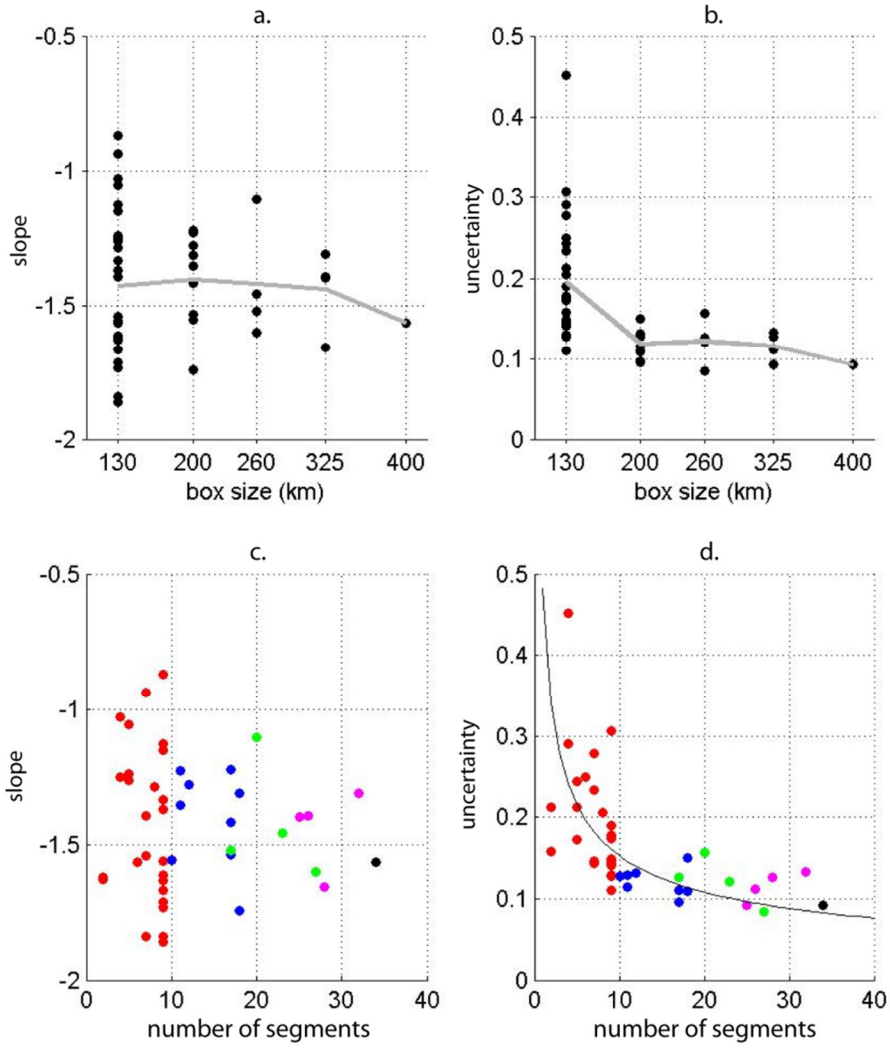

Figure 6.8: *Comparison of phytoplankton spectral slope estimates (a.) and uncertainties (b.) as a function of survey area size. For each survey area, 9 transects are used. Bigger boxes provide larger transects which are divided into 130 km long segments. The relationship of slope estimate (c.) and uncertainty (d.) with the number of segments for areas of size 130 km (red), 200 km (blue), 260 km (green), 325 km (pink) and 400 km (black) are also shown.*

The decrease in uncertainty can therefore be estimated when using an increasing number of segments. The prediction is shown with the black curve in Figure 6.8d. The decrease in slope uncertainty corresponds closely to the decrease expected due to the added number of segments. Increasing the area does therefore not apparently contribute significantly to decreasing the uncertainty. This could also have been measured by selecting the same number of evenly distributed segments for different sized areas for estimating the slope uncertainty and removing the problem of different number of transect. This was not done because it did not consist of a realistic *in situ* sampling strategy.

An additional experiment focusing only on the slope estimates using survey areas of dimension 200 km was made to evaluate further whether increasing the number of transects (here by reducing the distance between them) reduced the variability in slope estimates. The experiment was run with 5, 10, 15 and 25 equally spaced transects (Figure 6.9) in each 200 km x 200 km survey area. Results are consistent Figure 6.9: increasing the number of transects reduces the level of uncertainty in the slope estimates (Figure 6.9b) but does not reduce the variability observed between slope estimates for different 200 km by 200 km boxes within the 400 km by 400 km area (Figure 6.9a). Spatial variability at the regional scale therefore exists and is not the result of uncertainty in the slope values.

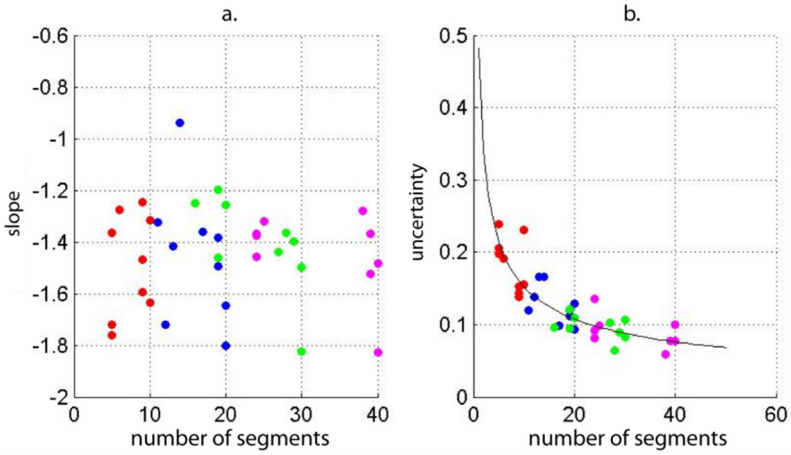

Figure 6.9: *Phytoplankton spectral slope estimates(a.) and uncertainty (b.) for the range 8-130 km calculated within a 400 km by 400 km area (Figure 6.5) using overlapping survey areas of size 200 km by 200 km. Results are obtained from surveying the survey areas with 5 (red), 10 (blue), 15 (green) and 20 (pink) equally spaced 200 km transects. The number of segments on the x-axis corresponds to the number of 130 km segments used to estimate the spectrum. For instance, in each cloud free 200 km transect, two 130 km segments overlapping by 50 % are potentially available for the estimation. However, different level of cloud cover in each survey area mean that not all can be used.*

6.3.3. Hypothesis 3: Satellite data show seasonal cycles in spectral slope

So far this chapter has focused on what satellite data can tell us about spatial variability in slope. However, Chapter 5 raised questions concerning how phytoplankton spectra evolve over time. For the subpolar region, the period of the spring bloom in the model corresponds to a transition period in slope steepness, from steeper winter values to flatter summer ones. For the transition region, significant temporal variability is observed but with no particular seasonal pattern. As the model is an idealized one, we now seek to explore this issue further using satellite data. More specifically, we explore whether there is a shift in spectral slope across the phytoplankton spring bloom. Two steps are taken to address this question. First, the time series of the

phytoplankton spectral slope is calculated over the spring and summer period. Second, the causes for the variations in slope are examined by comparing the levels of variability in the spectrum at large and small scales.

Three boxes were investigated in the subpolar area (denoted S1, S2 and S3 - Figure 6.10) and four in the transition region (T1, T2, T3 and T4 - Figure 6.11). Their size was chosen to limit the influence of sub-regional variability on the phytoplankton spectral slope, as was shown in the previous section when selecting smaller areas. Larger boxes were not used, partly to optimise the chance of suitably less cloudy images. Additionally, as the focus is on the spring bloom and the evolution of the phytoplankton slope relative to the phytoplankton concentration peak, the timing of the bloom needs to be consistent across the area studied. With the timing of the phytoplankton peak varying with latitude, the risk with taking a larger box is that data within it are at different points in time relative to the phytoplankton peak. For instance pre-bloom conditions may be evaluated in one corner of the box whilst in the other corner the bloom may have already started. An illustration of how much variability exists in peak time between different boxes is shown later in Figure 6.12 and 6.13.

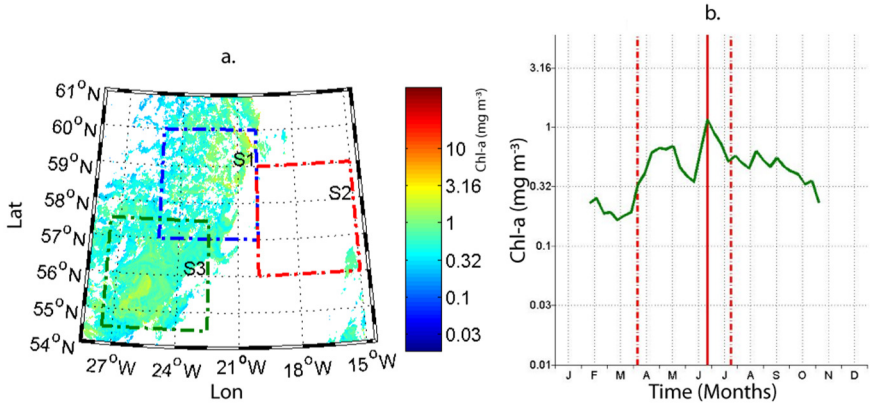

Figure 6.10: *Location of the three survey areas (S1, S2 and S3) in the subpolar region (a.) used for estimating the spectral slope evolution of phytoplankton over the course of the summer. Note the varying level of cloud cover affecting the different boxes. Also shown (b.) is the seasonal cycle in phytoplankton mean concentration for the area shown in (a.) with the studied period marked as dashed red lines).*

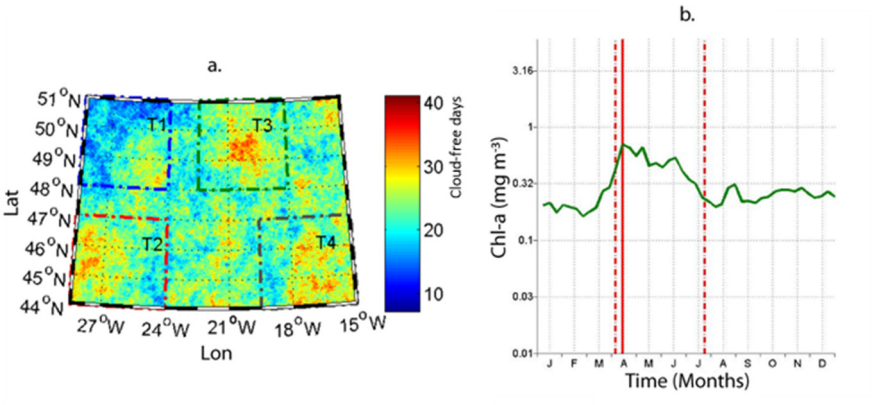

Figure 6.11: *Location of the four survey areas (T1, T2, T3 and T4) in the transition region (a.) used for estimating the spectral slope evolution of phytoplankton over the course of the summer. Also shown (b.) is the seasonal cycle in phytoplankton mean concentration for the area shown in (a.) with the studied period marked as dashed red lines). The colours in (a.) refer to the number of cloud free days for each pixel in the image during the period studied. It was used to identify subsets with most cloud free data.*

For both regions, images were analysed by extracting longitudinal transects. The direction of the transects in these regions does not matter for the spectral analysis because the size of the physical features populating them (~100 km or smaller) is smaller than the size of the transects (400 km). Direction of sampling however, would likely matter in regions dominated by large scale jets (e.g. Gulf Stream). A smaller interval of 5 km between transects was chosen relative to the previous section to improve slope uncertainties. The interval however is large enough to prevent duplicate measurements in neighbouring transects. Each transect is approximately 400 km long and was subdivided into 130 km overlapping segments for which the phytoplankton spectrum was estimated. In total, for a cloud free picture of a survey area, up to 325 segments can be estimated. Nevertheless, cloud cover limited the number of segments available in all survey areas. Only images with a minimum of 20 segments were considered for calculating the combined spectrum of phytoplankton for that day. This minimum number was chosen to ensure that a large enough area is covered and therefore minimising the impact of sub-regional variability that exists within an area of size roughly 400 km by 400 km. In addition, as shown in Figure 6.9 low uncertainties are obtained for the slope when using 20 segments. For reasons given earlier, the combined spectrum for each daily image was obtained by selecting the median estimate at each length-scale for which the variability was estimated. For ease of comparison, both subpolar and subtropical regions are initially analysed for the same period. Results for the subpolar and transition region are displayed in Figures 6.12 and 6.13 respectively.

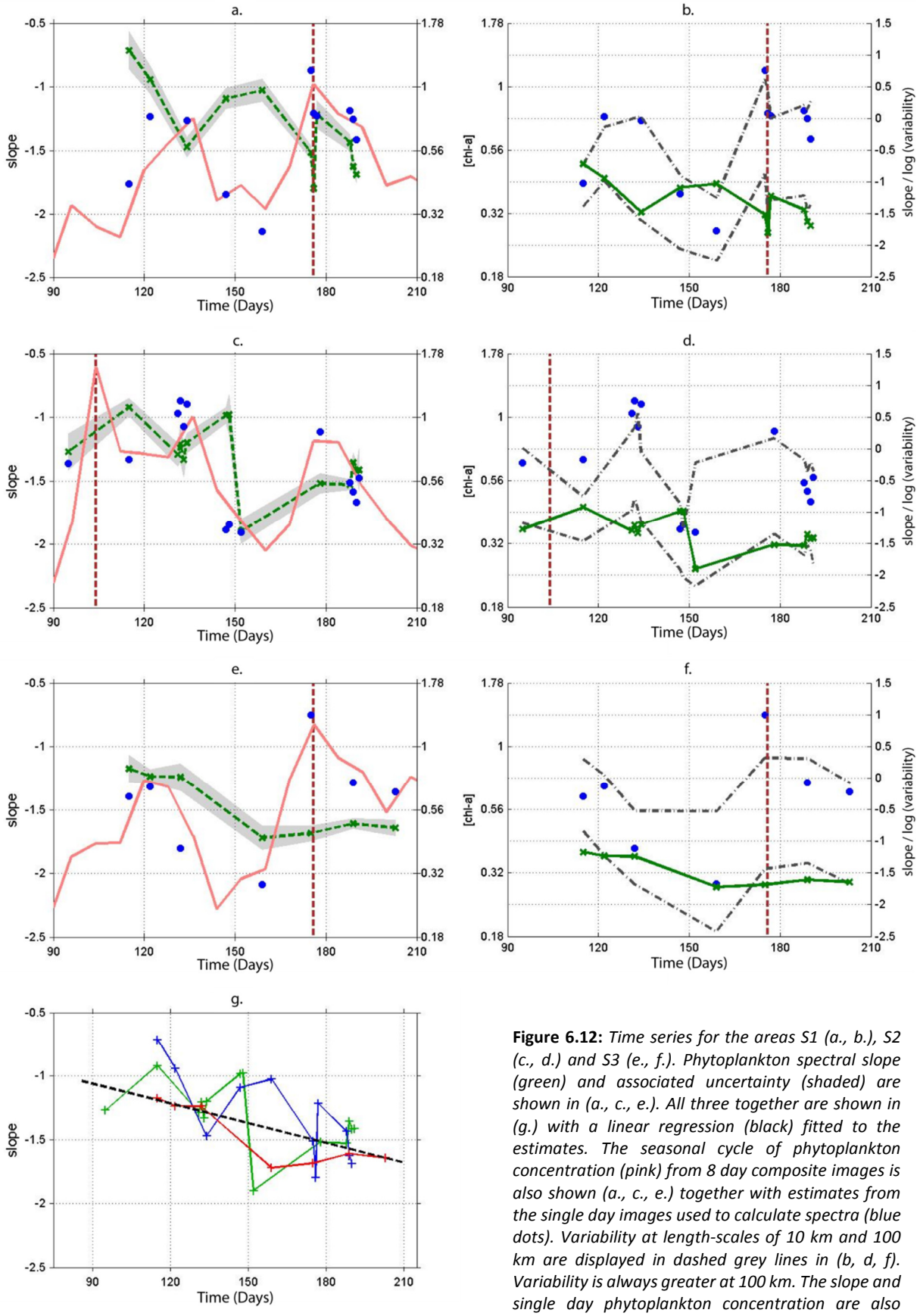

Figure 6.12: *Time series for the areas S1 (a., b.), S2 (c., d.) and S3 (e., f.). Phytoplankton spectral slope (green) and associated uncertainty (shaded) are shown in (a., c., e.). All three together are shown in (g.) with a linear regression (black) fitted to the estimates. The seasonal cycle of phytoplankton concentration (pink) from 8 day composite images is also shown (a., c., e.) together with estimates from the single day images used to calculate spectra (blue dots). Variability at length-scales of 10 km and 100 km are displayed in dashed grey lines in (b, d, f). Variability is always greater at 100 km. The slope and single day phytoplankton concentration are also shown in (b., d., f.) to aid comparison.*

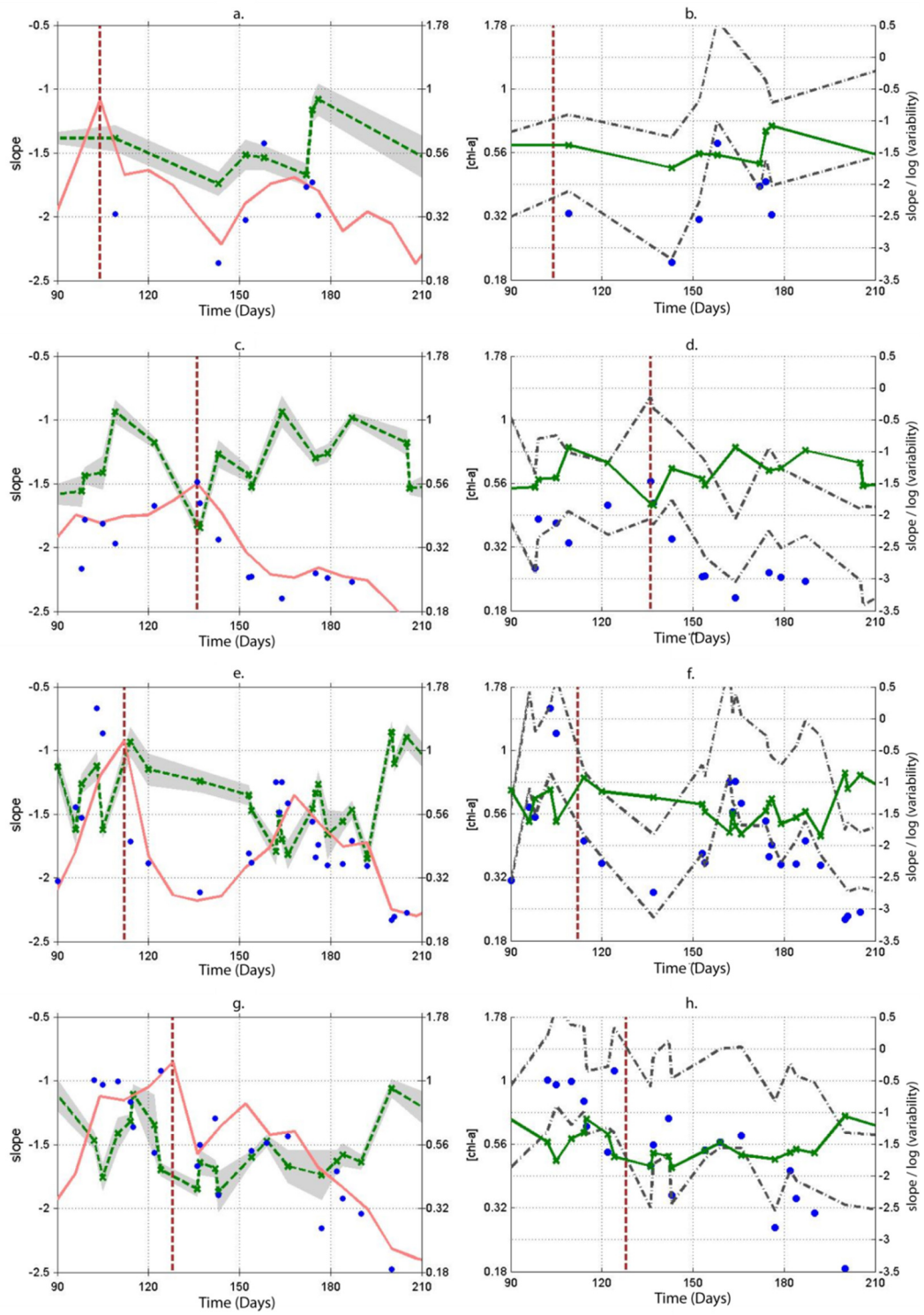

Figure 6.13: *Time series for survey areas T1 (a., b.), T2 (c., d.) and T3 (e,f)and T4 (g., h.) in the transition region. Phytoplankton spectral slope (green) and associated uncertainty (shaded) are shown in (a., c., e., g.). The seasonal cycle of phytoplankton concentration (pink) from 8 day composite images is also shown (a., c., e., g.) together with estimates from the single day images used to calculate spectra (blue dots). Variability at lengthscales of 10 km and 100 km are displayed in dashed grey lines in (b., d., f., h.). The slope and single day phytoplankton concentration are also shown in (b., d., f., h.) to aid comparison.*

Subpolar region:

Because of concerns over gaps caused by cloud cover, in addition to mean phytoplankton abundance in each survey area being calculated from the daily 1 km resolution images, the timing of the peak in phytoplankton concentration was also identified using 8 day composites of 4 km resolution images (Figure 6.12 a, c and e). For each of the survey areas there were two peaks in abundance: on JD 140 and JD 176 for S1; on JD 104 and JD 180 for S2; on JD 120 and JD 176 for S3.

Trends in phytoplankton slope relative to the largest phytoplankton concentration peak cannot be distinguished. Insufficient estimates are available to identify trends reliably for S1 and S3 where only two and three estimates, respectively, are available after the main peak. In S2, where the largest peak occurs earlier (JD104), the 13 estimates post peak show a variable but steepening slope. Extensive cloud coverage means no data are available outside the period shown in Figure 6.12 for any of the 3 survey areas. Trends for the period, rather than relative to the phytoplankton peak for each survey area (Figure 6.12g), show a tendency of slope to steepen with time. This is confirmed by a linear regression fitted to the combined time series for all three areas but a low r-squared value (0.41) suggests that the relationship is weak. Furthermore, the differences in bloom timing between the three sites suggest that any such relationship should be treated with caution.

Despite being potentially more exposed to sub-regional variability due to the small area covered, estimates obtained with only 20 to 25 transects, are nevertheless largely consistent in value with neighbouring estimates in time. For instance, in S1 the slope at JD 115 (-0.53), obtained with 23 segments, is similar to the slope at JD 122 (-0.71) obtained with 39 segments. One exception is found for S2 at a point when three estimates are available within a period of 6 days. For JD 147 and 148 slope values of -0.99 and -0.98 are found using 116 and 33 segments respectively. For JD 152, the slope estimate of -1.92, obtained from 23 segments only, is significantly steeper. The image for this area shows that the spectrum was calculated using a portion of the full survey area of only approximately 130 km by 130 km in size (Figure 6.14a). Therefore variability of slope between sub-regions of S2 relative to the regional value may exist. In particular, the cloud free zone in Figure 6.14a is traversed by a marked filamental feature which is perpendicular to the direction of the transects. This can generate a steeper spectrum due to the level of energy that is introduced at larger scales by the strong phytoplankton gradient. This measurement may therefore not be representative of the regional value. The same is true in S3 at JD 159 (Figure 6.14b). The feature should also be compared to that studied *in situ* in Chapter 3.

To first order, variability at large and small scale in the spectrum follows the changes in Chl-a concentration in the area (Figure 6.12 b, d and f). This is true for all three areas and consistent with the model results in Chapter 5. However, once again as in Chapter 5, this does not lead to the slope tracking variations in mean concentrations because it is the relative change in variability between the two length-scales that causes the changes in slope and this follows a more random pattern.

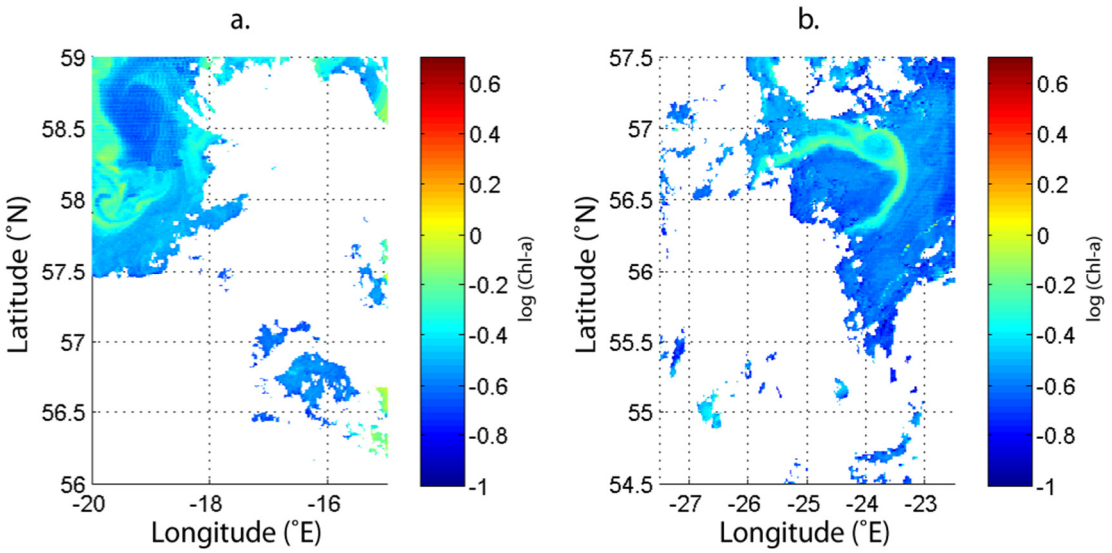

Figure 6.14: *Example of satellite derived Chl-a in the subpolar region for S2 on JD 152 (a.) and S3 on JD 159 (b.) for which only ~20 segments were used to estimate the phytoplankton spectra. The striking phytoplankton spatial features dominating these images caused the slopes to differ appreciably from estimates from images before and after.*

Transition area:

As for the subpolar region, the timing of the peak in phytoplankton concentration varies between areas but also in magnitude (Figure 6.13). For instance in T2, the South-western area, the peak is lower with concentration 0.56 mg m^{-3} and occurs later (JD 136) than elsewhere. The seasonal cycles in T1 and T3, covering the same latitudes, are well correlated. T4 also presents a strong peak (JD 128) but differs from T1 and T3 by presenting a more gradual decline with concentration, remaining above 0.5 mg m^{-3} for over 40 days. As a larger number of estimates was available due to less cloud coverage than in the subpolar region a minimum of 30 subsets for estimating the spectrum was set.

Relative to the date of the phytoplankton peak abundance, no consistent trend in slope is distinguishable across any of the four boxes investigated. Following the peak, cases for which spectral slopes are steepening (T3 and T1), flattening (T2) and stagnating (T4) are all observed.

Generally, the region as represented by the four areas displays large temporal variability in the phytoplankton slope. These variations remain present when considering slope estimates obtained from a minimum of 70 transects.

At both large and small scales of the spectrum, the changes in variability follow the phytoplankton mean concentration (Figure 6.13). As with the subpolar region, the changes in variability do not, however, introduce trends into the phytoplankton slope to correlate with the trend in phytoplankton concentrations. In the case of T4, a drop in variability is observed at both small and large scale of the spectrum from the phytoplankton peak at JD 128 to JD 210, but slopes increase over that time because the drop at large scale is smaller. A similar pattern is observed in T2.

As a further test that the number of segments does not influence the estimate of the slope unduly, it is possible to exploit the fact that for the transition area data are available until JD 270. The comparison of time series between T3 and T4 when using a minimum of 30 and 70 segments is shown in Figure 6.15. The degree to which the variations in slope are coincident for the two regions is not apparently affected by the number of segments. Comparison of time series between other areas is shown in Appendix A6.3. Once again, results show that over that significant temporal variability is present in the estimates of the phytoplankton slope over several months.

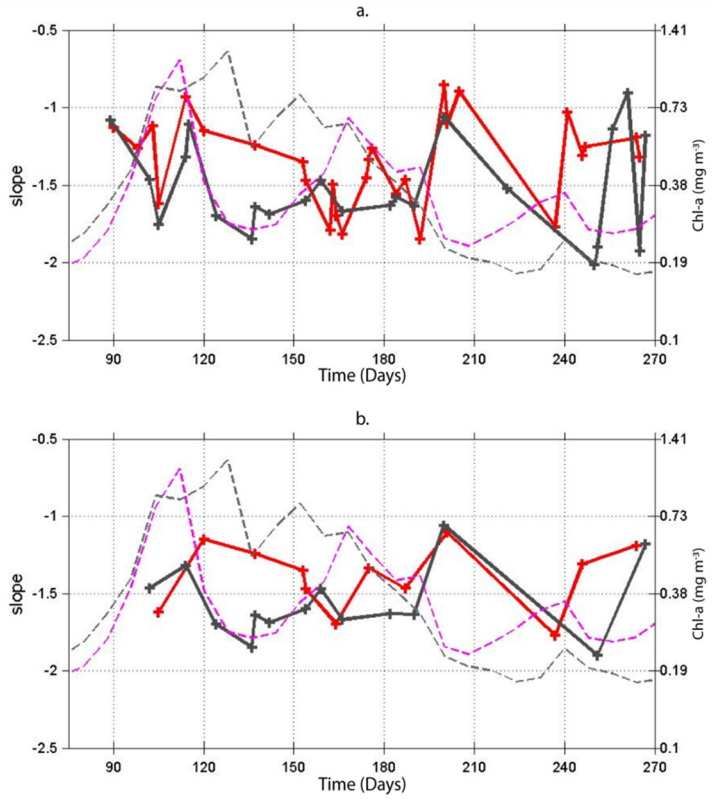

Figure 6.15: *Phytoplankton spectral slopes for areas T3 (red) and T4 (grey) of the transition area using 30 transects (a.) and 70 transects (b.) for the evaluation of the slope over a longer period. The variation in phytoplankton concentration is displayed in dashed colour for both areas.*

6.4. Discussion

Phytoplankton slope variability has been investigated earlier in this thesis (Chapters 4 and 5) over a range of time-scales from a few days up to a year. For time-scales of months to a year, variability in slope was evaluated from a model perspective with *in situ* data simply being too limited in time. Both model and *in situ* data indicated that phytoplankton slope also presents variability in space. In this chapter satellite data have shown that significant variability exists in the slope of phytoplankton over time-scales of days to months and spatially at the sub-regional scale. Combined together, satellite data further supports findings from *in situ* and models challenging the idea of the existence of universal scaling properties for phytoplankton in both space and time.

Satellite and in situ have consistent spectra:

It has been shown, based on an area for which both satellite and *in situ* phytoplankton data are available, that spatial variability seen in observations from satellite are consistent with estimates from *in situ*. Satellite estimated spectral slopes for the range 8-130 km are, however, steeper than those from *in situ* due to an under-evaluation of the power at small scales

Two aspects differentiate the *in situ* and satellite datasets that may explain the discrepancy: the resolution of the data (1 km and 4 km for satellite and *in situ* data respectively) and the manner that the data points are obtained in each data set. *In situ* data consist of data points approximately 4 km apart with each data point obtained from averaging around 20 data points collected over approximately a 100 m distance (Chapter 3). In contrast satellite data consist of 1 km averages with 1 km resolution.

A simple artificial time series replicating a phytoplankton transect can be generated by converting into the time domain a spectrum with pre-defined power-law (see Chapter 2). From this time series, two data sets were obtained reproducing the data collection and processing of satellite and *in situ* surveying. The spectral analysis of these two data sets consistently reveals that the spectrum obtained with the satellite-like data is steeper than that simulating the *in situ* data. As seen in Chapter 2 (Section 2.4.4.), a flatter slope than the true slope is found when using the data simulating *in situ*. In contrast, with simulated satellite data, a steeper slope than the true slope is found. Decreasing the resolution of the simulated satellite data to 4 km reduces the difference in slope with *in situ* but does not remove it.

The *in situ* – satellite comparison done to address Hypothesis 1 provides only one example and more comparisons are needed to evaluate the robustness of the relationship. These should cover different regions. As demonstrated above, further understanding of the effect of resolution and averaging on the spectral slope can also be obtained from comparing satellite data of different resolution (4 km and 1 km).

More generally, differences in slope estimates found between the two sources of data for the same region and time imply that phytoplankton slope estimates found in the literature and obtained from different data sources cannot be used together to argue for variability in phytoplankton slopes. The difference could simply be an artefact from different data being used. However, when used on its own, like is done in this chapter, satellite data can be used effectively to examine such variability in slope. Given the spatial and temporal coverage they provide,

satellite data therefore provide a valuable and complementary tool for patchiness studies, to address questions that could not be answered using *in situ* data.

Variability in slope at sub-regional scale

Satellite data show that considerable spatial variability exists in the slope of phytoplankton at the regional scale when using a sample the size of an *in situ* ship survey of 130 km by 130 km. In the case study covering a 400 km by 400 km area, phytoplankton slope values varied between -0.87 and -1.86. This covers a large part of the range of observed phytoplankton slope values found in the literature (Chapter 1) potentially explaining why so much difference is observed. Note, however that it is assumed that the magnitude of the differences observed in the satellite spectral slopes within this region is not amplified due to the under-evaluation of the power at small scale.

Obtaining a robust value of the regional slope can be obtained by sampling larger areas. This has implications for *in situ* sampling, as discussed below. Increasing the size of the study area reduces the variability observed in the slope. This improvement in estimation is the result of a larger area being covered and not because more transects are sampled. The number of transects used for the slope estimation affects the uncertainty of the slope but the uncertainty associated with the slope estimate should not be seen as a measure of how well the regional value is estimated. A phytoplankton slope with very low uncertainties can be obtained from a 130 km by 130 km area if sampled with many transects, but would still not be a good estimate of the regional slope value.

The size of physical features relative to the size of the survey area has a significant effect. For instance, in mid-latitudes eddies typically of size 50-100 km mean that transects within a typical 130 km x 130 km survey area only sample one such feature. The spectral slope is therefore strongly dependent on the variability induced by that eddy. Similarly spectra in neighbouring areas are themselves being influenced by other such features, explaining the variability in slope at sub-regional scale. Evidence of this happening is seen in both Chapter 3 for the subpolar area and Chapter 4 for the subtropical area. Larger survey areas would admit more mesoscale features such as eddies and therefore provide closer estimation of the regional slope value. Ships may best be used by sampling transects with a larger distance between them, set to exceed the size of eddies, to maximise the number of features covered within the 3 day period necessary to keep the exercise synoptic.

Variability in slope over time-scale of months

Temporal variability over the spring and summer period was observed in both the subpolar and transition area of the North Atlantic. The subtropical area was not studied for reasons given in the introduction to this chapter.

Phytoplankton slope time series for the subpolar region show that large variation exists over the period from the end of April to July. Values range between -0.92 and -1.90. In Chapter 5, model results suggested that during the spring bloom, the slope may change from steeper winter values to flatter summer ones. No particular pattern is distinguishable in the slope obtained from satellite data around the phytoplankton peak. More specifically, no flattening trend is observed. If anything, satellite data suggest a potential steepening over that period (Figure 6.12g). Longer time-scales could not be studied in the subpolar region due to high level of cloud coverage. However, a longer period was studied for the transition area with large variability also observed, with values ranging between -2.10 and -0.86. Changes in slope were not correlated to mean phytoplankton concentrations.

Care is needed when interpreting the time series of slope. The presence of cloud means that for different days, different parts of the 400 km by 400 km survey area contribute to the slope estimate. It also means that only a fraction of the total area is used for most slope estimates. Given the large spatial variability in slope that exists at sub-regional scale, it is important to ensure that the variability seen in the slope time series corresponds to temporal variability and not to spatial variability present at sub-region.

The level of variability in the time series remains when using a larger number of segments (Figure 5.14). This gives confidence that the variability in the time series is temporal. Furthermore, the similarities in the slope time series obtained between neighbouring 400 km by 400 km boxes (Figure 5.14) also indicate that the variability is not the result of sub-regional spatial variability. Satellite results therefore support those obtained from model (Chapter Section 5.3.4.) that temporal variability exists in the slope of phytoplankton over time-scales of months.

The spatial variability at small and large length scales generally follows changes in concentrations. The only exception seen is for one area in the transition area (Figure 6.13a and b) for which variability in the spectrum increases over time while phytoplankton concentration decreases. It has been shown though that this does not imply a relationship between slope and phytoplankton abundance as it is the difference in variability between large and small scales that counts. Phytoplankton can be forced at a number of scales, an example being by upwelling of

nutrients associated with winter convection, eddies and filaments. The non-uniformity of forcing across length-scales causes relative changes in variability at large and small scales creating the variations observed in the slopes.

Impact of sub regional variability on in situ surveying

One conclusion that can be drawn from this chapter is that a reliable estimate of the regional phytoplankton spectrum slope cannot be obtained using an *in situ* survey mapping an area of 130 km by 130 km. A larger area needs to be covered. However this cannot be achieved with a single ship as sampling would take too long for it to remain synoptic. For a survey longer than 3 days too much change occurs in both the oceanic flow and the phytoplankton distributions between the start and the end of the sampling period to obtain a representative picture of the area and its patchiness.

If evaluating larger areas is the only manner to obtain improved estimates of the phytoplankton slope, the question of how this can be realised with *in situ* approaches can be posed. One option is that a larger number of ships are required. The case study in Section 6.3.2.4. of an area having been evaluated by 30 survey areas can be taken as an example. It shows a mean phytoplankton slope of -1.43 for the regions with a variability of 0.29 when sampling it with an area of 130 km by 130 km. Let us say that an estimation of the slope within 0.1 of the regional mean value is wanted. Using three ships sampling simultaneously three randomly chosen areas of size 130 km by 130 km, there is a 46 % probability to obtain the desired accuracy. This increases to 52 % when using four ships to sample four areas instead. Although a precise figure can't be put on the accuracy, the results of this chapter suggest a more efficient solution. Both taking data from a wider area and keeping transects spaced by the size of the local mesoscale features have both been shown to improve estimates. Therefore, a significant improvement could be obtained, still using just one ship for the same period, but instead steaming round the edges of 130 km side boxes instead of the radiator pattern used for the *in situ* studies discussed in Chapters 3 and 4.

6.5. Conclusion

Provided that a sufficient area is covered, temporal variations in phytoplankton slope can be measured with satellite data reliably. Such estimates show that phytoplankton spectral slope

displays significant temporal changes over time-scales of months. These temporal variations do not, however, follow any particular patterns and are therefore not supporting data hypothesis of a seasonal pattern in slope. An understanding of the temporal variations cannot be obtained with satellite means alone as they are the result of component range of influences (e.g. submesoscale physics) many of which are poorly captured by satellites. This clearly makes the study of phytoplankton patchiness challenging. New sampling and surveying techniques need to be developed, particularly *in situ* methods better able to investigate forcing processes. In this chapter, it was shown that the phytoplankton slope displays large spatial variability at the regional scale. This means that the current localised slope estimations (Chapters 3 and 4) from one *in situ* survey cannot be used as a representative estimate for the region. *In situ* surveys need rethinking if they are to allow the robust comparison of slopes in different regions.

Chapter 7: Discussion

The power spectrum has proved to be a popular tool for quantifying phytoplankton patchiness. Heterogeneities in phytoplankton spatial structure have been quantified using spectral analysis for field and satellite observations (Mackas and Boyd, 1979, Washburn *et al.*, 1998, Martin and Srokosz, 2002) and for describing spatial variability of phytoplankton in model predictions (Steele and Henderson, 1992, Lévy *et al.*, 2001, Lévy and Klein, 2004, Bracco *et al.*, 2009). This thesis has shown that significant inconsistencies exist between the three approaches even though such studies have shed considerable light on patchiness.

Essential questions remain: can a correct estimate of the phytoplankton spectrum be made? Does a single universal spectrum for phytoplankton actually exist? Sources of uncertainty are large and often associated with the limits of our current phytoplankton sampling capabilities.

In Section 7.1. of this Discussion chapter, I will discuss the sources of uncertainty encountered in estimating the phytoplankton power spectrum and in Section 7.2., I will address the question of whether a single universal spectrum for phytoplankton exists.

7.1. Can we measure what we need to measure accurately?

7.1.1. Different spectral techniques give different estimates

A major challenge in using spectral analysis for evaluating phytoplankton patchiness is the ability to obtain a robust estimate of the true power spectrum. Results in this thesis show that a number of factors need to be taken into consideration.

This study shows that estimating the true spectral estimate of a power-law signal like phytoplankton is difficult, with each combination of spectral method and smoothing technique providing differing values for the slope estimates (Chapter 2 Section 2.4.4.). Not all methods have been evaluated here. In particular, to remain consistent with the most suitable analysis for cruise survey data, which are disproportionally sampled in one direction, it was chosen to use spectral methods in one dimension. Furthermore, the relatively low number of data points,

and the short span of scales they spanned, made methods like structure functions not suited to describe the statistics of the phytoplankton spatial variability.

The Fast Fourier Transform (FFT) has been used. This is a very popular spectral technique for studying plankton, but it is not suited to process unevenly spaced measurements as is often the case with phytoplankton *in situ* (Chapter 4) and satellite observations (Chapter 6). The Lomb Scargle periodogram (LSP) (Chapter 3 Section 5.1.) offers an alternative method but has been rarely applied; most studies favour interpolation to make data evenly spaced instead, but in the process add noise in a situation where noise is already a problem. In this thesis the approach has been to stay as close to the raw data, using the LSP unless data were evenly spaced. However, poor implementations of the method as a routine package in programming languages like Matlab, in contrast to FFT and interpolation functions, hinders its widespread use and development. In particular, this does not contribute favourably to the routine use of the most robust method to estimate the spectrum of phytoplankton in a given situation.

Furthermore, FFT does not always perform well for signals with a power law, the characteristic of phytoplankton spatial distribution that many seek to explore. For signals that have a power law behaviour with exponent steeper than -2, it overestimates the level of variability in spectra with a magnitude that increases with decreasing length-scale (Chapter 2 Section 4.4.). This leads to flatter slopes being estimated for the spectrum unless a pre-whitening step is applied prior to the spectral estimation. Other tapering options such as applying a window, e.g. a Hann window, did not improve results for the data studied here (Chapter 2 Sections 2.4.4. and 2.4.5.), even though this approach has been used for several studies in the literature (Weber *et al.*, 1986, Washburn *et al.*, 1998).

For the two spectral methods (FFT and LSP) and two different smoothing techniques (Hann window and pre-whitening) tested in this thesis, large differences exists between the different combinations when the same signal is being evaluated. Further differences may also exist with methods not considered here (e.g. variograms, structure function, wavelet analysis). The inconsistent ability to capture power-law signals makes a comparison of phytoplankton spectra between studies that have used different methods problematic.

For instance, phytoplankton spectral slopes in the literature have been measured between -0.6 and -3. Although it is known to improve estimations for power-law signals, particularly for signals with slopes of -2 and steeper, pre-whitening has not been systematically applied. With many studies estimating the slope to be within -1.5 and -2.5 (Horwood, 1978, Weber *et al.*, 1986, Yoder

et al., 1993, Washburn *et al.*, 1998, Seuront *et al.*, 1999) much of the variability could be the result of different methods being used. It should be acknowledged that studies used spectral methods for their own purpose at the time and the results were not originally intended to be used in a comparative study. Additionally, power spectra are known to be noisy (Jenkins and Watts, 1968). The problem therefore comes if values from a variety of sources and methods are being used to support a hypothesis that variability exists in the spectral slope of phytoplankton. In this thesis, by designing a method which has been tested against power-law signals of different strengths, it has been possible to quantify differences in spectral estimations between different data sources, and ultimately to determine whether variability in the scaling properties of phytoplankton independent of the method used.

7.1.2. Different sources of data give different spectra

In addition to the choice of method to calculate spectra, this study also shows that the type of data also affects the estimate. By applying an identical method the differences in spectra estimated using different sources of data could be investigated. Chapter 6 showed a case for which both *in situ* and remote-sensed Chl-a based estimates were simultaneously available, but that where a significant difference existed in the slopes of the spectra. A steeper slope was found using satellite data (-1.23 ± 0.19) than using *in situ* data (-0.72 ± 0.27). The most notable difference in the spectra is an under-estimation of energy below a length-scale of 25 km in the satellite spectrum relative to the *in situ* one (Chapter 6).

A simulation of the effect of sampling on the slope spectrum in Chapter 6 provides an explanation for the discrepancy. Important differences in data come from *in situ data* being sample points every 4 km, and satellite data being 1 km averages at 1 km intervals. When data is averaged over space into 1 km data points equally spaced by a 1 km interval it systematically generates a power spectrum for the range 8-130 km length-scales with a slope steeper than when the same data are averaged over 100 m with data points spaced by 4 km instead. Doing the same experiment but with the 1 km average data points spaced by 4 km instead reduced the difference but did not eliminate it. However like for *in situ*, the estimated slope was now flatter than the signal's slope.

This raised two points. First, the resolution of the data affects slope estimates. Higher resolution data, i.e. containing information below the shortest length-scale covered, gives a better estimation of the spectrum. A simple reason is that more points are available to evaluate the

power at the shortest length-scale covered than if only three measurements per wave are available, like for the *in situ* case. An experiment in Chapter 2 showed that flatter than true slopes are estimated for signals simulating *in situ* data. The second point concerns the averaging of the data. *In situ* data are effectively point estimates compared to satellite data which are average values from within a 1 km by 1 km pixel. Chapter 4 showed that large differences in slopes for the range 10-100 m existed between the different areas surveyed. Slope values for this range varied between -3.7 and -2.4, when averaged over a 130 km by 130 km area. Although this only covers part of the range below 1 km, it gives an indication of how patchy plankton are within that range. Averaging smoothes out such variability within the pixel, possibly propagating it into other scales.

The issue of resolution can be addressed by carrying out *in situ* surveys at a higher resolution than the surveys studied in this thesis. The 4 km resolution of the data in Chapters 3 and 4 is a consequence of measuring phytoplankton at multiple depths with the undulating vehicle. Fluorimeters are fast-sampling enough (1 measurement per second) to provide a much higher resolution map of an area if the instrument is deployed for a fixed depth during a survey. This has been done before with SeaSoar (Hodges and Rudnick, 2006). A comparison of spectra for the range 8-130 km can then be made using both high and low resolution data. The same experiment can be conducted using satellite data with different resolution. Satellite data are available at 4 km, 1 km and sub-kilometre resolution. Using all of these to estimate the spectrum at 8–130 km length-scales would be another recommendation for future work to explore this issue.

Until the differences between satellite and *in situ* estimates are resolved, such estimates cannot be used together as evidence to support the existence of variability in phytoplankton scaling properties. Nevertheless, used separately they can both reveal much about the patchiness of phytoplankton.

7.1.3. Minimising uncertainties and capturing variability in slope estimates

This thesis has demonstrated that a number of minimum requirements are needed to obtain a good spectrum estimation.

The number of transects carried out during a survey significantly affects the slope uncertainty of the phytoplankton spectrum. It is therefore important that, depending on the level of

uncertainty wanted for the estimation, a sufficient number of transects is sampled. Results for a 130 km by 130 km area using satellite data, showed a decrease in the uncertainty of slope from 0.19 to 0.14 when using 9 transects instead of 4.5.

Low uncertainties however do not necessarily mean that the estimate is a robust estimation of the slope at the regional scale. For this, an area sufficiently large needs to be sampled. An analysis of a 400 km by 400 km region using satellite data showed that large spatial variability exists in the slope estimate for the range of length-scales 8-130 km within such region when using a sample area the size of the *in situ* survey analysed in Chapters 3 and 4 (approx. 130 km by 130 km). Calculating the spectral slope for multiple *in situ* sized surveys within this region produced values ranging between -0.8 and -1.9. This range, obtained at a regional scale covers a considerable fraction of the range of slopes values previously found globally (see Chapter 1). With the majority of *in situ* research studies carried out within a limited space, for practical reasons, differences in slope estimates between different geographical regions may reflect more the spatial variability present at regional scale than differences between regions or over time.

A reason for why the slope may vary regionally can be found in the typical contents of a mesoscale survey area. Variability induced by the presence or absence of eddies within a survey area was found in both subpolar (Chapter 3) and subtropical (Chapter 4) regions. For both cases, the slopes obtained from transects that crossed the eddy were flatter than those obtained from transects that didn't. The large size of mesoscale features such as eddies relative to the size of the sampling area means that the spectral slope will inevitably be influenced by such features. Sampling larger areas, with transects spaced by a distance at least equal to the local eddy size, will obtain a more representative estimate of the regional spectral slope.

Long single transects, rather than a grid, may be a good alternative approach to obtain a good regional slope estimate. Such sampling already takes place and has been used for calculating the spectrum of phytoplankton (Hodges and Rudnick, 2006). Whether such strategy obtains a better estimation of the spectrum for a region needs to be tested in more detail however. The transect should be long enough to be representative of the region of interest. A bonus is that a single long transect provides more segments (through overlapping) than the same cumulative distance of grid surveying, helping to reduce uncertainties in slope estimates. Such a strategy could be tested beforehand by using satellite data. Potential *in situ* survey areas can then be targeted to determine the maximum transect length beyond which larger scale gradients influence the signal. Some regions may already be covered by transacted by regular commercial routes. Some Ships Of Opportunity (SOOP) already carry on board fluorimeters that sample the water at a

frequency of two measurement per minute (Hartman *et al.*, 2014) which corresponds to approximately one sample every 300 m. Near-coastal areas are regularly sampled in Europe (www.ferrybox.org), with similar projects in the US and Canada (Codiga *et al.*, 2012) for studies on ocean acidification (Gledhill *et al.*, 2008), variability of the Gulf Stream (Rossby *et al.*, 2010) and phytoplankton biomass (Halverson and Pawlowicz, 2013). Sampling along open ocean routes also takes place on SOOPs with some routes being sampled up to 18 times a year (http://www.aoml.noaa.gov/phod/goos/xbt_network/).

7.1.4. Vertical issues

The vertical distribution of phytoplankton across the euphotic zone adds an additional layer of complexity to measuring the spectrum of phytoplankton when it extends below the mixed layer.

Depending on the time of year and their geographical location, phytoplankton can form a Deep Chlorophyll Maximum (DCM). Sometimes, like for the D381 survey area in Chapter 4, both surface and subsurface concentrated distributions can occur within the same survey area.

In situ results for the subtropical gyre (Chapter 4 Section 3.3.1.), where a DCM is observed, show that the manner in which data are selected significantly influences the estimated slope of the phytoplankton spectrum. The slope can more than double depending on whether the data are selected on a fixed depth or along an isopycnal (Chapter 4 Section 3.3.1.3.).

On a fixed depth, data are extracted from different density layers. As water moves predominantly along isopycnals, the data collected can incorporate signals from internal waves. The displacement of the phytoplankton vertical structure across a given depth as the wave lifts and drops isopycnals transfers vertical structure into the horizontal data. Selecting data along isopycnals removes that problem but produces another one. Phytoplankton on isopycnals may be at different depths and hence receive different amounts of light, a major control on phytoplankton abundance. Once again this can propagate vertical structure into the spectrum. In Chapter 4 maximum concentrations were centred on 120 m depth and when plotted against isopycnals present a bimodal distribution with peaks at 26.2 kg m^{-3} and 26.3 kg m^{-3}. When plotted against depth the distribution was unimodal, suggesting the strong influence of light.

A more practical limitation is that phytoplankton patchiness below the mixed layer cannot be reliably captured by satellites which only measure the top few metres. Obtaining high resolution

data at depth spanning the necessary range of scales can only be completed with towed vehicles or gliders.

7.1.5. Chl-a is not always a good proxy for phytoplankton

Another source of uncertainty associated with measuring phytoplankton variability comes through the use of the pigment Chlorophyll-a (Chl-a) as a proxy for phytoplankton abundance. Chl-a has proved very popular for spatial studies of phytoplankton due to the continuous measurements that can be obtained with a fluorimeter. The concentration of the pigment, from which abundance is quantified, also affects the colour of the ocean and therefore can also be estimated remotely by measuring the ocean colour.

In regions of high light availability phytoplankton have lower Chl-a to biomass content such that Chl-a does not always correlate well with the abundance of organisms (Zubkov and Quartly, 2003) .The most striking case is for the subtropical oligotrophic regions for which only a poor Chl-a signal exists at the surface despite the abundance of photosynthesising plankton such as cyanobacteria e.g. *Prochlorococcus*. If Chl-a only captures a portion of what constitutes phytoplankton abundance, the spectrum derived from it will not be a good indicator of the phytoplankton spatial structure. Where Chl-a ceases to be a good proxy, other alternative estimates need to be used. Flow cytometry has previously been used to quantify spatial variability of microorganisms (Martin *et al.*, 2008), but the method is time consuming to achieve kilometre scale resolution. Recent advances in automated identification and classification of microorganisms with FlowCam may alleviate this problem.

All the factors detailed in the above sub-sections introduce uncertainties in the slope estimate of phytoplankton. If a consistent approach is not used for patchiness studies then the existence of universal properties in the spectrum cannot be robustly tested as any changes in method affects the slope estimate. Such sensitivity to differences in methodology renders comparison of observations between research studies in the literature challenging at best.

However, by acknowledging these limitations, a robust methodology can be implemented to investigate all aspects of universality, starting from understanding what occurs at small time and spatial scales and using it to understand what occurs at larger ones. For instance, universality in slope with season can only be examined once a thorough understanding of variability in slope

at day or weekly scales is obtained. Equally, geographical differences can only be evaluated once the degree of local variability is fully understood and it has been shown that variability in both time and space need to be addressed simultaneously. Only by doing so can each facet defining universality be robustly tested.

7.2. Do universal scaling properties in the spectrum of phytoplankton even exist?

One of the characteristics that has attracted most interest in the phytoplankton spectrum is that observations have shown scaling behaviour, such that variability varies as a power of length-scale (giving a straight line in a log-log representation).

As described throughout this thesis, this behaviour of a linear decrease in log(variability) with decreasing log (length-scale) is consistently found for *in situ* observations (Chapter 3 and 4), satellite data (Chapter 6) and modelling studies (Chapter 5). Scaling behaviour in the phytoplankton spectrum was found in the subtropical and subpolar gyres and intergyre transition regions of the North Atlantic open ocean. The presence of such power-law behaviour across regions shows that a degree of universality does exist in the spatial pattern of phytoplankton.

It has been suggested that the detailed characteristics of such scaling properties in phytoplankton distribution may additionally be universal (Platt and Denman, 1975, Powell and Okubo, 1994), by analogy with similar scaling behaviour displayed by the underlying flow field. The implication is that across space and time it is the same processes that control the spatial variability across the range of length-scales for which the scaling is observed. The range studied in this thesis is the mesoscale and below. The argument is that the source of heterogeneity originates at scales larger than the largest covered in the spectrum, and that therefore patchiness at the mesoscale and below is the result of this original heterogeneity being broken down to smaller scales.

However, the growing evidence that the mesoscale is a regime subject to upwelling of fresh nutrients (e.g. Strass, 1992, Lévy *et al.*, 2001, Allen *et al.*, 2005, McGillicuddy *et al.*, 2007, Klein *et al.*, 2008), whereby extra variability at intermediate scale is introduced, is questioning the validity of such scaling behaviour. The question of whether universality in scaling characteristics

of the spectrum of phytoplankton, over time and geographically, actually exists is therefore now examined from different perspectives.

7.2.1. High frequency variability

Numerical simulations suggest there is considerable variability in the phytoplankton spectral slope at time-scales of days to weeks (Chapter 5 Section 5.3.1. and 5.3.4.). This corroborates indications from *in situ* results. In the subtropical gyre, *in situ* slope estimates were found to vary considerably over the space of a month with values of -0.36, -0.84 and -0.71 found using fixed depth data from three consecutive surveys (Chapter 4 Section 4.3.3.). Spectra obtained from data along isopycnals also displayed strong variability with slopes of -0.98, -1.78 and -1.43. By using a model, the potential existence of such short term variability was corroborated. Intra-monthly variability has been shown to be present across the year and across regions. Such short term variability is not, however, constant across the year, with significant month to month changes.

In addition to undermining any notion of universality in phytoplankton scaling characteristics, such variability highlights the complexity underlying the spatial structure of phytoplankton, with rapid changes in its statistical properties. It is not clear what processes cause such variability over days and weekly time-scales. Physical processes like eddy pumping, (McGillicuddy *et al.*, 1998), submesoscale upwelling and subduction of water masses (Lévy *et al.*, 2001) all potentially modulate the spatial distribution of phytoplankton. However, to measure their effect on the variability of phytoplankton spectra requires simultaneous mapping of the three-dimensional flow. This is traditionally achieved with the radiator style surveys analysed in Chapters 3 and 4 which, as discussed above, are far from optimal for estimating spectra.

Robust *in situ* measurements of short term variability still need to be made. The short term variability cannot be tested with satellite data because not enough cloud free data exist within one month for an area that is large enough (400 km by 400 km) to sufficiently minimize the noise from spatial variability.

Gliders may offer an alternative for quantifying this temporal variability due to their ability to operate autonomously for up to 6 months (Rudnick *et al.*, 2012) and collect simultaneous physical and biological parameters (Suberg *et al.*, 2014). Gliders move up and down the water column by changing their buoyancy with wings allowing them to move horizontally at a speed of approximately 25 cm/s. A complete dive can reach 1000 m depth, collecting data on the way down and up to give two vertical profiles. Typically, one dive takes 4 hours to complete. It would

take less time, and provide finer horizontal resolution, if dives only reached 100 m depth. A large amount of data could thus be collected every day. Additionally, their regular communication via satellite allows their movement to be controlled so surveys using multiple gliders can therefore be coordinated. However, their slow movement means that the gliders are exposed to strong current and therefore following a defined transect may not always be straightforward and cause problems of alignment between gliders and erratically spaced data. Some other Autonomous Underwater Vehicles (AUV) e.g. Autosub have an advantage over gliders in that they move faster through the water which means fewer of them would be required, but their cost means only a small number of them exist for marine research.

An alternative solution for capturing and examining such high frequency variability may come from a new perspective on an old observational technique - moorings. Part of the NERC Ocean Surface Boundary Layer research programme OSMOSIS project, that started in 2012 at the Porcupine Abyssal Plain (PAP) in the North Atlantic, consisted of the deployment of 2 sets of 4 mooring stations organised in two concentric squares of side 15 km and 1.5 km centred on a central ninth mooring, continuously collecting hydrographic measurements over the course of the year. Using a similar array with fluorimeters fitted on each mooring, possibly at different depths, the difference in measurements between pairs of moorings would offer simultaneous measurements of variability covering many scales from 1.5 km to 21 km. Although the spatial coverage is limited, the many combinations provide between 2 and 8 measurements at any instant for each of the following length-scales 1.5 km, 2.1 km, 9.6 km, 10.7 km, 11.7 km, 15 km and 21 km. These cannot be used to calculate a power spectrum covering the full mesoscale, but the data would offer a considerable insight into the high frequency variability of phytoplankton structure at these scales. Furthermore, the addition of another square of moorings with side 75 km would provide an even greater spatial coverage with data collected across the full mesoscale and submesoscale as information on the variability of phytoplankton would be extended to length-scales as large as 106 km. Such an approach would benefit from the use of semi-variograms to calculate the spectrum. The technique has previously been applied to phytoplankton patchiness (Deschamps *et al.*, 1981, Yoder *et al.*, 1987, Yoder *et al.*, 1993) . The advantage of the technique is its ability to evaluate variability for data that is irregularly spaced in two dimensions, unlike power spectra for which methods perform best with straight line transects. Semi-variograms quantify how much variability is expected between 2 data points at a given distance apart, say r_i, for the field of interest. The more pairs of sample points being at distance r_i apart the better the estimate at that length-scale. For the OSMOSIS double square case, 1.5 km $\leq r_i \leq$ 21 km and for each length-scale 2, 4 or 8 pairs of data points

are available at each sample time which could be hourly. The semi-variogram may also be suited to use with fleets of gliders. Indeed, by deploying 6 gliders, 10 combinations of pairs of measurements are continuously being made. With gliders sampling for up to 6 months, the daily semi-variograms obtained with such high resolution data would provide much information on the magnitude of high frequency variability.

7.2.2. Geographical variability

Investigating geographical variability in the phytoplankton slope constitutes a difficult challenge, and one closely linked to the short term variability discussed in the previous section. In this thesis, most understanding of geographical variability was obtained from the model. Differences in slope between regions are not always distinguishable due to the large temporal variability occurring at the scale of weeks.

For the summer period when all 3 *in situ* surveys (Chapters 3 and 4) were carried out, model slope standard deviations of 0.33, 0.42 and 0.53 were found in the subpolar, transition and subtropical regions respectively. This means that unless very large differences exist between regions, they cannot currently be detected. Even three *in situ* surveys within one month (like D369 in Chapter 4) do not sufficiently eliminate such temporal variability. Model results suggests that when three surveys are made for each cruise and when cruises in two different regions take place simultaneously, then the difference between the regions can be correctly measured only provided that true difference is larger than 0.5 (Chapter 5 Section 5.3.2.3.), almost as large as previous observational estimates for the slope itself. Therefore, the observed differences between regions discussed in this thesis may not accurately reflect any underlying relationship.

Currently *in situ* surveys, due to being limited in space and time, cannot quantify the sub-regional and sub-monthly variabilities and therefore cannot be used to quantify variability on larger time and space scales. Based on the model predictions, the high frequency variability could explain the difference in *in situ* phytoplankton spectra observed between regions (Chapter 4) but replaces a potential failing of a universal scaling geographically with a potential failing of it in time.

Measuring geographical differences in slope requires that a sufficiently large area is sampled but also sampled frequently enough to remove both spatial and temporal variability at small scales. This can potentially be accomplished by satellite provided sufficiently large cloud free

images are available for both the regions compared over the period investigated. Obtaining such favourable conditions would, however, be unusual based on the satellite study done in Chapter 6.

7.2.3. Monthly, and seasonal variability

Further doubts have been cast on the universality of the scaling properties of the phytoplankton spectrum over longer time-scales by this thesis because such properties have been shown to also vary on seasonal time-scales. Even the extent of short term variability changes across the year, with periods of high variability e.g. spring and autumn and periods of lower variability (Chapter 5 Section 5.3.2.2.).

In the subpolar region the model suggested the existence of a seasonal cycle in the phytoplankton slope, specifically a rapid flattening of the spectrum during the phytoplankton bloom followed by a more gradual slow steepening over the course of the summer (Chapter 5 Section 5.4.). There was some evidence for this in for all four years investigated, though there was considerable shorter scale variability superimposed upon it. The seasonal changes in slope occur at a similar time to the spring bloom but the timing relative to the peak of the bloom is inconsistent.

Although satellite observations did not give the same temporal resolution as the model, there was still sufficient evidence to corroborate the model predictions that phytoplankton scaling properties vary over the year (Chapter 6 Section 6.3.3.). However, there was no evidence of the above seasonal pattern. The poor temporal resolution, because of the intermittency produced by clouds, means that it is still not possible to reject the hypothesis of a seasonal cycle in phytoplankton slope. The high frequency variability discussed in the previous section may alias any seasonal signal that is present. The existence of a seasonal cycle may be better tested using multi-year satellite data. Such an approach would increase the number of spectral slope estimates in each month and would compensate for the poor resolution of data from a single year. If such a seasonal cycle is a characteristic feature of phytoplankton patchiness it should become apparent in the reconstructed annual variations of phytoplankton spectral slope obtained from the multi-year records. The timing and abruptness of seasonal changes would not be as clear as for a single year, though, because like the bloom itself, such a signal might vary in timing and intensity between years.

Changes in the spectral slope, happening during the spring period of high biological activity, would highlight the importance of biological processes in modifying the phytoplankton spatial structure. The impact on the spatial distribution of non-linearities in the interactions between biogeochemical species remains difficult to understand. The motivation for further exploring the existence of a seasonal cycle in slope comes from analysis of a single model and so the robustness of the results needs to be tested with other models. Biogeochemical interactions, such as the type of functional responses to grazing by zooplankton or the nature of the spectrum relative to how nutrient upwelling is imposed, impact strongly on the spatial and relative spatial distribution of interacting species (Abraham, 1998, Englund and Leonardsson, 2008, Martin *et al.*, 2008). The results may therefore be specific to this model. An illustration of this problem is provided in Chapter 3 with existing theories disagreeing on the nature of the nitrate-phytoplankton relationship. Future work on the robustness of these results should be carried out using other basin scale models (e.g. Oschlies, 2002, McGillicuddy *et al.*, 2003). To investigate the length-scale range studied here (30–150 km), the resolution of such models (1/9° and 0.1° respectively) resolves the mesoscale, but not the submesoscale. Even the nominal ~10 km resolution will not be achieved due to imposed dissipation at small scales which will artificially cause the spectrum to roll off.

Nevertheless, performing different model runs may contribute to understanding the origin of such variability and what causes such large variations. By simply comparing the trends in phytoplankton patchiness time series over an identical range (30-150 km) for model runs with different grid resolutions e.g. 1/27° and 1/9°, the extent of the submesoscale contribution may be assessed.

Ships of opportunity once again may provide a means of study *in situ* as several operate set routes throughout the year. Some already accommodate multiple sensors on board to provide underway simultaneous measurements. The temporal coverage and resolution associated with this method of sampling provides an ideal opportunity in studying spatial variability over time-scales of seasons that scientific cruises cannot offer.

7.2.4. Phytoplankton relationship with other tracers

Understanding of phytoplankton patchiness can also be obtained by studying the spatial relationship between phytoplankton and the other interacting components of the ecosystem, in particular its evolution over time. However, studies on different biogeochemical variables have

used observations at one time, in one location. The result is that conclusions have often been inconsistent. For instance, no consensus emerges for the relationship between phytoplankton and zooplankton spectral slopes (Mackas and Boyd, 1979, Piontkovski *et al.*, 1997, Martin and Srokosz, 2002). It may be that studies struggle to fully capture the mechanisms generating the relative difference between tightly coupled biogeochemical components. With evidence from this thesis that variability in space and time, at many scales exists in the spatial statistics of phytoplankton, an important issue is how this variability compares with other components and how their relationship evolves over time. This highlights the importance of future observations carrying out measurements of multiple tracers in multiple locations, at multiple times.

The *in situ* data analysis of Chapter 3 demonstrated that nitrate and phytoplankton, although tightly coupled biochemical species, can display distributions with different statistical properties. Here, nitrate has a significantly steeper spectrum (- 1.29) than phytoplankton (-0.5). Even though it was a small, single dataset such observations already enhance our understanding of patchiness by contradicting a number of existing theories for patchiness that predict equal slopes (Hernández-García *et al.*, 2002, Bracco *et al.*, 2009). Model simulations in Chapter 5 suggest that large differences in slope for phytoplankton and nitrate are not uncommon. In the model, however, it is more likely that phytoplankton slope is steeper than nitrate over the summer period studied in Chapter 3. It may be that the observations witness a rare event, but it is too early to have too much confidence with such a level of detail in models. It is therefore important to obtain more observations of the relationship in the same place and time to build up the statistics and form a clearer view.

Models only represent an idealised view of the real world. Care is therefore needed when interpreting their results. The dynamics of the different biogeochemical components is based on how the interactions are defined. As mentioned in the previous section, the non-linearities in the functional responses, such as phytoplankton growth, zooplankton grazing and mortality can generate different relationships between the spatial distribution of phytoplankton and zooplankton (e.g. Steele and Henderson, 1992, Martin *et al.*, 2008) according to how they are parameterised. For instance, white noise forcing of the zooplankton mortality term is shown to generate a red spectra for phytoplankton and zooplankton(Steele and Henderson, 1992). This transfer of variability across scales is the result of the non-linear interactions. However, other types of forcing, such as on phytoplankton growth can also give a different spatial relationship with other components of the ecosystem such as zooplankton and nitrate. Currently the understanding of nutrient forcing is incomplete, with the relative importance of the different

pathways (winter convection, mescoscale upwelling …), acting on different length-scales for upwelling nutrients not known. The spectral shape of this forcing impacts on the resulting patchiness of plankton. Different nitrate spectra are predicted by models depending on the dominant pathways for nitrate injection into the euphotic layer. In the case of large scale forcing (Abraham, 1998), variance is driven across length-scales by the horizontal advection that cascades the variability to smaller scales. On the other hand, a regime dominated by small scale injections generates a different form of patchiness made of smaller structures (Lévy *et al.*, 2001). The first regime generates steeper slopes for nitrate spectra than the second one. The effect on phytoplankton spectral slope is not so clear due the non-linear interactions. Furthermore, over the course of the year, the influence of the different nutrient pathways varies and may therefore modulate the distribution of phytoplankton seasonally. For instance, in the subtropical regions the impact of small scale injection by submesoscale processes becomes gradually more important as the nitrate stockpiles from winter mixing are depleted. Observations across this transition would shed light on the nature and evolution of the nitrate-phytoplankton spatial relationship.

The relationship of the phytoplankton distributions to physical fields, such as temperature and salinity, has been found, here and elsewhere, to be inconsistent. Alternatively, numerical studies have shown that phytoplankton spectral slope may be correlated to relative vorticity (Lévy and Klein, 2004). Currently, satellite derived altimetry data provide geostrophic velocities maps in 1/3° grids as 8 day composites. These can only be used to evaluate whether there is a relationship between vorticity and phytoplankton spectral slope on seasonal and annual cycles. Furthermore, submesoscale events, at the margins of eddies or in filaments, are very localised and ephemeral. These fine details will disappear in the average over time and space obtained for each pixel. Such work may, however, soon become possible with future satellites (e.g. Sentinel-3, Wavemill and SWOT) potentially providing altimetry measurements at a 2km scale.

7.3. Conclusion

Obtaining a robust measurement of phytoplankton spatial structure is challenging with many limitations in the data contributing to adding noise and uncertainties in the estimates. It has been shown that provided sufficient spatial coverage is available, the patchiness of phytoplankton can be accurately quantified using power spectrum. Universal properties of the

phytoplankton spectrum have been tested from a model and observational (*in situ* and satellite) perspective covering a large range of temporal scales, from a few days to a year, and spatial ones, sub-regional and regional. A power-law behaviour in the phytoplankton spectrum was consistently found across the sources of data used and the range of scales studied, 8-130 km and 10-100m supporting to a certain degree the existence of universal properties for the phytoplankton spectrum. However, stronger universality, in common scaling exponents for the phytoplankton spectrum, is dented by the significant variability in slope that is consistently observed across the spatial and temporal scales studied and present across the data and model output used. A summary of all the results from *in situ*, satellite and model from this research study in Figure 7.1 illustrates the scale of this variability.

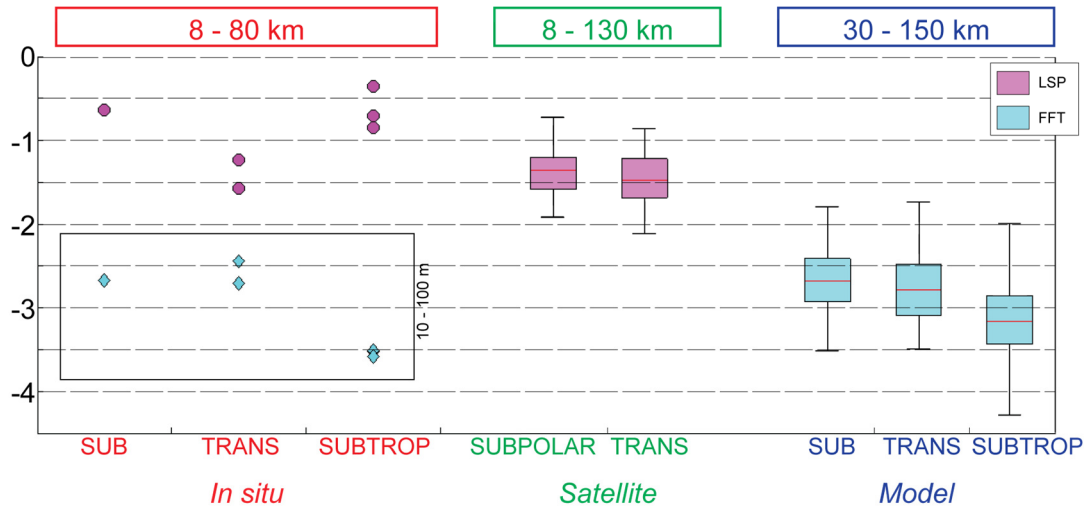

Figure 7.1: *Spectral slope of phytoplankton using in situ, satellite observations and model output for areas in the subpolar (SUB), transition (TRANS) and subtropical (SUBTROP) regions of the North Atlantic for length-scales covering the mesoscale. The range of length-scales vary between types of data due to the specificity of the data sets. For in situ, slopes for the range 10 -100 m are also calculated (diamonds). Slopes are estimated using the Fast Fourier Transform (FFT) with whitening the data (pink) or using the Lomb Scargle Periodogram (LSP) (blue).* For satellite and model, slopes are displayed in a box with the median value (red line) and 25th and 75th percentiles (edges), the whiskers correspond to the most extreme slope values.

Had the universality of scaling properties been confirmed, power spectra would present a computationally cheap method for describing sub-gridscale phytoplankton variance in coarse resolution models. Reactions in the phytoplankton ecosystem occurring below the 100 km length-scale play a central role in the distribution of organisms such as phytoplankton and zooplankton(Levy and Martin, 2013) suggesting at least an implicit representation of their spatial variability at those scales is necessary. Such a 'closure' for parameterising phytoplankton heterogeneity in global coarse resolution biogeochemical models could potentially improve

mean field estimates. Two things would still get in the way of such plans. First, there is the evidence of the presence of a critical length-scale at which a shift in power law behaviour occurs, estimated to be within the 0.1-8 km range (Chapter 3 Section 3.3.). This shift provides a challenge to a potential implementation, as it occurs at a length-scale which is not currently explicitly modelled and questions such as the exact length-scale at which the shift occurs, the nature of the shift and whether this shift occurs in all biogeochemical components remain to be answered. Closures, accounting for variance and correlations of phytoplankton at smaller scales, are already being carried out (Englund and Leonardsson, 2008, Wallhead *et al.*, 2013) and showing promising results as compared to the more usual mean field biogeochemical models. However, none of them address the consequences of the shift in scaling behaviour seen in Chapter 3 and elsewhere.

The understanding of patchiness is not complete. I showed that fluctuations in phytoplankton spatial properties at the mesoscale exist. The natural following question is therefore whether there is also structure in the manner in which these properties vary and are not simply random. This thesis sets the groundwork for this. So far, the clearest signs of structure come from the model study (Chapter 5) which shows a seasonal cycle in the slope of phytoplankton in the subpolar region. It also shows that temporal differences exist in how variable phytoplankton spatial properties are across the year in the subtropical region, with peaks of variability observed in spring and autumn. The scale of the variability in slope highlighted in this thesis demonstrates the need for both high resolution and global data to fully capture the phenomenon. New approaches and technology mean that obtaining such information is at last becoming realistic. Doing so may reveal the existence of provinces delimited by changes in phytoplankton spatial properties or behaviour as was hinted by the model results of this thesis.

Additionally, a simple yet important reason for deepening our understanding of phytoplankton patchiness is the testing of models. The resolution of global models keeps increasing and it is only a matter of time before global models will resolve fully the mesoscale and submesoscale. Yet, such models would still need to be tested. A number of metrics already exists to assess models (Stow *et al.*, 2009) e.g. the correlation coefficient, root mean squared error or absolute error, but these are based on a point by point comparison of the model predictions and observations by doing statistics on the difference at each point.

The problem is that no matter how fine resolution they become models will never predict the position of the numerous small-scale fronts and eddies populating the oceans correctly. This limits the use of these metrics as models explicitly resolve the highly variable mesoscale and

smaller. Peaks and troughs of concentrations in phytoplankton are associated with eddies and fronts meaning that metrics using point comparison will suffer from the mismatch in position of these dynamical features.

However, if in addition to these metrics, information on the spatial properties of the phytoplankton field between model and observations can be compared, this would increase the quality of the model assessment. This is where the spectral slope as a metric may be a powerful option. The spectral slope of phytoplankton indicates how the variability of the phytoplankton field is distributed across spatial scales. A comparison between spectral slope from observations and from the model therefore assesses how well the spatial properties are captured independent of the position of the features that generate this variability.

If the spectral properties of phytoplankton can be quantified globally via the techniques detailed in the discussion chapter, these can be used to validate biogeochemical models. The skill of a model could be assessed by how well it reproduces the spectral properties of phytoplankton. For instance for a given region, how close are the model mean slope, range and variance to those obtained from observations? Given the growing importance attributed to models to support decision making, it is essential that models about to resolve the mesoscale can be thoroughly tested. This makes spectral slope as a metric for phytoplankton a valuable tool.

It is therefore important that further research is done to obtain a global coverage of phytoplankton slope properties. From a wider perspective, this will also enable us to better understand the complexity and continuously evolving spatial structure of phytoplankton across the many spatial scales and understand how they adapt to and influence different environments. At a time when environments are fast changing with global warming potentially affecting ocean circulation and acidification (Intergovernmental Panel on Climate Change (IPCC), 2013), increasing pressure is being put on the marine ecosystem. Understanding how phytoplankton is structured may shed light on how well they will adapt to potential future changes. The position of phytoplankton at the base of the marine food web, makes this question an essential one.

Appendices

A5.1: *Time series for the phytoplankton slope (in colour) for the subpolar area for year 1 (a.), 2 (b.), 3 (c.) and 4 (d.) overlaid by mean slope for the 4 years (black).*

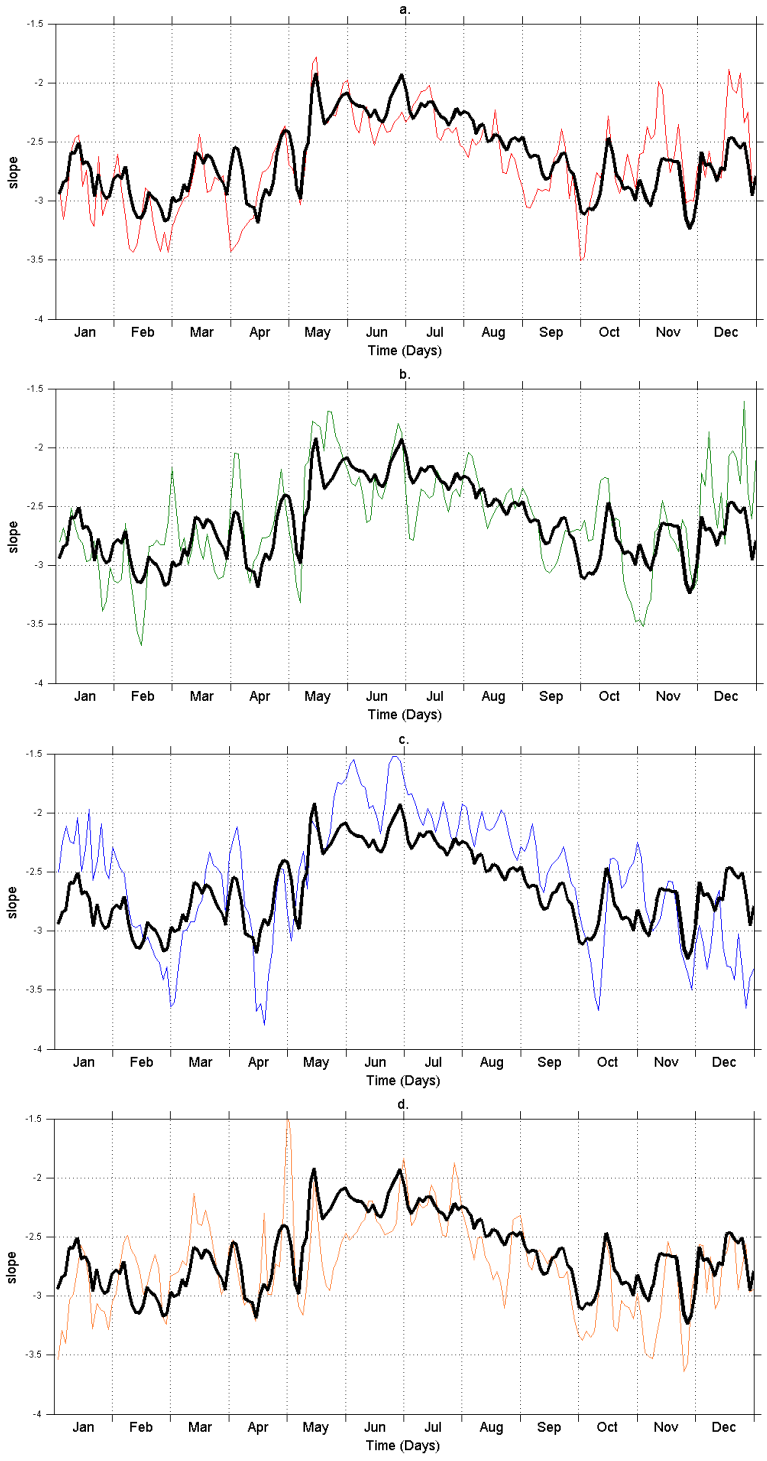

A6.1: *Detail of time series for the D321 area sampled in the East-West (a.) and North-South (b.) direction. The respective spectra for each transect are in (c.) and (d.). Mean spectra are displayed in bold green. The spectra all display a power law as a function of length-scale.*

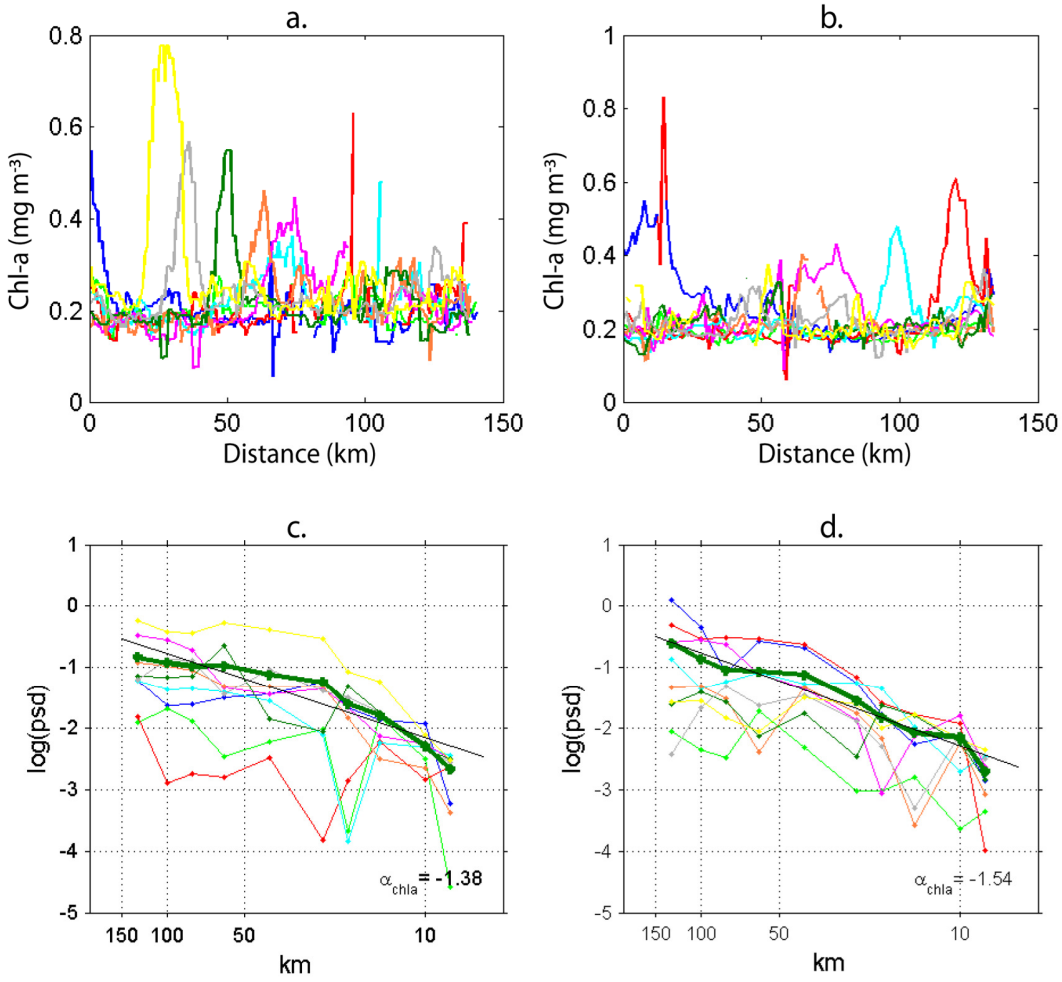

A6.2*: Spectral analysis of satellite Chl-a data for the region surrounding the location of the D321 cruise. The area of 400 by 400 km, was subdivided into subsets of size 130 by 130 km overlapping in the latitudinal and longitudinal direction by 50 %. Slope estimates and standard deviation are shown for each box .In brackets it is shown the number of transects used for the analysis. The lower number of transects used is due to some transects having more than 20 % of data hidden by clouds. Cells with 'Cloud' means the slope of phytoplankton was not calculated due to clouds covering more than 30% of the area. Position in the table corresponds to positions on the map (Figure 6.5).*

Cloud	Cloud	-1.39 ± 0.24 (4)	-1.70 ± 0.18 (9)	-1.91 ± 0.13 (9)	-1.92 ± 0.11 (9)
Cloud	-1.25 ± 0.19 (6)	-1.38 ± 0.19 (7)	-1.29 ± 0.16 (8)	-1.71 ± 0.16 (9)	-1.74 ± 0.13 (9)
Cloud	-1.32 ± 0.22 (8)	-1.19 ± 0.15 (9)	-1.15 ± 0.16 (7)	-1.54 ± 0.14 (9)	-1.46 ± 0.16 (9)
-1.94 ± 0.44 (3)	-1.58 ± 0.18 (9)	-1.18 ± 0.21 (7)	-1.33 ± 0.27 (4)	-1.48 ± 0.18 (9)	-1.06 ± 0.26 (9)
-1.69 ±0.19 (8)	-1.67 ± 0.18 (8)	-1.55 ± 0.17 (3)	-1.20 ± 0.17 (6)	-1.31 ± 0.25 (7)	-0.96 ± 0.30 (5)

A6.3:

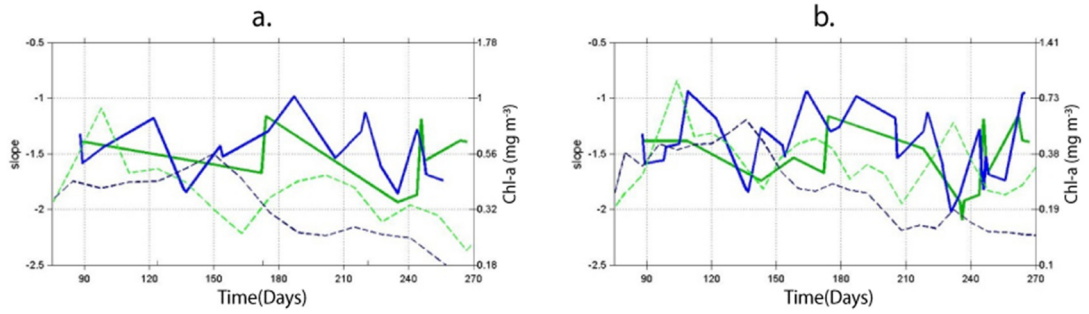

A) *Comparison of phytoplankton spectral slopes for areas T1 (green) and T2 (blue) using 30 transects (a.) and 70 transects (b.) for the evaluation of the slope.*

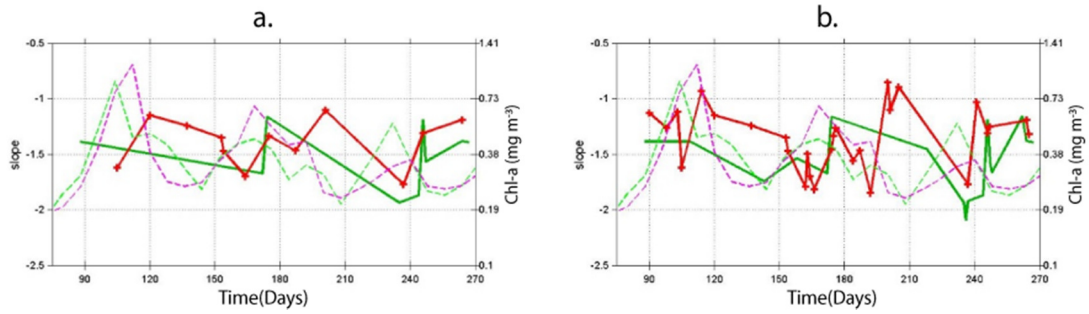

B) *Same as above but between T1 (green) and T3 (red).*

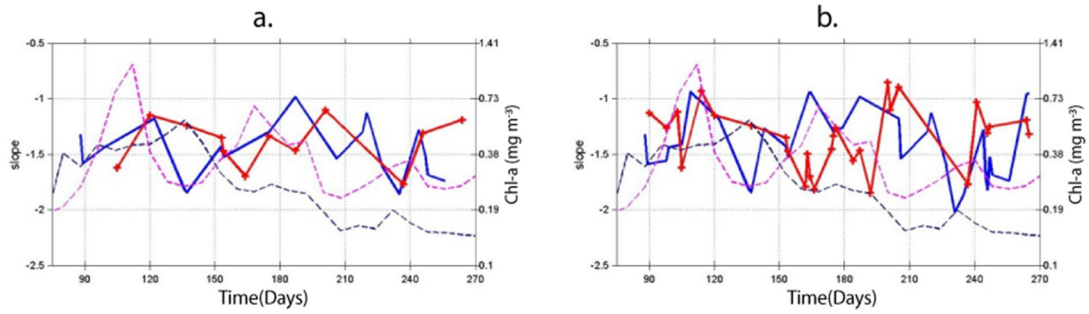

C) *Same as above but between T2 (blue) and T3 (red).*

Bibliography

Abraham, E. R. (1998). "The generation of plankton patchiness by turbulent stirring." Nature **391**(6667): 577-580.

Allen, J. T. (2008). RRS Discovery Cruise 321, 24 Jul-23 Aug 2007. Biophysical interactions in the Iceland Basin 2007. National Oceanography Centre Southampton Cruise Report, 23, Southampton, UK, National Oceanography.

Allen, J. T., L. Brown, R. Sanders, C. Mark Moore, A. Mustard, S. Fielding, M. Lucas, M. Rixen, G. Savidge, S. Henson and D. Mayor (2005). "Diatom carbon export enhanced by silicate upwelling in the northeast Atlantic." Nature **437**(7059): 728-732.

Allen, J. T. and A. Naveira-Garabato (2012). RRS Discovery Cruise 381, 28 Aug - 3 Oct 2012

Ocean Surface Mixing, Ocean Sub-mesoscale Interaction Study. National Oceanography Centre Cruise Report, National Oceanography Centre.

Barale, V. and C. C. Trees (1987). "Spatial variability of the ocean color field in CZCS imagery." Advances in Space Research **7**(2): 95-100.

Behrenfeld, M. J., R. T. O/'Malley, D. A. Siegel, C. R. McClain, J. L. Sarmiento, G. C. Feldman, A. J. Milligan, P. G. Falkowski, R. M. Letelier and E. S. Boss (2006). "Climate-driven trends in contemporary ocean productivity." Nature **444**(7120): 752-755.

Bendat, J. S. and A. G. Piersol (1971). Random Data: Analysis and Measurement Procedures, John Wiley & Sons, Inc.

Bracco, A., S. Clayton and C. Pasquero (2009). "Horizontal advection, diffusion, and plankton spectra at the sea surface." J. Geophys. Res. **114**(C2): C02001.

Bracco, A., S. Clayton and C. Pasquero (2009). "Horizontal advection, diffusion, and plankton spectra at the sea surface." Journal of Geophysical Research-Oceans **114**.

Callies, J. and R. Ferrari (2013). "Interpreting Energy and Tracer Spectra of Upper-Ocean Turbulence in the Submesoscale Range (1–200 km)." Journal of Physical Oceanography **43**(11): 2456-2474.

Chelton, D. B., P. Gaube, M. G. Schlax, J. J. Early and R. M. Samelson (2011). "The Influence of Nonlinear Mesoscale Eddies on Near-Surface Oceanic Chlorophyll." Science **334**(6054): 328-332.

Codiga, D. L., W. M. Balch, S. M. Gallager, P. M. Holthus, H. W. Paerl, J. H. Sharp and R. E. Wilson (2012). "Ferry-based Sampling for Cost-Effective, Long-Term, Repeat Transect Multidisciplinary Observation Products in Coastal and Estuarine Ecosystems. Community White Paper, IOOS Summit, Herndon, VA (November, 2012).".

Coles, W., G. Hobbs, D. J. Champion, R. N. Manchester and J. P. W. Verbiest (2011). "Pulsar timing analysis in the presence of correlated noise." Monthly Notices of the Royal Astronomical Society **418**(1): 561-570.

Denman, K. L., A. Okubo and T. Platt (1977). "Chlorophyll fluctuation spectrum in sea." Limnology and Oceanography **22**(6): 1033-1038.

Denman, K. L. and T. Platt (1976). "The variance spectrum of phytoplankton in a turbulent ocean." Journal of Marine Research **v. 34(4)** p. 593-601.

Deschamps, P.-Y., R. Frouin and L. Wald (1981). Satellite determination of the mesoscale variability of the sea surface temperature.

Emery, W. J. and R. E. Thomson (2001). Chapter 5 - Time-series Analysis Methods. Data Analysis Methods in Physical Oceanography. W. J. Emery and R. E. Thomson. Amsterdam, Elsevier Science**:** 371-567.

Englund, G. and K. Leonardsson (2008). "Scaling up the functional response for spatially heterogeneous systems." Ecology Letters **11**(5): 440-449.

Fasham, M. J. R. and P. R. Pugh (1976). "Observations on the horizontal coherence of chlorophyll a and temperature." Deep Sea Research and Oceanographic Abstracts **23**(6): 527-538.

Field, C. B., M. J. Behrenfeld, J. T. Randerson and P. Falkowski (1998). "Primary Production of the Biosphere: Integrating Terrestrial and Oceanic Components." Science **281**(5374): 237-240.

Folt, C. L. and C. W. Burns (1999). "Biological drivers of zooplankton patchiness." Trends in ecology & evolution (Personal edition) **14**(8): 300-305.

Fox-Kemper, B., G. Danabasoglu, R. Ferrari, S. M. Griffies, R. W. Hallberg, M. M. Holland, M. E. Maltrud, S. Peacock and B. L. Samuels (2011). "Parameterization of mixed layer eddies. III: Implementation and impact in global ocean climate simulations." Ocean Modelling **39**(1-2): 61-78.

Fox-Kemper, B. and R. Ferrari (2008). "Parameterization of mixed layer eddies. Part II: Prognosis and impact." Journal of Physical Oceanography **38**(6): 1166-1179.

Fox-Kemper, B., R. Ferrari and R. Hallberg (2008). "Parameterization of mixed layer eddies. Part I: Theory and diagnosis." Journal of Physical Oceanography **38**(6): 1145-1165.

Gledhill, D. K., R. Wanninkhof, F. J. Millero and M. Eakin (2008). "Ocean acidification of the Greater Caribbean Region 1996–2006." Journal of Geophysical Research: Oceans **113**(C10): C10031.

Gower, J. F. R., K. L. Denman and R. J. Holyer (1980). "Phytoplankton patchiness indicates the fluctuation spectrum of mesoscale oceanic structure." Nature **288**(5787): 157-159.

Halverson, M. J. and R. Pawlowicz (2013). "High-resolution observations of chlorophyll-a biomass from an instrumented ferry: Influence of the Fraser River plume from 2003 to 2006." Continental Shelf Research **59**(0): 52-64.

Hartman, S. E., M. C. Hartman, D. J. Hydes, D. Smythe-Wright, F. Gohin and P. Lazure (2014). "The role of hydrographic parameters, measured from a ship of opportunity, in bloom formation of Karenia mikimotoi in the English Channel." Journal of Marine Systems(0).

Hernández-García, E., C. López and Z. Neufeld (2002). "Small-scale structure of nonlinearly interacting species advected by chaotic flows." Chaos: An Interdisciplinary Journal of Nonlinear Science **12**(2): 470-480.

Hodges, B. A. and D. L. Rudnick (2006). "Horizontal variability in chlorophyll fluorescence and potential temperature." Deep Sea Research Part I: Oceanographic Research Papers **53**(9): 1460-1482.

Horwood, J. (1981). "Variation of fluorescence, particle-size groups, and environmental parameters in the southern North Sea." Journal du Conseil **39**(3): 261-270.

Horwood, J. W. (1978). "OBSERVATIONS ON SPATIAL HETEROGENEITY OF SURFACE CHLOROPHYLL IN ONE AND 2 DIMENSIONS." Journal of the Marine Biological Association of the United Kingdom **58**(2): 487-502.

Intergovernmental Panel on Climate Change (IPCC), W. G. I. W. (2013). Summary for Policymakers. Climate Change 2013: The Physical Science Basis. T. F. Stocker and D. Qin, Cambridge Univ. Press, Cambridge, U. K., and New York.

Jenkins, G. M. and D. G. Watts (1968). Spectral analysis and its applications. Oakland, CA., Holden-Day.

Klein, P., B. L. Hua, G. Lapeyre, X. Capet, S. Le Gentil and H. Sasaki (2008). "Upper ocean turbulence from high-resolution 3D simulations." Journal of Physical Oceanography **38**(8): 1748-1763.

Klein, P. and G. Lapeyre (2009). The Oceanic Vertical Pump Induced by Mesoscale and Submesoscale Turbulence. Annual Review of Marine Science. **1:** 351-375.

Kolmogorov, A. N. (1991). "The Local Structure of Turbulence in Incompressible Viscous Fluid for Very Large Reynolds Numbers." Proceedings: Mathematical and Physical Sciences **434**(1890): 9-13.

Kraichnan, R. H. (1967). "Inertial Ranges in Two-Dimensional Turbulence." Physics of Fluids (1958-1988) **10**(7): 1417-1423.

Lekan, J. F. and R. E. Wilson (1978). "SPATIAL VARIABILITY OF PHYTOPLANKTON BIOMASS IN SURFACE WATERS OF LONG ISLAND." Estuarine and Coastal Marine Science **6**(3): 239-251.

Lévy, M. (2003). "Mesoscale variability of phytoplankton and of new production: Impact of the large-scale nutrient distribution." J. Geophys. Res. **108**(C11): 3358.

Lévy, M., M. Gavart, L. Mémery, G. Caniaux and A. Paci (2005). "A 4D-mesoscale map of the spring bloom in the northeast Atlantic(POMME experiment): results of a prognostic model." J. Geophys. Res. **Vol. 110**(C7,C07S10).

Lévy, M., D. Iovino, L. Resplandy, P. Klein, G. Madec, A. M. Tréguier, S. Masson and K. Takahashi (2012). "Large-scale impacts of submesoscale dynamics on phytoplankton: Local and remote effects." Ocean Modelling **43-44**: 77-93.

Lévy, M. and P. Klein (2004). "Does the low frequency variability of mesoscale dynamics explain a part of the phytoplankton and zooplankton spectral variability?" Proceedings of the Royal Society of London. Series A: Mathematical, Physical and Engineering Sciences **460**(2046): 1673-1687.

Lévy, M., P. Klein and A.-M. Tréguier (2001). "Impact of sub-mesoscale physics on production and subduction of phytoplankton in an oligotrophic regime." Journal of Marine Research **59**: 535-565.

Lévy, M., P. Klein, A. M. Tréguier, D. Iovino, G. Madec, S. Masson and K. Takahashi (2010). "Modifications of gyre circulation by sub-mesoscale physics." Ocean Modelling **34**(1–2): 1-15.

Levy, M. and A. P. Martin (2013). "The influence of mesoscale and submesoscale heterogeneity on ocean biogeochemical reactions." Global Biogeochemical Cycles **27**(4): 1139-1150.

Lévy, M., L. Resplandy, P. Klein, X. Capet, D. Iovino and C. Ethé (2012). "Grid degradation of submesoscale resolving ocean models: Benefits for offline passive tracer transport." Ocean Modelling **48**(0): 1-9.

Lévy, M., L. Resplandy and M. Lengaigne (2014). "Oceanic mesoscale turbulence drives large biogeochemical interannual variability at middle and high latitudes." Geophysical Research Letters **41**(7): 2467-2474.

Lomb, N. R. (1976). "Least-squares frequency analysis of unequally spaced data." Astrophysics and Space Science **39**(Feb. 1976): 447-462.

Lorenzen, C. J. (1966). "A method for the continuous measurement of in vivo chlorophyll concentration." Deep Sea Research and Oceanographic Abstracts **13**(2): 223-227.

Lovejoy, S., W. J. S. Currie, Y. Tessier, M. R. Claereboudt, E. Bourget, J. C. Roff and D. Schertzer (2001). "Universal multifractals and ocean patchiness: phytoplankton, physical fields and coastal heterogeneity." Journal of Plankton Research **23**(2): 117-141.

Mackas, D. L. and C. M. Boyd (1979). "Spectral Analysis of Zooplankton Spatial Heterogeneity." Science **204**(4388): 62-64.

Mackas, D. L., K. L. Denman and M. R. Abbott (1985). "Plankton patchiness: biology in the physical vernacular." Bulletin of Marine Science **37**: 652-674.

Madec, G. (2008). NEMO ocean engine. Note du Pole de modelisation de l'Institut Pierre-Simon Laplace No 27.

Mahadevan, A. and J. W. Campbell (2002). "Biogeochemical patchiness at the sea surface." Geophysical Research Letters **29**(19): 32-31-34.

Martin, A. P. (2003). "Phytoplankton patchiness: the role of lateral stirring and mixing." Progress In Oceanography **57**(2): 125-174.

Martin, A. P. and K. J. Richards (2001). "Mechanisms for vertical nutrient transport within a North Atlantic mesoscale eddy." Deep Sea Research Part II: Topical Studies in Oceanography **48**(4–5): 757-773.

Martin, A. P. and M. A. Srokosz (2002). "Plankton distribution spectra: inter-size class variability and the relative slopes for phytoplankton and zooplankton." Geophysical Research Letters **29**(24).

Martin, A. P., M. V. Zubkov, M. J. Fasham, P. H. Burkill and R. J. Holland (2008). "Microbial spatial variability: An example from the Celtic Sea." Progress in Oceanography **76**(4): 443-465.

McGillicuddy, D. J., L. A. Anderson, N. R. Bates, T. Bibby, K. O. Buesseler, C. A. Carlson, C. S. Davis, C. Ewart, P. G. Falkowski, S. A. Goldthwait, D. A. Hansell, W. J. Jenkins, R. Johnson, V. K. Kosnyrev, J. R. Ledwell, Q. P. Li, D. A. Siegel and D. K. Steinberg (2007). "Eddy/Wind Interactions Stimulate Extraordinary Mid-Ocean Plankton Blooms." Science **316**(5827): 1021-1026.

McGillicuddy, D. J., L. A. Anderson, S. C. Doney and M. E. Maltrud (2003). "Eddy-driven sources and sinks of nutrients in the upper ocean: Results from a 0.1 degrees resolution model of the North Atlantic." Global Biogeochemical Cycles **17**(2).

McGillicuddy, D. J., A. R. Robinson, D. A. Siegel, H. W. Jannasch, R. Johnson, T. D. Dickey, J. McNeil, A. F. Michaels and A. H. Knap (1998). "Influence of mesoscale eddies on new production in the Sargasso Sea." Nature **394**(6690): 263-266.

Mudelsee, M. (2010). Climate Time Series Analysis: Classical Statistical and Bootstrap Methods. Dordrecht Heidelberg London New York, Springer.

Oschlies, A. (2002). "Can eddies make ocean deserts bloom?" Global Biogeochem. Cycles **16**(4): 1106.

Pidcock, R., A. P. Martin, J. Allen, S. C. Painter and D. Smeed (2013). "The spatial variability of vertical velocity in an Iceland basin eddy dipole." Deep Sea Research Part I: Oceanographic Research Papers **72**(0): 121-140.

Pidcock, R., M. Srokosz, J. Allen, M. Hartman, S. Painter, M. Mowlem, D. Hydes and A. P. Martin (2010). "A Novel Integration of an Ultraviolet Nitrate Sensor On Board a Towed Vehicle for Mapping Open-Ocean Submesoscale Nitrate Variability." Journal of Atmospheric and Oceanic Technology **27**(8): 1410-1416.

Piontkovski, S., R. Williams and W. Peterson (1997). "Spatial heterogeneity of the planktonic fields in the upper mixed layer of the open ocean." Oceanographic Literature Review **44**(9).

Platt, T. (1972). "Local phytoplankton abundance and turbulence." Deep Sea Research and Oceanographic Abstracts **19**(3): 183-187.

Platt, T. and K. L. Denman (1975). "Spectral Analysis in Ecology." Annual Review of Ecology and Systematics **6**: 189-210.

Pollard, R. T. and L. A. Regier (1992). "Vorticity and Vertical Circulation at an Ocean Front." Journal of Physical Oceanography **22**(6): 609-625.

Powell, T. M. and A. Okubo (1994). "Turbulence, Diffusion and Patchiness in the Sea." Philosophical Transactions of the Royal Society of London Series B-Biological Sciences **343**(1303): 11-18.

Prairie, J. C., K. R. Sutherland, K. J. Nickols and A. M. Kaltenberg (2012). "Biophysical interactions in the plankton: A cross-scale review."

Press, W. H., S. A. Teukolky, W. T. Vetterling and B. P. Flannery (2007). Numerical recipes : the art of scientific computing. Cambridge, Cambridge University Press.

Rossby, T., C. Flagg and K. Donohue (2010). "On the variability of Gulf Stream transport from seasonal to decadal timescales." Journal of Marine Research **68**(3-1): 503-522.

Rudnick, D. L., M. Crowley, O. Schofield, R. Baltes, C. M. Lee and C. Lembke (2012). A national glider network for sustained observation of the coastal ocean. Oceans, 2012.

Sanders, R., S. A. Henson, M. Koski, C. L. De La Rocha, S. C. Painter, A. J. Poulton, J. Riley, B. Salihoglu, A. Visser, A. Yool, R. Bellerby and A. P. Martin (2014). "The Biological Carbon Pump in the North Atlantic." Progress in Oceanography(0).

Sarmiento, J. and N. Gruber (2006). Ocean Biogeochemical Dynamics. Princeton, NJ, Princeton University Press.

Scargle, J. D. (1982). "Studies in astronomical time series analysis. II - Statistical aspects of spectral analysis of unevenly spaced data." Astrophysical Journal, Part 1 **263**(Dec. 15, 1982): 835-853.

Seuront, L., F. Schmitt, Y. Lagadeuc, D. Schertzer and S. Lovejoy (1999). "Universal multifractal analysis as a tool to characterize multiscale intermittent patterns: example of phytoplankton distribution in turbulent coastal waters." Journal of Plankton Research **21**(5): 877-822.

Smith, R. C., X. Zhang and J. Michaelsen (1988). "Variability of Pigment Biomass in the California Current System as Determined by Satellite Imagery 1. Spatial Variability." J. Geophys. Res. **93**(D9): 10863-10882.

Steele, J. H. and E. W. Henderson (1992). "A simple model for plankton patchiness." Journal of Plankton Research **14**(10): 1397-1403.

Stow, C. A., J. Jolliff, D. J. McGillicuddy Jr, S. C. Doney, J. I. Allen, M. A. M. Friedrichs, K. A. Rose and P. Wallhead (2009). "Skill assessment for coupled biological/physical models of marine systems." Journal of Marine Systems **76**(1–2): 4-15.

Strass, V. H. (1992). "Chlorophyll patchiness caused by mesoscale upwelling at fronts." Deep Sea Research Part A. Oceanographic Research Papers **39**(1): 75-96.

Strutton, P. G., J. G. Mitchell, J. S. Parslow and R. M. Greene (1997). "Phytoplankton patchiness: quantifying the biological contribution using fast repetition rate fluorometry." Journal of Plankton Research **19**(9): 1265-1274.

Suberg, L., R. B. Wynn, J. v. d. Kooij, L. Fernand, S. Fielding, D. Guihen, D. Gillespie, M. Johnson, K. C. Gkikopoulou, I. J. Allan, B. Vrana, P. I. Miller, D. Smeed and A. R. Jones (2014). "Assessing the potential of autonomous submarine gliders for ecosystem monitoring across multiple trophic levels (plankton to cetaceans) and pollutants in shallow shelf seas." Methods in Oceanography(0).

Tsuda, A., H. Sugisaki, T. Ishimaru, T. Saino and T. Sato (1993). "White-noise-like distribution of the oceanic copepod Neocalanus cristatus in the subarctic North Pacific." Marine Ecology-Progress Series **97**(1): 39-46.

Wallhead, P. J., V. C. Garçon and A. P. Martin (2013). "Efficient upscaling of ocean biogeochemistry." Ocean Modelling **63**(0): 40-55.

Washburn, L., B. M. Emery, B. H. Jones and D. G. Ondercin (1998). "Eddy stirring and phytoplankton patchiness in the subarctic North Atlantic in late summer." Deep-Sea Research Part I-Oceanographic Research Papers **45**(9): 1411-1439.

Weber, L. H., S. Z. El-Sayed and I. Hampton (1986). "The variance spectra of phytoplankton, krill and water temperature in the Antarctic Ocean south of Africa." Deep Sea Research Part A. Oceanographic Research Papers **33**(10): 1327-1343.

Yoder, J. A., J. Aiken, R. N. Swift, F. E. Hoge and P. M. Stegmann (1993). "Spatial variability in near-surface chlorophyll a fluorescence measured by the Airborne Oceanographic Lidar (AOL)." Deep Sea Research Part II: Topical Studies in Oceanography **40**(1-2): 37-53.

Yoder, J. A., C. R. McClain, O. B. Jackson and L.-Y. Oey (1987). "Spatial Scales in CZCS-Chlorophyll Imagery of the Southeastern U. S. Continental Shelf." Limnology and Oceanography **32**(4): 929-941.

Zubkov, M. V. (2012). RRS Discovery Cruise 369, 09 Aug -15 Sep 2011. Influence of advection and sedimentation on linking microbial phosphorus, carbon and nitrogen cycling in the North Atlantic subtropical gyre (LINK). P. G. Hill, Southampton, UK, National Oceanography.

Zubkov, M. V. and G. D. Quartly (2003). "Ultraplankton distribution in surface waters of the Mozambique Channel‹flow cytometry and satellite imagery." Aquatic Microbial Ecology **33**(2): 155-161.